Wanted: Scalable Tracers for Diffusion Measurements

Supporting Information 1
Candidate Species for Biomembranes

Michael J. Saxton

Department of Biochemistry and Molecular Medicine, University of California, One Shields Ave., Davis, California 95616
E-mail: mjsaxton@ucdavis.edu
Phone: (530) 752-6163. Fax: (530) 752-3516

Supporting Information 1 considers candidate species for probes of 2D diffusion in biomembranes, including a more detailed discussion of the structure, design, and diffusion of the tracers.

As mentioned in the text, if distinct series of scalable tracers must be used to cover the entire range of sizes required, the radii of successive series ought to overlap. Thus, for biomembranes one might use a series of macrocyclic polyamides, a series of multipass transmembrane α-helices, and a series of β-barrels, with overlap minimally at one radius, ideally at several. As also discussed, one would use a scalable series to test size dependence alone, and a nonscalable series to test the sensitivity of diffusion to details of composition. The transmembrane segment would be varied with the hydrophilic regions constant, and vice versa.

For membrane protein structures see the excellent review of Vinothkumar and Henderson [1], and reviews of computational modeling of membrane proteins. [2,3]

Self-Assembled Amphiphiles: Lipid Domains

Lipid domains – say gel-phase in a fluid-phase bilayer or liquid-ordered in liquid-disordered – have the advantages that they are naturally occurring and their size varies almost continuously. A disadvantage is that the experimenter has limited control over their size. The diameter varies among domains and with time, so the sizes of individual domains must be measured along with the diffusion coefficient. Also, the boundary layer is likely to be different from that of transmembrane proteins. Repulsion between domains may be important, [4,5] implying that domains ought to be used at low densities, as tracers but not as crowders. The pioneering experimental work was done by Klingler and McConnell [4] and further developed by Cicuta et al. [6] Rotational diffusion of diamond-shaped gel phase domains in giant unilamellar vesicles was measured by Petrov et al. [7]

Peripheral Proteins

In artificial peripheral proteins, a scalable headgroup is bound to the membrane by lipid tails. GPI-linked lipids could be used, or a lipid linked to the headgroup via avidin plus biotin or via Ni chelate plus a His tag. Linkages are reviewed briefly in Lohmüller et al. [8] In pioneering work on the mechanism of patching and capping, Wolf et al. [9,10] measured diffusion of stearoylated dextran bound to artificial bilayers and to plasma membranes of 3T3 cells.

Most of the tracers discussed in this review emphasize the nondraining or solid limits, but some work has been done at the free-draining limit. Diffusion measurements were made on tracers in which 1, 2, or 3 pleckstrin homology domains were coupled by flexible linkers with a length of 4–6 nm, and the domains were bound to PIP_3, phosphatidylinositol-(3,4,5)-trisphosphate. [11,12]

Macrocyclic Polyamides

The macrocyclic polyamide tracers developed in the Petersen lab were explicitly designed to be scalable. These were based on synthetic macrocyclic amide rings, dimers through hexamers, with their arms terminated by nitrilotriacetic acid. The first experiments [13] used these rings to link dodecyl chains, giving surface areas in the range 0.3–3.0 nm^2, compared to a phospholipid area ~ 0.65 nm^2. Later work [14] used various numbers of transmembrane helices, specifically a His-tagged peptide from the *b* subunit of *E. coli* F_1F_0-ATP synthase.

An important design principle is that the size of the macrocyclic polyamide headgroup must be varied, not just the number of acyl chains on a fixed headgroup. If one simply uses a hexamer and increases the number of acyl chains, the probe shape varies from conical to cylindrical, and the membrane properties of the probe vary accordingly.

Transmembrane α-Helices

Tracers based on transmembrane α-helices are an obvious choice. Tests of the Saffman-Delbrück equation using natural transmembrane proteins were described in the text. Here we discuss extending the size range with natural multipass α-helical proteins, which are not rigorously scalable, and the construction of their scalable counterparts.

Requirements

The ideal building block for scalable transmembrane helix (TMH) probes would be a diffusionally neutral TMH, that is, one that does not perturb the bilayer and has no attractive or repulsive force between probe molecules. The basic requirement is to avoid oligomerization, aggregation, or repulsion among the tracers, and to avoid lipid domain formation by the tracers. Direct interactions such as van der Waals attraction and charge repulsion must be minimized, and likewise lipid-mediated interactions.

To minimize lipid-mediated interactions, the TMH length must be matched to the membrane thickness. Much work has been done on hydrophobic matching, [15–17] including NMR of isotopically labeled forms, and coarse-grained molecular dynamics simulations. The emphasis has been on WALP and other simple synthetic single-TMH species. The WALP peptides are made up of a hydrophobic sequence of alternating leucine (L) and alanine (A), with pairs of tryptophans (W) at each end as membrane anchors, and a single glycine (G), for example WALP16, acetyl-GWW-$(LA)_5$-WWA-ethanolamide, and WALP19, acetyl-GWW-$(LA)_6$-LWWA-ethanolamide. The tryptophans localize near the lipid carbonyl groups, anchoring the peptides vertically. Domański et al. [18] present simulations.

An important point is that in synthetic peptides with two pairs of tryptophan anchors, interfacial matching – matching the Trp-Trp distance to the membrane thickness – is more important than hydrophobic matching, at

least for the particular systems examined.[19] This view is supported by fully atomistic molecular dynamics simulations that give a detailed picture of the energetics of various responses to mismatch.[20,21] These results suggest that to make a diffusionally neutral TMH, both distances ought to be matched to the bilayer.

Gambin et al.[22] measured diffusion of Leu-based peptides vertically positioned in the membrane by Lys. The surfactant system used in these experiments had the advantage that the thickness could be tuned continuously but the disadvantage that the membrane was not made of phospholipids. Ramadurai et al.[23] made diffusion measurements by fluorescence correlation spectroscopy (FCS) on WALP and related peptides in giant unilamellar vesicles. Hydrophobic mismatch had little effect on the diffusion coefficient.

Sparr et al.[24] measured self-association of WALP23 in membranes by means of excimer formation in peptides labeled with pyrene on the C or N termini. If the peptide and membrane are hydrophobically matched, the peptide does not self-associate at low concentrations, but hydrophobic mismatch in either direction promotes association. The peptide associates to form antiparallel dimers as shown experimentally, and the association was attributed to electrostatic interactions between the dipole moments of the α-helix backbone, on the basis of computer modeling.

Biologically driven dimerization is an important consideration in designing scalable α-helical tracers. Dimerization motifs[25–27] can be used internally to assemble multispan tracers but must be avoided on the outer surface of tracers. Testing for self-association is essential. See for example the work of Chakrabarti et al.[28] on self-association of MHC class I glycoprotein HLA-A2 in liposome and cell membranes. The most sensitive measurements of association used rotational diffusion or FRET. A more generic form of this approach is to design into the helices hydrophilic and hydrophobic faces appropriate to the folding pattern sought.

Designing and validating a diffusionally neutral series of scalable tracers would be an interesting test of our understanding of protein-lipid interactions.

Natural α-Helices

To what extent can naturally occurring proteins be used? Ramadurai et al.[29] made FCS measurements on a variety of proteins in giant unilamellar vesicles, of diameter 15–40 μm to avoid curvature and undulation effects. The proteins were labeled at an engineered Cys site. Explicit tests for anomalous subdiffusion showed diffusion to be normal. The measurements covered a significant range of protein sizes, from single TMHs of radius 0.5 nm such as synaptobrevin 2 and WALP23 synthetic peptide to MscS, the mechanosensitive channel of large conductance, a heptamer of radius 4.0 nm.

What are the size limits? In a review of membrane protein structure Vinothkumar and Henderson[1] list some larger proteins such as *E. coli* multidrug transporter EmrE with 8 TMHs; *E. coli* lactose permease LacY with 12 TMHs; sodium-dependent secondary transporters Mhp1, LeuT, BetP, and vGlt1 with 15 TMHs, two of which are interrupted; and the *E. coli* ammonia channel AmtB, a trimer with 11 TMHs per monomer. The ABC = ATP-binding cassette importers have 10–20 TMHs. So there are many possibilities for larger proteins. The limitation with this approach is that the tracers are not scalable, and they may be bound in mobile complexes or to the cytoskeleton.

Another large species is aquaporin-1, a tetramer which each monomer has six TMHs. Crane and Verkman[30] made single-particle tracking (SPT) measurements on aquaporin-1 in COS-7 and MDCK cells. The authors explicitly tested for anomalous subdiffusion and found free diffusion over long distances, predominantly normal diffusion, implying a low level of specific interactions with membrane components. Tetramers of aquaporin-4 further associate to form large structures called orthogonal arrays of particles. Dynamics of association and diffusion were also examined, including the dependence on isoform and the effect of mutations.[31]

Another class of large multihelix proteins are the pore-forming toxins (PFT), reviewed by Iacovache et al.[32] and in more detail by Parker and Feil[33]. The α-PFTs include colicins, diphtheria toxin, and *E. coli* hemolysin A.

Synthetic α-Helices

Early work on synthetic multipass TMH proteins is summarized in the review of computational design of proteins by Perez-Aguilar and Saven[2]. Recent references on synthetic α-helices include work of the Deber group on partially randomized "helical hairpin" peptides with two TMH joined by a 6-residue loop[34] and development of artificial proteins with 4 TMH as engineered scaffolds for cofactors. These may be independent helices assembled by porphyrins[35] or helices linked by hydrophilic loops.[36]

Transmembrane β-Barrels

As the work of Gambin et al.[37] suggests, transmembrane β-barrels may be a useful set of scalable membrane probes. These are proteins of the outer membrane of Gram-negative bacteria, and also of mitochondria and chloroplasts. The proteins are cylindrical with a hydrophobic exterior and a hydrophilic interior. They are made up of β-strands, sequences of $\sim$ 10 amino acids with alternating hydrophilic and hydrophobic residues. The β-hairpin is a pair of antiparallel β-strands connected by a short loop of $\sim$ 5 residues in the periplasm. A β-barrel is a cylinder of β-hairpins connected by loops of various lengths in the extracellular region. The strands are parallel and form a closed cylinder to permit hydrogen bonding between successive strands. The strands are at an angle with respect to the barrel axis, typically in the range 37° to 51°, and the angle is a key factor determining the cross-sectional area. The number of β-strands is even in almost all cases. Two bands of aromatic residues are located on the hydrophobic surface near the edges of the membrane to fix the vertical position of the barrel in the membrane,

just as in transmembrane α-helices. Some β-barrel proteins have long loops that can fold into the lumen to gate the pore. β-barrels may be a single polypeptide or a self-assembled structure.

Transmembrane β-barrels have been reviewed by several authors.[38–43] The table of β-barrel radii[41] is calculated from the number of strands and the shear number, which is related to the angle between the strands and the barrel axis. The calculations assume ideal cylindrical β-barrel geometry and use the exact formula of Murzin et al.[44] Reboul et al.[45] discuss the geometry of small versus giant β-barrels similarly. These results are useful first approximations but eventually actual structural measurements are needed. The Wimley group has studied bioinformatics of β-barrels.[46,47] Fairman et al.[48] list the structures of the known small β-barrel membrane proteins, with PDB (Protein Data Base) numbers but not literature references, and summarizes online resources for the structures.

Small β-Barrels: Structure

The small β-barrels are highly promising as scalable tracers. Their size ranges from 8 to 24 β-strands. Some examples are given here; Galdiero et al.[43] give further examples.

Among the 8-stranded β-barrels are OmpX, involved in bacterial adhesion and entry into mammalian cells, and OmpA, which stabilizes the outer membrane by connecting it to the peptidoglycan layer, and is also involved in bacterial conjugation. These β-barrels have different tilts of the β-strands with respect to the barrel axis. The diameter of OmpX is ~ 2 nm, with an axis ratio of 1.6, and the axis ratio for OmpA is 1.2. The interior of OmpA contains a network of hydrogen bonds and salt bridges, with no passage even for water. The network is rigid, as shown by the low B-factors in the X-ray structure. The network in OmpX is different but similarly dense.[49,50]

The porins are passive diffusion channels of the outer membrane. The 16-strand porins such as OmpC and OmpF are general pores, and the 18-strand porins provide specific transport, such as the sucrose transporter ScrY and the maltose oligosaccharide transporter LamB. The porins have a kidney-shaped cross-section and form homotrimers. The review of porins by Zeth and Thein[51] is a good general starting point for thinking about design of β-barrel tracers.

The main exception to the even-strand rule is VDAC, the voltage-dependent anion channel of mitochondria, with 19 strands.[48] The mammalian VDAC[51] is very nearly circular, with diameters ~ 3.1 and ~ 3.2 nm.

The 22-strand β-barrels include FhuA, FepA, and FecA, all transporters of iron complexes, and the vitamin B12 transporter BtuB. These are monomers. FhuA, the ferric hydroxamate uptake protein, has an elliptical cross-section with axes 3.1 nm and 4.4 nm, and has an N-terminal plug domain of 160 residues. It has been used in pore engineering studies described in the next section.[52]

The largest small β-barrel known is PapC from the bacterial chaperone/usher pathway. It is 24 strands, with a plug domain, and some structural irregularities giving a kidney-shaped barrel with outside dimensions 6.5×4.5 nm.[53]

One way to obtain larger structures, at the cost of some geometric regularity, is to make trimers, well established in nature.

Small β-Barrels: Design

The small β-barrels seem to be an excellent starting point for design of scalable tracers. The goal would be a rigorously scalable series covering the full range of sizes from 8 to 24 strands, with an attempt to make larger barrels. The properties wanted are (1) uniform strands; (2) uniform loops; (3) strand length matched to the membrane thickness; (4) pore-pore association sites eliminated; (5) loops modified to rigidify the pore and give it a circular cross-section; (6) pores blocked. Blocking the pore is essential if β-barrels are to be used as tracers in cell membranes. Some small β-barrels are pores, and a major class of giant β-barrels are the pore-forming toxins. In a rigorously scalable set of tracers, the barrel elements ought to be uniform, with the irregularities in strands and loops removed, such as those in PapC discussed by Remaut et al.[53]

The 22-stranded BtuB vitamin B12 transporter is asymmetric, with the barrel length varying between 2.5 nm and 3.7 nm, leading to distortions in the bilayer around the barrel. Ellena et al.[54] presented experimental evidence, discussed hydrophobic matching, and pointed out that this asymmetry could lead to lipid-mediated attraction. Ideally one would compare diffusion of uniform barrels to barrels with different exteriors, as an example of using scalable tracers to find the size dependence of diffusion and nonscalable tracers to find the variation due to differences in composition.

The feasibility of making a scalable series of β-barrels is strongly supported by published work on the modification of membrane β-barrels for biotechnology applications. The review of β-barrels by Galdiero et al.[43] says that they are "especially amenable to engineering studies," and a short review of biophysics of membrane proteins by White[55] says "Need a larger boundary? Just add a few more hairpins." The review of β-barrels by Schulz[40] summarizes early work on modification. Johansson et al.[56] designed the so-called β-barrel platform for the development of novel protein functions. This is a simplified form of OmpA with all four extracellular loops shortened. Naveed et al.[57] modified the trimerization sites in OmpF porin. Arnold et al.[58] showed that gene duplication of the 8-stranded β-barrel OmpX produced a functional 16-stranded pore, as did the even-numbered intermediate pores. The conductance of the pores in black lipid membranes was measured and structural requirements were found for folding into pores. Lolicato et al.[59] found a consensus sequence for β-hairpins in β-barrels, used it to make various sizes of β-barrels, and studied the conductance of the hexamer (12 β-strands) in black lipid membranes.

Recently Movileanu and colleagues have published a

series of papers on designing and building nanopores by modifying the 22-strand β-barrel FhuA, ferric hydroxamate uptake component A from *E. coli*. Krewinkel et al.[60] increased the barrel diameter by enlarging it to 24 strands. They added a β-hairpin and a loop copied from first two N-terminal strands, thus increasing the channel area by 16 percent. They also removed the plug domain. Muhammad et al.[61] increased the height of the barrel to improve hydrophobic matching with a block copolymer membrane. The hydrophobic region was lengthened by 1 nm by copying the last five amino acids of each strand. A constraint is reconstitution; the barrel must match the *E. coli* membrane thickness well enough that the protein can insert and be properly folded in *E. coli*. Mohammad et al.[62] shortened some extracellular loops and removed the plug domain.

β-barrels have a variety of cross-sectional shapes.[39] Zeth and Thein[51] point out that bacterial porins are oval and mitochondrial porins are nearly circular, even though their sizes are very similar. Scalable membrane probes ought to be circular, rigid, and nonporous. These criteria can be met by the choice of interior residues, loops, and segments folding into pore. Many examples useful in engineering the shape are available in nature, and likewise examples of loops and terminal domains that act as plugs.

In summary it appears that β-barrels can be made into scalable tracers, made by scalable chemistry – just add a DNA sequence. The design problem is more the barrel-head than the barrel.

Giant β-Barrels: Structure

Nature provides an interesting variety of examples of larger β-barrel structures,[45] but they are less readily scalable than small β-barrels. The best-understood group of giant β-barrels is the β-pore forming toxins.[32,33] One example is *Staphylococcus aureus* α-hemolysin, a self-assembled heptamer. The assembled pore is mushroom-shaped, with a 14-strand β-barrel stalk and a hydrophilic head. The stalk diameter is 2.6 nm and the head diameter is 10 nm. The X-ray structure shows extensive contacts between the monomers.[63] Aerolysin has a similar structure, a heptamer giving a mushroom-shaped pore with a stalk diameter of 4.6 nm and a head diameter of 14.0 nm.[33] Another prominent class of giant β-barrels is the cholesterol-dependent cytolysins, such as pneumolysin, streptolysin, and perfringolysin O, reviewed by Tweten[64]. The structure of pneumolysin was determined by cryo electron microscopy.[65] The pore is made up of $\sim$ 40 monomers, each contributing two β-hairpins, so 4 antiparallel β-strands and a total of $\sim$ 160 β-strands. The actual number of monomers varied, with peaks at 38 and 44. Diameters ranged from 32 to 43 nm. The other main group of giant β-barrels, the MACPF proteins – membrane attack complex, perforin – is reviewed by Dunstone and Tweten[66].

Giant β-Barrels: Constraints

The giant β-barrels have the advantage of large size but they are much less easily scalable than small β-barrels. The problem is the unscalable chemistry. One needs to be able to vary the size readily without having to redesign much of the protein.

The question of stoichiometry must be examined for each protein. Variable stoichiometry is common.[32] A cholesterol-dependent cytolysin may have between 30 and 50 monomers per pore, so the resulting variation in radius must be taken into account. The range of variation is limited; to go outside these limits would require considerable redesign of the monomer.

Another limitation is that the giant β-barrels involve too much biology themselves to be convenient probes of other biology. An essential feature is that a water-soluble protein must be converted to a membrane-bound form. In some proteins, monomers require proteolytic activation before assembly can occur. In general, membrane insertion and self-assembly are required; the order depends on the protein. Particular membrane components may be required for insertion, such as a GPI-linked membrane protein for aerolysin, or cholesterol for the cholesterol-dependent cytolysins. Some self-assembly is required, so if the cell is perturbed in an experiment, one must verify that the tracer is not affected.

Wanted: Scalable Tracers for Diffusion Measurements

Supporting Information 2
Candidate Species: Spherical Tracers

Michael J. Saxton

Department of Biochemistry and Molecular Medicine, University of California, One Shields
Ave., Davis, California 95616
E-mail: mjsaxton@ucdavis.edu
Phone: (530) 752-6163. Fax: (530) 752-3516

Here we consider candidate spherical tracers for 3D aqueous systems such as the cytoplasm and the nucleus. We discuss in detail lipid droplets, quantum dots and various types of fluorescent beads. We discuss briefly some interesting exotic fluorophores, and gold beads used as point scatterers in some SPT experiments.

Diffusion in cells may depend on how the label is introduced. Hale et al.[67] pointed out that endocytosed beads measure mechanics along the endocytotic pathway, which involves motor proteins, but microinjected or bombarded beads measure the mechanics of the cytoplasm. Similarly Duits et al.[68] made SPT measurements on particles in the cytoplasm of human microvascular endothelial cells (Hmec-1) and found that ballistically injected beads behaved differently from endogenous granules, which were identified as lipid droplets and mitochondria by their staining.

Some of the candidate tracers are colloidal particles, so anyone considering high-precision measurements ought to read the recent reviews on the pitfalls in measuring radii and volume fractions of colloids, and in preparing hard-sphere colloids.[69,70]

Core-shell structures are standard in quantum dots but can be used with other bead structures to adjust particle size, provide attachment points for covalent linkages, and modify surface properties. See the highly informative review of core-shell structures by Schärtl[71].

Preventing aggregation of colloidal tracers is of particular importance. This is usually done by Coulomb repulsion or by attaching free chains to the surface to give entropic repulsion ("hairy sphere"). Charge would be a complication here and entropic repulsion is preferable. See the discussion of the DLVO and hairy sphere interactions in Supporting Information 5. For example, poly(methylmethacrylate) beads were coated with poly(12-hydroxystearic acid) to prevent aggregation.[72] Nanoparticles of diameter 15–20 nm were prepared with a fluorescent polystyrene core and a shell of dendrons.[73] Similarly, glycopolymers were chemically grafted to polymer nanoparticles,[74,75] and enzymatic synthesis of hyperbranched oligosaccharide was used to form a coating ("artificial glycocalyx") on a silicon surface.[76]

Self-Assembled Amphiphiles: Lipid Droplets

Lipid droplets are the 3D analog of lipid domains in membranes. The droplets occur naturally in cells. They have a high refractive index compared to cytoplasm so they are detectable in SPT without labeling. They are often used in the physics literature[77–81] for SPT measurements of diffusion in cytoplasm, or for laser tweezer measurements of viscosity. The droplets consist of neutral lipids, mostly triacylglycerols and sterol esters, surrounded by a phospholipid monolayer. Proteins are associated with the droplets. The diameters are nonuniform, in the range 0.1 – 5 μm, so the size of each particle must be measured along with its diffusion coefficient. In adipocytes the lipid droplets may be much larger, around 100 μm.

It is essential to remember, however, that lipid droplets are not just inert droplets of fat, but "an organelle that is dynamic, fully engaged with the biology of the cell, and actively involved in a diversity of cellular processes" as the review of Saka and Valdivia[82] puts it. This review discusses topics such as the assembly of hepatitis C viruses on lipid droplets, and lipid droplets as modulators of immune response. Furthermore, there are enough droplet-associated proteins to warrant proteomic studies. The presence of a phospholipid monolayer rather than a bilayer constrains the structure of associated proteins.[83] Lipid droplets can be transported by motor proteins, as discussed in the review of Fujimoto and Parton[84]. In addition, the surface proteins might lead to transient binding of lipid droplets to immobile structures in cells.

Artifical lipid droplet analogs have been made by microinjection of fluorescent-labeled soybean oil into sea urchin egg cytoplasm.[85] The fluorescent lipid analog spread from the droplet to the endoplasmic reticulum but not to other organelles. This experiment was important as a demonstration of the continuity of the endoplasmic reticulum membrane, but for our purposes it implies that the oil droplets must be stabilized if they are to be used as scalable tracers. It would be interesting to examine what cellular species partition into the droplets.

Quantum Dots

The favorable fluorescence properties of quantum dots (semiconductor nanocrystals) are well known. The absorption peak is broad and the absorption cross-section is large. The emission band is narrow, and the peak is tunable by the choice of quantum dot size. There are many recent reviews, including applications to cell biology[86] and engineering the semiconductor bandgap to control optical properties.[87]

Several layers are used to make standard quantum dots and these layers enlarge the quantum dot significantly. The core is surrounded by an inorganic shell (for example CdSe surrounded by CdS) to passivate surface trapping sites and to isolate the core from the environment. (The shell is part of the quantum mechanics, the edge for the particle-in-a-spherical-box.) Next is a hydrophilic layer, and finally whatever antibodies or ligands are needed to attach the quantum dot to its target. Small core-shell quantum dots can be made by proper choice of the organic layer bound to the outer shell; Howarth et al.[88] made quantum dots of hydrodynamic diameter 11.1 nm compared to 20–30 nm for commercial quantum dots.

The main limitation on the use of quantum dots is blinking, that is, random transitions to dark states that can have very long lifetimes. Blinking can be diminished by several approaches: the use of antioxidants such as β-mercaptoethanol in the medium,[89,90] engineering the potential at the core-shell interface,[91] and the use of thick shells. For example, Mahler et al.[92] used a CdSe core 2.5 nm in diameter with a CdS shell 5 nm thick. Chen et al.[93] made somewhat larger core-shell structures, with 18–19 successive monolayers of CdS on a CdSe core, to a total diameter of 15–20 nm. The monolayer thickness

of CdS is around 0.34 nm. Chen et al.[93] used the so-called SILAR technique, successive ion layer absorption and reaction,[94] to build up the shell one monolayer at a time.

One could thus make a series with constant core size and various shell thicknesses. For example, Brovelli et al.[95] grew quantum dots with a fixed CdSe core of radius 1.5 nm and CdS shells of 4, 7, 14, and 19 monolayers. The growth of thick shells and their effects on emission have been studied in detail.[96,97] At a fundamental level, recent work using electrochemical charge injection showed two distinct mechanisms of blinking.[98]

One could also make a series with various core sizes and constant total diameter, so that the color of the fluorescence can be used to connect individual SPT images into trajectories. The Lagerholm group[99] distinguished four different colors of quantum dots in the same field by using a beam splitter, dichroic mirrors, and filters. The Lidke group[100] developed a high-speed hyperspectral line-scanning microscope that resolved eight different colors of quantum dots.

In addition to core-shell quantum dots, one could make null quantum dots, with inert shells only and no fluorescent cores. These could be used in model fluid experiments to give a low concentration of fluorescent spheres and a high concentration of otherwise identical nonfluorescent spheres.

Standard biochemical separation techniques may be useful in preparing quantum dots. Analytical ultracentrifugation has been used to find the size distribution and surface properties of quantum dots[101] as well as stoichiometric gold nanoclusters.[102] For quantum dots linked to biological targeting molecules, gel electrophoresis has been used to select quantum dots of defined valency.[88,103,104]

Fluorescent Beads: Organic and Inorganic

Fluorescent beads have several favorable properties. There are many fluorophores per particle. Photobleaching is reduced because the fluorophores are shielded from molecular oxygen. Fluorescence quenching is reduced because the dye is less mobile and the environment is more rigid. A potential disadvantage is stickiness; the outermost layer must be chosen appropriately. The most commonly used fluorescent beads are based on colloidal silica, polystyrene, or poly(methylmethacrylate) (PMMA). Fluorophores may be incorporated by adsorption, covalent linkage to a precursor, or covalent linkage after particle preparation. Covalent linkage is preferable unless a core-shell structure is used and the adsorbed fluorophore is sealed in the core by the shell. Fluorescent beads are reviewed briefly by Pellach et al.[105] and in more detail by Burns et al.[106], Sokolova and Epple[107], and Hermanson[108].

Van der Waals forces can be suppressed by refractive index matching, which in most cases requires organic solvent mixtures. Index matching also eliminates light scattering, and sedimentation is suppressed if the solvents are chosen to match the particle density.[109] Caveats regarding index matching are given by Royall et al.[70]

Core-shell structures have uses beyond shielding the fluorophore and increasing the particle size. Titania has a high refractive index, and the high refractive index contrast to the medium makes it well suited to laser tweezer experiments. Demirörs et al.[110] described a general method to coat colloidal particles – silica, silver, polystyrene – with a titania shell with a thickness adjustable between 10–250 nm. The core-shell particles were monodisperse. Viravathana and Marr[111] made silica-coated titania particles so that the solvent could be index-matched to the silica shell to suppress van der Waals interactions and the titania core would allow laser tweezer experiments.

Commercial. A size series of fluorescent beads is the best set of scalable tracers commercially available, assuming that the proprietary chemistry is constant. The smallest ones seem to be 20–50 nm diameter and the largest, 5–25 μm, depending on the supplier.

It would be useful to extend the series to smaller beads and to characterize how spherical and deformable the smaller beads are. Around 5 nm diameter, one needs to begin to consider the actual number of monomers and crosslinks in the sphere, at least at the level of simple calculations that assume that all crosslinkers in the reaction mixture are incorporated into the polymer. Nunes and Asua[112] presented a strategy for nanolatex synthesis and prepared PMMA nanoparticles down to a diameter of 13 nm.

Homemade. The van Blaaderen group has long been active in preparing fluorescent nanospheres, in part in order to use mixtures of fluorescent and nonfluorescent nanospheres as a model fluid or glass in which individual particles can be observed by confocal microscopy.[109,113] For example, the group prepared monodisperse core-shell ZnS-silica and silica-ZnS particles with diameters in the range of 0.16–2.8 μm,[114] and monodisperse fluorescent core-shell PMMA particles[115] with diameters in the range of 0.35–1.3 μm. Recent work[116] reports the synthesis of monodisperse, highly crosslinked PMMA particles containing various fluorophores including NBD and rhodamine derivatives. Particles were either homogeneous or core-shell with the shell fluorescent. Diameters were varied between 1–2 μm. Nanosphere tracers for model fluid and glass experiments are usually made large enough that they can be resolved readily by optical microscopy. Smaller diameters would be useful for measurements in cells.

The Bräuchle laboratory prepared various perylene-labeled silica nanoparticles to take advantage of the high photostability of perylenes. A monofunctional perylene derivative plus silica gave a sphere 80 nm in diameter. The spectrum was solvent-dependent, indicating that the dye was at the surface. Another type of nanoparticle, diameter 30–100 nm, had a 10–30 nm polysiloxane core containing the dye, and a nonfluorescent silica shell. The spectrum was not solvent-dependent.[117]

One of the most promising families of scalable tracers is silica core-shell particles.[118,119] These tracers are brightly fluorescent silica nanoparticles, monodisperse with diameter 30 nm, and are more photostable than the original dye. They are prepared by first covalently attaching a small organic dye such as FITC, TRITC, or various Alexa dyes to 3-aminopropyltriethoxysilane to make the core precursor. Then the core is made by a condensation reaction that includes this precursor. Finally, the shell is grown using unlabeled tetraethylorthosilicate. Both core-shell and homogeneously labeled particles were made. The size can be varied; the review of Burns et al.[106] shows scanning electron micrographs of core-shell particles of diameters 50, 150, 250, 500, and 1500 nm, and later work[120] gave diameters 3.3 and 6.0 nm.

Ultrabright fluorescent silica particles, diameter 40 nm, have been prepared using hydrophobic groups in the matrix to retain the Rhodamine 6G fluorophore[121] though these were not core-shell structures.

Exotic (for now)

Nanodiamonds, particulaly the negatively charged nitrogen vacancy center, have favorable fluorescence properties.[122,123] Fluorescent metal nanoclusters are highly photostable but the quantum yields are often low[124] except for the dendrimer-gold complexes mentioned in the section on dendrimers, or in the case of two-photon excitation.[125] All these would require development of a shell layer to adjust the size. See Graf et al.[126] for a method of silica encapsulation of colloidal particles including gold, silver, and polystyrene.

Gold Bead Scatterers

Colloidal gold is a strong light scatterer so it has long been used as an unbleachable label in SPT (that is, a point source of darkness). A typical diameter is 30–40 nm. The diameter d is much less than the wavelength of light, so Rayleigh scattering occurs and the scattering is proportional to d^6. Colloidal gold is inherently scalable except for the detectability limits set by the d^6 dependence. The area has been reviewed by De Brabander et al.[127] and by Kusumi et al.[128]

Wanted: Scalable Tracers for Diffusion Measurements

Supporting Information 3
Candidate Species: Globular Proteins

Michael J. Saxton

Department of Biochemistry and Molecular Medicine,
University of California, One Shields
Ave., Davis, California 95616
E-mail: mjsaxton@ucdavis.edu
Phone: (530) 752-6163. Fax: (530) 752-3516

Calculations of D

Diffusion measurements in aqueous media often use a variety of globular proteins as tracers. The basic size effect is given by the Stokes-Einstein equation for a spherical particle in dilute solution

$$D = kT/6\pi\eta R(hydro) \quad \text{(S1)}$$

where kT is the thermal energy, η is the viscosity, and $R(hydro)$ is the hydrodynamic radius. One method to account for tracer geometry is to assume that the protein is an ellipsoid of revolution and to apply the standard Perrin corrections.[129,130] A more refined approach is based on the actual molecular structure. Garcia de la Torre and collaborators have published programs to calculate hydrodynamic properties from atomic coordinates by means of atomic-level bead shells, residue-level beads, or residue-level bead shells.[131,132] The alternative approach of Aragon[133] represents the surface as a triangulation. Both procedures have been well tested. The thickness of the solvation shell is important in these calculations, and the values used in the different methods agree well. These algorithms make it possible to calculate diffusion coefficients at the small-proteome scale.

Large-Scale Compilations of D

One widely-used set of experimental biochemical diffusion coefficients is the compilation of Tyn and Gusek[134]. They used the Stokes-Einstein relation and took the hydrodynamic radius be directly proportional to the experimental $R(gyr)$, in most cases obtained from small-angle X-ray scattering. These are literature values so the values of both D and M_r reflect differences among methods and laboratories. We examine this data set in detail in the next section.

Dill et al.[135] obtained a distribution of D's for cell proteins based on a scaling relation for the radius, $R(scaling) \propto N^{0.392}$, with N the number of amino acid residues.[136] The rest of the calculation is standard, based on the Stokes-Einstein equation with $R(hydro) \propto R(scaling)$ and the proportionality constant of Tyn and Gusek[134]. The plot of D versus $\log N$ of Dill et al.[135] based on the Tyn-Gusek data set gives more confidence about the usefulness of the correlation than the original plot of $\log D$ versus $\log N$ does. From this and other data Dill et al.[135] argued that the observed protein density in cells maximizes biochemical reaction rates.

McGuffee and Elcock[137] carried out inspiringly comprehensive Brownian dynamics simulations on a 51-component model of *E. coli* cytoplasm, with macromolecular shapes from atomic-level structures and concentrations approaching those in vivo. They used two models, "steric" with repulsive forces only, and "full" including approximate electrostatic and hydrophobic interactions. Input to the simulations included infinite-dilution diffusion coefficients from the bead model of García de la Torre et al.[131] A single global interaction parameter was adjusted to match the simulated diffusion coefficient of GFP to experiment. Effects of crowding on diffusion and anomalous subdiffusion were examined in detail.

Recent work by Kalwarczyk et al.[138] found D for the entire proteome of *E. coli* in cytoplasm. Diffusion coefficients in dilute solution were obtained from the Stokes-Einstein equation using the scaling relation of Dill et al.[135] for the hydrodynamic radius of proteins and similar power laws for RNA and DNA. The main objective of this work was to represent diffusion in complex fluids in terms of the authors' "scale-dependent viscosity reference curve," which interpolates smoothly between microscopic and macroscopic viscosity. This curve is fit to a small number of experimental values of D for each complex fluid, such as the cytoplasm of a given cell type. Their results are consistent with the "full" case in the simulations of McGuffee and Elcock[137] for sizes < 6 nm. But most of the data points are in the range $R(hydro) = 2--6$ nm. There is significant scatter in their plot of D versus $R(hydro)$, and the plot is of $\ln D$, not D. Few data points are available for most of their curve, a limitation they note. Scalable tracers would be well suited to generating their reference curve for a particular cell type. A wide range of sizes is needed; as Kalwarczyk et al.[138] point out, tracer sizes should be uniformly distributed on a logarithmic scale, say 0.1–300 nm. Nonscalable tracers would be used to find the scatter in D due to shape, surface properties, etc. Both the mean and the variation are potentially important in cell-level simulations.

The FRAP measurements of Kumar et al.[139] on proteins in *E. coli* are noteworthy for the number and variety of proteins examined, both cytoplasmic and transmembrane, enabling the authors to evaluate the size dependence, though neither series of proteins was scalable. A strength of this data set is that all the diffusion coefficients were obtained using essentially the same methods of experiment and analysis. Importantly, measurements on eYFP were included; this permits cross-calibration of their results with other laboratories. Experimentalists ought to adopt one of the intrinsically fluorescent proteins as a calibration standard. But Nenninger et al.[140] found much less sensitivity to size in their diffusion measurements of GFP multimers in *E. coli* cytoplasm. They found that D followed the Stokes-Einstein equation for monomers through tetramers (27–111 kDa), but was significantly lower for pentamers, possibly due to size-related obstruction. Nenninger et al.[140] suggested that the greater size dependence found by Kumar et al.[139] was due to specific interactions.

How Good Are the Predicted D's?

Are the usual set of nonscalable proteins good enough, or is it necessary to make a set of scalable tracers? Here we examine the data of Tyn and Gusek and some more recent data sets. It is far beyond the scope of this work to systematically update and extend the Tyn-Gusek data set, and a detailed examination of some of that data seems more antiquarian than scientific. But some useful points can be made without a full review.

Tyn and Gusek[134] presented a log-log plot of calculated D versus observed D for 198 data points – proteins, DNA,

RNA, and viruses – ranging from ribonuclease, 12640 Da, to tobacco mosaic virus, 50 MDa. Fig. S1 *a* shows the Tyn-Gusek data set as a log-log plot of observed D versus M_r. The obviously fibrous species are marked: flagellin,[141] meromyosin, collagen, fibrinogen, myosin, RNA, and DNA. Viruses (including phages) are also marked. The line is a power-law approximation

$$D = 465.9/M_r^{0.392} \tag{S2}$$

with D in units of 10^{-7} cm^2/s and M_r in Da, calculated as in Dill et al.[135] The exponent is fixed at the value obtained by Hong and Lei[136] and the coefficient is from a least-squares fit to the entire Tyn-Gusek data set. The viruses follow approximately the same power-law dependence as the globular proteins because most of the viruses are isometric, that is, practically spherical. Phage lambda is approximately spherical because the measurements were on the head alone. Alfalfa mosaic virus is bacilliform, that is, rod-shaped with hemispherical ends. Several forms of this virus are known; the most asymmetric is the B form, with a length/diameter ratio of 3.1. The one geometrically extreme virus is tobacco mosaic virus, a cylinder with a length/diameter ratio of 16.7. Convenient websites for data on virus structures are Descriptions of Plant Viruses (www.dpvweb.net)[142] and VIPERdb (viperdb.scripps.edu).[143]

Most of the outliers are fibrous. The remaining outliers are the "aggregated" and "less aggregated" forms of β-casein; β-casein is known to form micelles.[144] One data point for γ globulin has a M_r similar to the four other values but a D around half that of the others. Both M_r and D for *E. coli* ribosomal 4S protein are seriously in error[145] but the corrected point is still within the globular protein cloud.

Fig. S1 *b* shows a plot of $\log D$ versus $\log M_r$ for an expanded data set, and Fig. S1 *c* shows the same data as a linear plot of D versus $\log M_r$. The plot includes the Tyn-Gusek values for globular proteins and viruses, and a variety of other data sets on globular proteins from the literature. Data points for various proteins are from the simulation papers of García de la Torre et al.[131], Aragon and Hahn[146], and Brookes et al.[147] Experimental data are shown but the simulations reproduce the data well. Experimental results for a set of large proteins and complexes (from urease, 480 kDa, to 70S ribosomes, 2.5 MDa) are also shown.[132] The full data sets from these references are shown; duplicates have not been purged. In addition, the simulation results of McGuffee and Elcock[137] for soluble proteins and ribosomes of *E. coli* are included. In view of the scatter in the Tyn-Gusek values for tobacco mosaic virus, recent values are included with the modern value of the M_r, and the observed range of D as pH and ionic strength are varied.[154] A recent value for eGFP is included as a reference point.[155]

The lines are power-law approximations. Eqn. S2 is a fit to the entire Tyn-Gusek data set, and Eqn. S3 is the corresponding fit to the globular protein subset of the Tyn-Gusek data, with the same fixed exponent,

$$D = 494.5/M_r^{0.392} \tag{S3}$$

to show that leaving out the viruses and the fibrous species has little effect. The Stokes-Einstein D, slope $-1/3$, is also included because the slope of the cloud of data points seems to lessen at large M_r.

Fig. S1 *b,c* show what might be called the "globular biomolecule cloud," in which a wide variety of compact biomolecules – globular proteins, protein complexes, and viruses – fall into a consistent cloud of points, approximated by a power-law relation. The width of the cloud reflects scatter due to the nonscalability of a large assortment of globular proteins, combined with experimental scatter. There is scatter in D due to differences in techniques, calibration, pH, ionic strength, etc., nicely described in a review paragraph in a modeling paper by Durchschlag and Zipper[156]. The values of the M_r are a surprisingly large source of scatter in the older (pregenomics) literature. Sometimes in the Tyn-Gusek data set, entries for single substance have the same D and differ only in M_r. For viruses the variation in M_r may reflect the difference between capsids and intact viruses. Statements in the older literature about fibrous versus globular structures need to be reexamined in light of current understanding of quaternary structures, as in the cases of α-crystallin[157] and α_2-macroglobulin.[158]

An updated version of the Tyn-Gusek data set would be needed to examine the dependence of D on M_r and shape systematically. The results might be of limited usefulness now that simulations can give good values of solution properties for proteins of known structure.

Some biomolecules – linear or branched random coils – are clearly outside the globular protein cloud. Fig. S1 *d* shows the merged globular protein data of Fig. S1 *b*, plus current results for DNA, and fractionated heparin, pullulan, and dextran. For references see the caption.

The old Tyn-Gusek DNA data is consistent with current DNA data, but the DNA size is precisely controlled in the current work. Robertson et al.[148] chose large DNA, 5900 to 287000 base pairs, 2.65–129 μm, so a minimum of $\sim$ 50 persistence lengths, and the exponent is equal to the value for a self-avoiding chain in a good solvent. The data set assembled from the literature by Amorós et al.[149] includes much shorter chains so there is a wide range of ratios of DNA length to persistence length, and the overall power-law fit is less interpretable.

The simplest way to understand this data is in terms of Flory-Huggins solvent types.[159,160] Table S1 gives values of the exponent ν in

$$R(hydro) \propto R(gyr) \propto N^{\nu} \tag{S4}$$

where N is the number of monomers, and $D \propto 1/R(hydro)$. Values of ν are also discussed in Supporting Information 4.

The exponent for globular proteins is 0.392, close to the Flory value of 1/3 for a poor solvent. That is, water is a poor solvent for (the hydrophobic interiors of) globu-

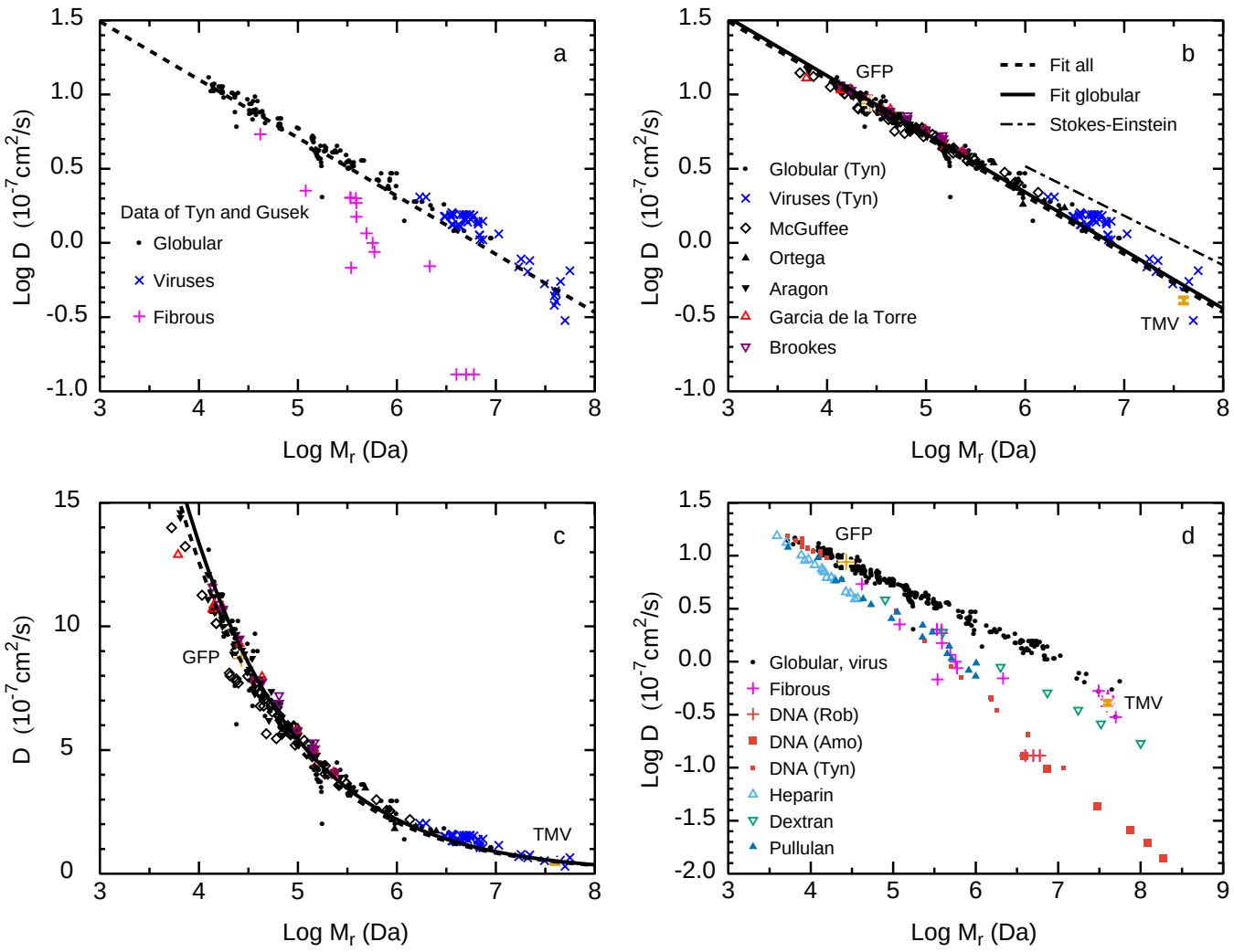

Figure S1. Diffusion coefficients as a function of $\log M_r$. Units: D in 10^{-7} cm^2/s, M_r in Da. *(a)* $\log D$ versus $\log M_r$ for the data set of Tyn and Gusek [134], separated into globular proteins, fibrous proteins as discussed in the text, and viruses including phages. The dashed line is Eqn. S2. *(b)* The cloud of globular biomolecules in a logarithmic plot. Log D versus $\log M_r$ for the Tyn-Gusek set of globular proteins, protein complexes, and viruses, along with simulated D's for *E. coli* proteins obtained by McGuffee and Elcock [137], and the entire experimental data sets used in the simulations of Ortega et al. [132], Aragon and Hahn [146], García de la Torre et al. [131], and Brookes et al. [147] Values for GFP and tobacco mosaic virus are also shown, as described in the text. The lines are power-law relations: Eqn. S2, Eqn. S3, and the Stokes-Einstein curve for large particles. Units: D in 10^{-7} cm^2/s, M_r in Da. *(c)* The cloud of globular biomolecules in a linear plot. D versus $\log M_r$ for the same data as in panel *(b)*, with the same power-law equations. *(d)* Random coils are distinct from the globular protein cloud. Log D versus $\log M_r$ for the globular proteins and the viruses in panel *(b)*. Note the change in scale from panels *(a)* and *(b)*. Values for GFP and tobacco mosaic virus are also shown, as described in the text. For comparison, data are shown for DNA from Robertson et al. [148], Amorós et al. [149], and Tyn and Gusek [134], and for the carbohydrates heparin, [150] pullulan, [151–153] and dextran. [152]

Table S1. Flory exponents ν

Theory **Solvent**	ν	
Poor solvent	0.333	
Theta solvent	0.5	
Self-avoiding chain in good solvent	0.588	
Good solvent	0.6	
Experiment **Species**	ν	
Globular proteins	0.392	[135,136]
Unfolded proteins	0.57 ± 0.02	[161]
Unfolded proteins	0.598 ± 0.028	[162]
DNA	0.589 ± 0.018	[148]
DNA	0.68	Fit to [149]
Heparin	0.62 ± 0.01	[150]
Pullulan	0.542	[152]
Pullulan	0.51	[151,153]
Dextran	0.441 at 25 C	[152]

lar proteins. Exponents for the linear carbohydrates are in the theta-solvent to good-solvent range. Nordmeier [152] attributed the low exponent of dextran to branching but the dextrans used in these experiments were 80 kDa to 100 MDa, and branching is considered important only for sizes > 100 kDa.[163] Experimental results for unfolded (chemically denatured) proteins are also included in the table. The exponents are close to the theoretical value for a self-avoiding chain in a good solvent.[161,162]

To summarize, one can find a reasonable estimate of $\log D$ for a globular protein just from the M_r. Is this good enough? It depends on the use. To analyze global properties of a generic cell [135], the estimates are certainly good enough. To analyze reaction kinetics in dilute solution, the estimates are good enough that the uncertainties can be treated by the usual analysis of propagation of errors. But in work on a crowded or inhomogeneous system, better values might be advantageous, and to determine the percolation threshold of cytoplasm, a series of scalable tracers would be essential.

Radius of Gyration Tensor

Quantitative measures of shape are needed to characterize a set of tracers and determine how similar their shapes are. Descriptors based on the radius of gyration tensor are convenient for known structures. Two sets of descriptors are commonly used. In one, all the descriptors are dimensional.[164] We use the other, in which $R(gyr)$ is dimensional but the other two shape parameters are dimensionless.[165]

The radius of gyration tensor (strictly, the moment of inertia tensor because mass weighting is used) is defined as

$$T = \begin{pmatrix} \langle x^2 \rangle & \langle xy \rangle & \langle xz \rangle \\ \langle xy \rangle & \langle y^2 \rangle & \langle yz \rangle \\ \langle xz \rangle & \langle yz \rangle & \langle z^2 \rangle \end{pmatrix} \tag{S5}$$

where the origin is at the center of mass, and the averages are defined as, for example

$$\langle xy \rangle = \frac{1}{M} \sum_i m_i x_i y_i, \tag{S6}$$

where m_i is the mass of the ith atom, M is the total mass, and the sum is over atoms. The eigenvalues of T are $\lambda_x \geq \lambda_y \geq \lambda_z$. The radius of gyration is given by the trace

$$R^2(gyr) = \mathrm{Tr}\ T = \lambda_x + \lambda_y + \lambda_z \tag{S7}$$

and the mean eigenvalue is

$$\bar{\lambda} = \mathrm{Tr}\ T/3. \tag{S8}$$

The asphericity Δ is defined as

$$\Delta = \frac{3}{2} \sum_{i=1}^{3} (\lambda_i - \bar{\lambda})^2 / (\mathrm{Tr}\ T)^2. \tag{S9}$$

It measures anisotropy, and ranges from 0 for a sphere to 1 for a rod. The shape parameter S is defined as

$$S = 27 \prod_{i=1}^{3} (\lambda_i - \bar{\lambda}) / (\mathrm{Tr}\ T)^3. \tag{S10}$$

It is negative for an oblate sphere and positive for a prolate. The range is [-1/4, 2].

Distributions of these shape parameters are given for a large, carefully chosen set of soluble proteins by Dima and Thirumalai [165]. They used PDBSelect [166] to obtain an independent subset of proteins with at most 25% similarity in sequences, and then they limited the subset to nonmembrane proteins with structures meeting specified completeness requirements. A total of 1177 proteins was used. This degree of care would be useful in work on D as a function of M_r.

Proteins in Text Fig. 1

Table S2 shows properties of the ten globular protein tracers for which the structures are shown in text Fig. 1.

The mass and the number of amino acid residues are as given by the PDB (Protein Data Base) web site. Values of the radius of gyration, asphericity, and shape parameters are calculated from the PDB files, with hydrogen atoms added using the NIDDK PDB Utility Server. These calculations are done in Mathematica, using the definitions in the previous section. Atoms are weighted by mass. The current version of Mathematica can parse standard PDB files but not some modified files (a single chain selected in Rasmol, for example), so all the files were parsed using Linux utilities. Asterisks indicate modifications from the PDB files as downloaded to select a single chain (1OVA, 4F5S) or to form the tetramer (1HHO). In these cases the coordinates are used as obtained, with no relaxation step for the interface. No hydrogen atoms were added for 1MFR.

Does the asymmetry illustrated in text Fig. 1 and quantified in Table S2 matter? Usually the tracers are assumed to be effectively spherical on account of fast rotational diffusion. For 3D diffusion of a sphere of radius a, the translational and rotational diffusion coefficients are [129]

$$\begin{aligned} D(trans) &= kT/6\pi\eta a \quad \text{in units of length}^2/\text{time} \\ D(rot) &= kT/8\pi\eta a^3 \ \text{ in units of radian}^2/\text{time} \end{aligned} \tag{S11}$$

and the characteristic times are

$$\begin{aligned} \tau(trans) &= \ell^2/6D(trans) \ \text{ for a distance } \ell \\ \tau(rot) &= 1/6D(rot) \qquad \text{for an angle 1 rad.} \end{aligned} \tag{S12}$$

So the times for translation over one radius and rotation over one radian are of the same magnitude,

$$\begin{aligned} \tau(trans) &= \quad \pi\eta a^3/kT \\ \tau(rot) &= (4/3)\pi\eta a^3/kT. \end{aligned} \tag{S13}$$

The reason the correlation times are often of much different magnitudes is that FCS or FRAP measurements of translational diffusion are on the length scale of the wavelength of light, not the particle size. A similar argument holds in the 2D case; see Saffman and Delbrück [167] for the translational and rotational mobilities. So in many diffusion measurements the asymmetry is averaged out. But as the time resolution of SPT experiments is improved, the averaging decreases, and in the cell, patchy specific interactions may be important.

Table S2. Globular protein properties

Protein	PDB ID	State	N	Mass Da	$R(gyr)$ nm	Δ	S
Cytochrome C	5CYT	monomer	104	12032.70	1.246	0.0421	0.0004
Lysozyme	6LYZ	monomer	129	14331.20	1.399	0.1235	0.0826
Myoglobin, oxy	1MBO	monomer	153	17979.65	1.522	0.0834	-0.0296
eGFP	2Y0G	monomer	252	28569.40	1.695	0.0912	0.0479
Peroxidase	1H5D	monomer	308	34704.10	1.900	0.1370	0.0962
Ovalbumin	1OVA*	chain A	386	43109.53	2.185	0.2222	0.2075
Chymotrypsinogen	2CGA	homodimer	490	51372.40	2.484	0.2939	0.3138
Hemoglobin	1HHO*	heterotetramer	574	64865.94	2.313	0.0370	0.0139
BSA	4F5S*	chain A	587	66637.69	2.678	0.0745	-0.0264
Ferritin	1MFR	homo-24-mer	4224	496125.86	5.298	0.0000	0.0000

Candidates

It would be useful to build a scalable series of tracers to serve as a probe of complex systems such as the cell, or the pores in a kidney. This would be a nonstandard challenge for designers of de novo proteins, to build a scalable series of generic globular proteins with minimal binding to naturally occurring proteins. Instead of starting with a scaffold and adding functionality, the problem is to make a scalable series of scaffolds. Blaber and Lee[168] provide an interesting discussion of bottom-up versus top-down protein design. The detailed design of scalable soluble proteins is beyond the scope of this review, but I will point out the requirements and describe a few examples to argue for feasibility.

One approach is to make proteins with a string of linked α-helices, with hydrophobic surfaces chosen to drive folding into parallel helices, possibly with disulfide bonds to stiffen the linkages between helices. The length of the α-helices could be varied to make the final structure more spherical than disk-shaped. The preparation of this series of tracers would be relatively scalable. This approach would extend current work on protein maquettes, that is, functional synthetic proteins simpler than the biological forms. Much work has been done on adding biochemical functionality to bundles of four α-helices.[169–172] Here a series of bundles of different sizes is needed, designed to avoid biochemical functionality.

Another approach is based on β-barrel or α/β proteins. Soluble β-barrels with a hydrophilic exterior include proteins as prominent as chymotrypsin, strepavidin, and green fluorescent protein, but the size is only 6–8 strands. Pure β-barrels are reviewed by Flower et al.[173] in terms of the calcyin structural superfamily, which is a group of proteins with closely related structures but little similarity in sequence. This superfamily includes lipocalins, which are usually 8-stranded with a few 6-stranded; avidin and metalloprotease inhibitors, which are 8-stranded and more circular in cross-section than lipocalins; and fatty acid binding proteins, which are 10-stranded. Lipocalins bind hydrophobic species; typically one end of the barrel is open and the other is plugged.[174] This structure suggests that one could engineer barrelheads in the ends to make the structure stiffer and with more circular, just as in transmembrane β-barrels. Synthetic analogs called anticalins have been prepared, though the emphasis is on obtaining selectivity via the loops at the open end, not on varying the barrel size.[175] Other β-barrels are the Greek key and jelly-roll structures.[176] A very common structure is the 8-stranded α/β barrel or TIM (triosephosphate isomerase) barrel; 10-stranded α/β barrels also occur.[176] A larger protein with mostly β-barrel structure is green fluorescent protein and its analogs, with 11 strands. Overall, the known examples of soluble β-barrels and α/β proteins cover a much smaller range of strand numbers than transmembrane β-barrels do.

A third approach would be to assemble the structures from small protein building blocks. This approach is successfully used in nature to make ferritins and viral capsids, for example, and in pioneering synthetic work to make nanostructures.[177] But the synthesis is not particularly scalable. Each size of tracer would require its own set of connections among building blocks, differing in angles.

Wanted: Scalable Tracers for Diffusion Measurements

Supporting Information 4
Candidate Species: Carbohydrates and Synthetic Polymers

Michael J. Saxton

Next we discuss carbohydrates and synthetic polymers. The organic fluorescent beads already considered are of course synthetic polymers but here we consider materials for which the standard analysis of polymer solution properties is useful.

Analysis

The diffusion properties of polymers are directly related to their size and branching so this section summarizes methods of characterization. Polymers are likely to be heterogeneous so the analysis is complicated, especially if branching occurs.

Traditional chemical analysis provides some information, particularly in the case of those polysaccharides for which highly specific enzymatic degradation can be used. Naessens et al. [178] reviewed chemical and biochemical approaches to dextran structure. NMR gives the fractions of branching points and terminal groups.

The standard approach to characterization is size exclusion chromatography (SEC) (also gel permeation chromatography, gel filtration chromatography) with multiple detection. The usual detection methods are differential refractometry, differential viscometry, multiangle (laser) light scattering photometry, and quasi-elastic light scattering. These methods yield solution properties as functions of elution volume. The refractive index measures concentration. Static and dynamic light scattering give the radius of gyration $R(gyr)$ and the hydrodynamic (Stokes) radius $R(hydro)$, and separate experiments give the thermodynamic radius from the second virial coefficient. The intrinsic viscosity gives the viscosity-averaged radius.

All the radii are expressed as power-law functions of the molecular mass M_r

$$R = KM_r^a \tag{S14}$$

where K and a are the Mark-Houwink parameters for each radius. For solid spheres, $a = 1/3$ and for $R(gyr)$ and $R(hydro)$ for random coils, $a = 0.5 - 0.6$. The intrinsic viscosity varies similarly, with $a = 0.5 - 0.8$. Branching is indicated by deviations from linearity in a log-log plot of radius versus M_r. The analysis is often complex because one must consider the particular average that each type of measurement yields (number, mass, viscosity, or z-average) and the effect of polydispersity on each of these averages. Rolland-Sabaté et al. [153] provide a convenient summary of the various radii, molecular masses, and power law relations, including tables of values for theoretical models and extensive experimental results for dextrans and other polysaccharides.

Deviations from the power law occur because SEC separates on the basis of hydrodynamic volume, not mass, so that there can be structural heterogeneity within a fraction of the same hydrodynamic volume. The heterogeneity can be resolved using temperature gradient interaction chromatography to bring in enthalpic factors, or multidimensional chromatography. Many reviews are available on special topics, including multiple detection,[153,179] branching,[180–182] temperature gradient interaction chromatography,[183,184] and universal calibration of SEC columns.[185,186]

Solvent quality is defined using the standard Flory-Huggins polymer model, in which solvent types differ in the exponent of the power-law relation between the polymer radius R and the number of monomers N. In a poor solvent, the monomer-monomer attraction is stronger than the solvent-monomer attraction, so the polymer tends to a compact conformation, with $R \propto N^{1/3}$ at low temperature. In a theta solvent, the solvent-monomer energetic attraction cancels the monomer-monomer excluded volume repulsion, and the polymer conformation is a random walk, with $R \propto N^{1/2}$. In a good solvent, the solvent-monomer attraction is stronger than monomer-monomer attraction so polymers tend to be in an extended conformation, with $R \propto N^{3/5}$ in the Flory approximation. An athermal solvent is a special case in which the monomer-monomer, solvent-monomer, and solvent-solvent interactions are equal, so energetic interactions have no effect and the conformation is purely a matter of entropy and excluded volume. The Flory-Huggins classification can be described formally in terms of excluded volume.[159,160]

Polysaccharide Structures

Polysaccharides may or may not be scalable in size. For some the size can be varied without varying the structure, but for others the degree of branching may vary with size or the diffusion mechanism may vary with environment.

Three classes of structures are considered: linear, branched, and hyperbranched. An important example of the linear class is pullulan, a nonionic, highly flexible polysaccharide that has been used as a calibration standard for SEC of polysaccharides.[181,187,188] Solution properties of pullulan and dextran are compared in detail by Nordmeier [152] and by Rolland-Sabaté et al. [189] Among branched polysaccharides, it is essential to distinguish between comb structures with many short side chains, and structures like dextran with some long chains. Experiments on various comb polysaccharides were reported by Stokke et al. [190] One example is schizophyllan, with a single-glucose side chain at every third backbone glucose. In solution, it forms a triple helix stabilized by hydrogen bonds. At the residue scale, schizophyllan is a comb but at the scale of a macromolecule in solution, it is linear. Dubin [191] recommended it as an SEC standard because it is one of the few stable nonionic helical polysaccharides, and the lack of charge is an advantage over DNA. Dubin suggested schizophyllan as a rodlike linear standard and pullulan as a flexible linear standard. The difference in flexibility is large. The persistence lengths for pullulan [192] were 1.4–3.1 nm for mass 100 kDa to 1 MDa but the values for schizophyllan [193,194] were in the 100–200 nm range. The branching structure of dextran is more complicated and is discussed in the next section. The final class of polysaccharide is hyperbranched, a random dendrimer-like structure discussed later in this Supporting Information.

Dextran

Dextrans[163,178] are commonly used as tracers and as crowders so they warrant a detailed review. Crude dextrans are large macromolecules (> MDa) obtained from fermentation of sucrose, commercially by the B-512F strain of *Leuconostoc mesenteroides*. Commercial dextrans are produced from the fermentation product by partial acid hydrolysis followed by fractional precipitation.

Structure. Dextran structure has been studied extensively by SEC-based methods but the branching topology is still incompletely understood. For standard commercial dextrans, a fair oversimplification for purposes of this review is as follows. Dextran is a $\alpha(1 \rightarrow 6)$ glucan with around 5% branching, but 85% of those branches are very short, only 1 or 2 glucose residues long, and chains that short have little effect on solution properties. The solution properties of dextrans are strongly influenced by a small fraction of long side chains, on the order of 50 residues. Naessens et al.[178] reviewed dextrans with other branching structures, not necessarily commercially available.

A widely accepted principle in dextran research is that solution properties are controlled by the small number of long branches, not the large number of short branches. But tracking down the evidence for this principle is not as simple as it might appear. One clear statement of the principle is in the experimental paper of Kuge et al.[195] analyzing branching by means of SEC and viscometry. Short chains "would give no appreciable contribution to the solution properties" on the basis of the arguments of Billmeyer[196]. A more complete and consistent treatment can be based on the results of Berry and Orofino[197] giving the contraction (or shrinking, or branching) factor g for comb polymers. Here g is defined as the ratio of the mean radius of gyration for the branched polymer to the mean radius of gyration for an unbranched polymer of the same M_r. Calculations of g assume that the backbone and side chains are pure random walks (that is, the polymer is in a theta solvent). Consider a regular comb polymer in which the repeating unit consists of a backbone segment and a single side chain. The key parameter is the ratio r of the side chain length to the distance along the backbone between branching points. For the side chains to have a significant effect, their length must be comparable to the separation of the branching points. Consider a polymer of length 100 repeating units. By definition $g = 1$ for $r = 0$. For short side chains, g is near 1, for example 0.909 for $r = 0.1$. But for $r = 1$, $g = 0.670$ and for $r = 2$, $g = 0.507$. For long polymers the value of g depends only weakly on the backbone length, so a length of 100 is representative. If $r = 1$, g varies by less than 1.5% when the backbone length is varied between 50 and 200 residues. An experimental complication for dextran is that the unbranched polysaccharide – the pure backbone without short chains – is not available. For workarounds see for example Ioan et al.[187]

Characterization. The evidence for the short chains is from chemical characterization and NMR.[198] The evidence for the long chains is from log-log plots of solution properties versus M_r, which show power-law dependence at low M_r and deviations at higher M_r. Solution properties include specific viscosity, the z-average $R(gyr)$ from dynamic light scattering, and the hydrodynamic radius from static light scattering. The plots show significant deviations from the expected behavior for random coils, even a random coil with short side chains, implying that the remainder of the branches must be long enough to give the observed solution properties.[152,153,199–201] Smaller dextrans, < 100 kDa, are random coils in solution, but larger dextrans show effects of branching. Dextrans with long branches are more compact than random coils. Recall that dextrans are prepared by hydrolysis of the original natural product, so the branching pattern may reflect effects of both synthesis and hydrolysis. Two recent detailed studies of dextran structure conclude that the chemical and solution structure are "not completely elucidated" according to Vollmer et al.[201] and the branching topology is "not fully understood" according to Rolland-Sabaté et al.[153]

Diffusion. Another question is the diffusive behavior. In work on renal permeability, Venturoli and Rippe[202] argued that dextran is linear and flexible so it is hyperpermeable compared with globular proteins. In artifical membranes with track-etched pores, dextran can pass through smaller pores than its hydrodynamic diameter would allow. Note that long branches would be expected to interfere with reptation. Oliver and Deen[203] presented a Monte Carlo model of transport of random coil dextran through a pore, including both entropic effects and the interaction energy with the pore wall. Weiss et al.[204] measured diffusion of dextrans in HeLa cell cytoplasm by FCS, and found that 40 kDa dextran was much more subdiffusive than 500 kDa dextran. They proposed that motion of the 40 kDa dextran was partially reptational, but the larger dextran was more globular and moved by obstructed diffusion. They further proposed using the anomalous diffusion exponent as a quantitative measure of crowding.

Conclusion. In view of the ambiguities about branch structure and diffusional dynamics, are dextrans the best choice as standard tracers and crowders? Is dextran a calibration standard or a research problem? An answer or a question?

Branch-on-Branch Polymers

Next we discuss branch-on-branch polymers,[205,206] specifically Ficoll, dendrimers, hyperbranched polymers, and dendrigraft polymers. The generic advantage of branch-on-branch polymers is that the cascading branches block a transition from ordinary diffusion to reptation. Their generic disadvantage is that there is no equivalent of the reducing ends of reducing polysaccharides, no unique site for fluorescent labeling post-synthesis. One must build the fluorophore into the core or build a protected attachment site into the core at the price of some loss of spherical symmetry. So a constraint for some branch-on-branch polymers is, some synthesis required,

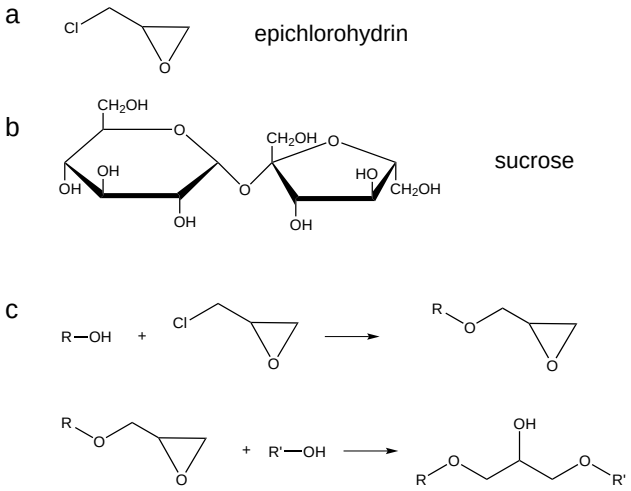

Figure S2. The crosslinking reaction used to make Ficoll. *(a)* Structure of epichlorohydrin. *(b)* Structure of sucrose. *(c)* The elongation reaction, in which epichlorohydrin crosslinks two molecules containing hydroxyls. Several outcomes are possible. Suppose that R is a random sucrose polymer. (1) If R′OH = HOH, the crosslinker (3 carbons) is added and there are two new terminal hydroxyls. (2) If R′OH = sucrose, the crosslinker and one sucrose are added to the chain, thus making Ficoll a copolymer. (3) If R′OH is a sucrose in the same chain as ROH, a ring is formed. (4) If R′OH is a sucrose in a different chain, the chains are crosslinked.

at least when the experiments are sensitive enough to require uniquely labeled tracers. The charge or surface properties of branch-on-branch polymers can be modified by capping the terminal groups with an appropriate moiety. Ficoll and some dendritic and hyperbranched polymers are commercially available.

Ficoll

Structure. Ficoll (now a trademark of GE Healthcare Life Sciences) is a commercial synthetic polysucrose often used as a crowder or a tracer. It is a copolymer made by reaction of sucrose and epichlorohydrin [1-chloro-2,3-epoxypropane, (chloromethyl)oxirane] in aqueous NaOH, as shown in Fig. S2, and fractionated by stepwise precipitation, as described in the patent.[207]

As shown in Fig. S2, 2,3-epoxypropyl ethers are formed at hydroxyls, and these epoxides are opened by reaction with water or a nearby hydroxyl. The resulting structure includes intramolecular diether crosslinks, intermolecular diether crosslinks, and monoether substituents. The reader can imagine the combinatorics, though some linkages are disfavored sterically. The short chains presumably have little effect on solution properties, just as in the case of dextrans, but they contribute to the chemical complexity. For examples of possible structures see the work of Holmberg et al.[208,209] on model compounds for Ficoll fragments. For more information on the chemistry and analytical methods, it is useful to go outside the Ficoll literature to references on epichlorohydrin crosslinking of polysaccharides such as maltodextrins,[210] partially hydrolyzed starch,[211] and especially the crosslinking of dextran to make Sephadex.[212] Dextran and Ficoll have been fractionated by chromatography on Sephadex G-200.[213]

Characterization. For applications to diffusion, crowding, and renal filtration, it would be useful to better characterize Ficoll, a point made by Groszek et al.[214]. This commercial product is less well characterized in the literature than commercial dextrans are. Some basic questions apparently unanswered are the density of crosslinks, the degree of branching, and the NMR spectra. Presumably these gaps are due to the chemical complexity and the nonuniformity of the random crosslinking. But note the comment of Fissell et al.[215] that their Mark-Houwink exponents for Ficoll 400 from 2010 agree closely with those of Lavrenko et al.[216] from 1986, implying consistent manufacturing over decades.

The most advanced analysis of Ficoll solution properties has been done in the renal filtration literature. Fissell et al.[215] used standard multidetector SEC on Ficoll to show that the Mark-Houwink exponents for the intrinsic viscosity were 0.34 (Ficoll 70) and 0.36 (Ficoll 400), between the value of 0 for a solid sphere and 0.5–0.8 for a random coil. Groszek et al.[214] used similar experiments to show that there was little difference between neutral and anionic forms of Ficoll. Georgalis et al.[217] found two different sizes of particles in Ficoll 70 by means of light scattering experiments.

In the SEC calibration literature, Wang and Dubin[218] found that the retention of Ficoll in SEC experiments depended on pH and ionic strength, implying that Ficoll was not neutral but weakly charged. The charge may be the result of oxidation of terminal aldehydes.

Diffusion. Briefly, Ficoll is more spherical than dextran. It is sufficiently crosslinked that it cannot reptate, but it is not a rigid sphere. This is basically the view of Asgeirsson et al.[219] based on experiments in vivo, but I will summarize the argument in terms of experiments on pores, artificial and natural, from Fissell et al.[220] Similar arguments are made by Venturoli and Rippe[202]. The text section Tunable Deformability discusses the views of Asgeirsson et al.[219] on deformability.

Ficoll is more spherical than dextran, as shown by Bohrer et al.[221] Narrow-molecular-mass fractions of dextran and Ficoll were prepared by SEC and their diffusion through a track-etched membrane was measured. Diffusion of Ficoll was close to theory for a sphere, but dextran diffused through the pores more readily. The pore diameters were varied between 30–70 nm, so the pores were much larger than the diffusing polymers. Similarly, Dubin et al.[222] used carboxylated starburst dendrimers of generations 0.5 to 7.5 as a calibration standard for SEC. The exponents in the power-law equations for intrinsic viscosity and D versus mass were close to those for an impenetrable sphere, and the curves of the chromatographic partition coefficient versus radius for dendrimers and Ficoll were very close. The Ficoll data were from the same

laboratory.[223] These experiments used a Superose 12 column, for which the pore size was 12 or 17 nm, in either case larger than the Ficoll. Similarly, experiments on rat kidney found that Ficoll was more spherical and protein-like than dextrans.[224]

But other experiments on rat kidney found that Ficoll is more deformable than globular proteins are.[219] Sieving coefficients were measured as a function of Stokes-Einstein radius for various polymers, and were fit to a two-pore model. The observed small-pore radius was 3.74 nm for rigid globular proteins, but larger for more flexible polymers: 4.66 nm for Ficoll, 6.42 nm for dextran, 6.73 nm for pullulan, and 8.24 nm for PEO.[219] Here the pore size was close to the size of the diffusing polymers. Fissell and collaborators[220] measured transport of Ficoll 70 through silicon slit nanopore membranes with slit widths of 8–90 nm. This experiment enabled them to vary the ratio of the polymer radius to the slit width over a wide range, and they interpreted earlier work in terms of this ratio. They measured the sieving coefficient of the rigid globular protein albumin as a function of this ratio and found good agreement with the predicted values for a rigid sphere. But Ficoll molecules could penetrate the pore even when the Stokes-Einstein radius was greater than the slit width, implying deformability.

Dendrimers

Structure. Dendrimers are "iteratively branched macromolecules"[225] made up of a core and branching groups. The synthesis is also iterative, so the branching is regular, systematic, and deterministic, but the synthesis is complicated. Each iteration to add a monomer shell requires a series of reactions to deprotect, link, and protect, as well as a purification step. Dendrimers are prepared either by divergent synthesis, in which generations are added successively to the core, or by convergent synthesis, in which branching structures (dendrons) are synthesized, purified, and then linked to the core. Dendrimers are described in terms of generations, each consisting of one shell of branching monomer. (Readers are cautioned to check what numbering scheme is used in each reference.) The dendrimers are uniform within each generation, at least for the first few generations. Work on very large dendrimers examines deviations from the ideal as the generation number increases.[225,226] In many of the preparations the monomer has two branches, but sometimes three or four are used. See the reviews of Tomalia et al.[227] and of Astruc et al.[228] A recent review of the synthesis of dendritic and hyperbranched polymers[229] provides an overview of what exists, useful even to a reader with no interest in the synthetic organic chemistry.

A fundamental limit to dendrimer size is that the number of monomers to be added increases exponentially with the generation number but the volume available only increases as the cube of the radius. An early model by de Gennes proposed that the limiting factor is the surface area, increasing as the square of the radius, a view reinforced by the usual 2D structural formulas of 3D dendrimer structures. Later work showed that for flexible dendrimers, backfolding of terminal groups implies that the limiting factor is volume, not surface area. Boas et al.[230] discuss the factors affecting backfolding. The steric limit on size can be evaded by using longer spacers or even by increasing the length of spacers at each generation. Typical diameters are 1–10 nm, a small range for probes but nicely in the range of "bioassemblies."[228,231] A publishably large dendrimer[225] was made from polyphenylene, generation 6, 271.6 kDa, diameter 28 nm.

Both rigid and flexible dendrimers have been prepared, and some are commercially available. Polyphenylenes are a prominent example of rigid dendrimers, with a mean persistence length around 20 nm, that is, 46 phenyl units.[232] Common examples of flexible dendrimers are poly(propylene imine) (PPI) and poly(amidoamine) (PAMAM), shown in Fig. S3. In PAMAM the terminal groups are all amines though backbending implies that the surface is not. One can use the standard amine-reactive fluorescent labels developed for proteins, but the more homogeneous and geometrically simple dendrimer surface might be unnatural enough to diminish biochemical interactions. A disadvantage of PAMAM is that ionization of the amines must be dealt with.

Many different branching monomers have been used, and many different substituents can be put on the terminal groups, so properties such as solubility can be varied considerably. Dendrimers include charged forms, lysine-based, sugar-coated, and PEG-coated. Water-soluble forms are emphasized for biomedical applications such as controlled drug release.[228]

Dendrimers and hyperbranched polymers (see next section) can be assembled around fluorescent or scattering cores. For fluorescence, published syntheses are of small (low-generation) branched polymers to enhance the quantum yield by preventing dye aggregation, including perylene in polyphenylene dendrimers[232] and fluorescein or perylene in polyglycerol dendrimers and hyperbranched polymers.[233–235] Dendrimers have been designed containing multiple dyes for vectorial energy transfer to the core acceptor.[232,236] Weil et al.[236] review work on water-soluble rylene fluorophores for biological applications.

Gold beads encapsulated in dendrimers or hyperbranched polymers have been prepared. In the work of Zill et al.[237], hyperbranched polyglycerol dendrons were linked via an amine to gold nanoparticles of diameter 13.5 nm, and in the work of Pérignon et al.[238] hyperbranched dendrons similar to those in PAMAM were linked to gold nanoparticles of diameter 4–9 nm. In much of the other work,[239–241] the gold particles were in the 1–2 nm range, too small to be useful as scatterers in SPT experiments. But fluorescence from small gold and silver particles has been reported, including some stabilized by dendrimers. For example Au_8 stabilized by poly(amidoamine) dendrimers showed a quantum yield of 42% though the emission peak was at 455 nm. Larger clusters gave longer-wavelength emission but at lower quantum yields.[242,243]

Characterization. Dendrimers have been characterized by standard SEC techniques, where they are the closest

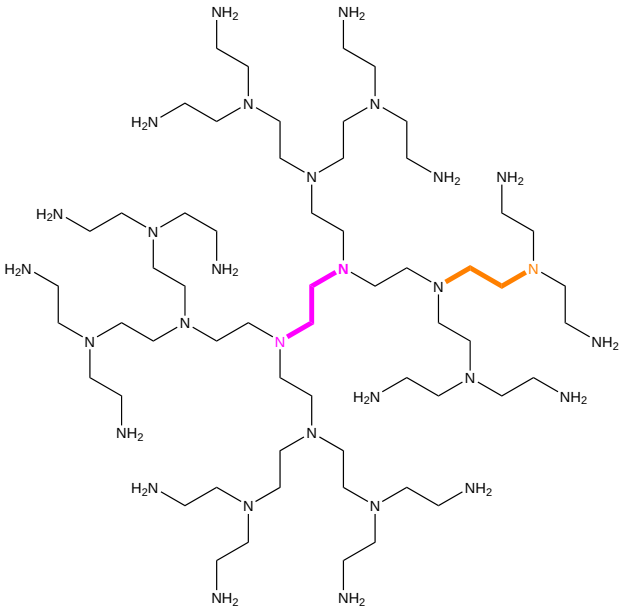

a. PEI

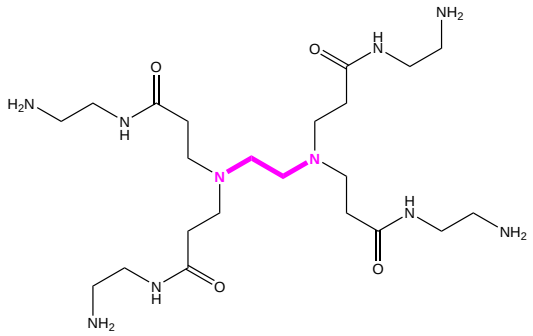

b. PAMAM

Figure S3. Structures of dendrimers. *(a)* Poly(ethylenimine) (PEI). Ethylenediamine core (magenta) plus three generations. The repeating unit is shown in orange. No internal chemical reactions are possible; reactions can occur only at the terminal amines. *(b)* Poly(amidoamine) (PAMAM). Ethylenediamine core (magenta) plus one generation, though this species is generally identified as G0. The repeated unit is added in two reaction steps so half-generations are available. Inner and terminal amines are chemically distinct.

approximation to an ideal nonprotein standard. Striegel et al.[244] used multidetector SEC to examine dilute solutions of dendrimers and polysaccharides, including PAMAM, PPI, dextrans, and maltodextrins from starch degradation. For dendrimers, the Mark-Houwink power law relation between intrinsic viscosity and M_r showed an inversion around the 3rd or 4th generation. The inversion was attributed to the transition from a disklike conformation to a spherical one.

Diffusion. Dendrimers have several structural advantages as scalable labels: the diameter is uniform within each generation, the terminal groups are uniform among generations, and the size can be varied systematically. The core can be chosen to be a fluorescent or scattering label, or terminal groups can be labeled. The disadvantages are the limited range of diameters and the complexity of the syntheses.

Dendrimers also have a dynamical advantage, that the branching structure suppresses reptation and entanglement. Dendrimer solutions have a lower viscosity than the corresponding solutions of linear polymers because the polymers are spherical instead of entangled. Direct comparison of dendrimers with their exact isomeric linear comb equivalents were carried out by Hawker et al.[245] on poly(benzyl ether), and their melt properties were examined by Hay et al.[246] Similarly, viscosities of hyperbranched polymers were compared with the linear analog for esterified polyglycerols.[247]

An important general solution property of dendrimers is that their interaction is soft. For flexible dendrimers, the peak density is in the core (dense-core model) due to backfolding of terminal groups, not at the periphery (dense-shell model). The soft matter physics of dendrimers and star polymers was reviewed by Ballauff and Likos[248] and by Likos[249].

Yu and Russo[250] used pattern FRAP and dynamic light scattering to measure diffusion of G3 and G5 PAMAM labeled with FITC. McCain et al.[251] used 3 generations of PAMAM dendrimers as diffusion probes in a model film of porous silica nanospheres. FCS and concentration jump measurements were made, both using total internal reflection fluorescence. A very interesting study by Cheng et al.[252] compared obstructed diffusion of dendrimers, dextran, the globular protein ovalbumin, and polystyrene latex beads. The obstacles were polymers: polyethylene oxide (40, 200, and 600 kDa) and guar galactomannan (2 MDa). The diffusion measurements were by fringe pattern photobleaching and confocal FRAP. Diffusion coefficients were discussed in terms of the fractal dimension and deformability of the tracers. For NMR measurements of diffusion of PAMAM dendrimers, see[253] for generations 0–7 in methanol, with two different terminal groups, and[254] for generations 0–3 in aqueous solution. A multiscale calculation of solution properties of dendrimers was presented by del Río Echenique et al.[255]

Hyperbranched Polymers

Structure. Hyperbranched polymers are polymers in which multiple layers of random branches make a structure resembling a dendrimer but with random branch points and branch lengths. Hyperbranched polymers can be regarded as imperfect dendrimers, structurally intermediate between linear polymers and dendrimers. Like dendrimers they have a large number of terminal groups. Their great advantage over dendrimers is ease of preparation: a one-step synthesis instead of a multi-step synthesis with purifications of intermediates. The disadvantage is that hyperbranched polymers are often highly poly-

disperse.. Separation procedures such as precipitation and preparative-scale SEC can be used to reduce polydispersity. Specialized synthetic methods such as polymerization in a dioxane emulsion yield more uniform products.[256,257]

One naturally occurring example is glycogen, with a protein core surrounded by polysaccharides consisting of linear $\alpha(1 \rightarrow 4)$ chains of glucose residues with $\alpha(1 \rightarrow 6)$ branching every ~ 10 glucoses. The spacing results from the chain length required for binding of the branching enzyme. And, as pointed out by Senti et al.[258] long ago in work on dextran, hyperbranching occurs because the branching enzyme has no way to distinguish between the original oligomer and later branches. Higher-order organization occurs; rat liver glycogen is organized into β-particles 20–25 nm diameter which assemble into α-particles 110–290 nm diameter. We do not consider glycogen as a tracer because the size and structure are highly sensitive to the source and details of preparation, and because glycogen can be metabolized by cells.[259–261]

Another natural example is amylopectin, one of the components of starch. The structure is the same as glycogen but branching occurs every 24–30 glucose residues. We do not consider amylopectin as a tracer. The structure is too complicated, and the literature emphasizes the various levels of higher-order organization involved in forming starch granules.[262] Furthermore, amylopectin can be metabolized by cells.

On the general requirement of metabolic inertness, Naessens et al.[178] pointed out that an advantage of dextran in clinical applications is that it has a high fraction of the slowly hydrolyzed $\alpha(1 \rightarrow 6)$ linkage, whereas the $\alpha(1 \rightarrow 4)$ linkage in glycogen and starch is hydrolyzed rapidly.

A very promising synthetic material for scalable tracers is hyperbranched polyglycerol,[257] shown in Fig. S4, a material of great interest for biomedical applications on account of its biocompatibility. It is structurally similar to poly(ethylene glycol); they are compared in Fig. S5. Large particles, up to 100 nm diameter, have been prepared, depicted as spheres made up of covalently bound smaller polyglycerol spheres.[263,264] Polyglycerol nanogels can be prepared with diameters of tens to hundreds of nm, and fluorescent forms have been made.[265] Fluorescent conjugates of hyperbranched polyglycerols with fluorescein or perylene diimide have been synthesized.[234] At least for proof-of-concept experiments, commercial hyperbranched polyglycerols could be used as scalable tracers, with nonspecific fluorescent labeling of hydroxyls by the method long used for dextrans.[266]

Another synthetic material is hyperbranched PAMAM, the random analog of the PAMAM dendrimer.[267] An advantage of PAMAM over polyglycerol is that PAMAM can be labeled readily with the usual amine-reactive protein labels. An advantage of polyglycerol is that it is neutral but the ionization of terminal amines must be considered in PAMAM. More accurately, polyglycerol is nominally neutral, and ought to be analyzed as in the work of Wang and Dubin[218] that found Ficoll to be weakly charged, not neutral.

Characterization. Solution properties of hyperbranched polyglycerol were measured by SEC[256] and by small-angle neutron scattering.[270] Dendrimers and hyperbranched polymers are more uniform than dextran, simplifying modeling, as in the random branching model of Konkolewicz et al.[271]

Hyperbranched polymers are described in terms of the fraction of monomers with various connectivities: dendrimeric (D), linear (L), and terminal (T), as shown in Fig. S4 *c* for polyglycerol.[268] The degree of branching DB is defined as

$$DB = 2D/(2D + L), \tag{S15}$$

and is 0 for linear polymers and 1 for perfect dendrimers. For random addition with trifunctional monomers, DB is 0.5 or 0.66 depending on the way the reaction is carried out. Observed values for hyperbranched polyglycerol are 0.53–0.59 from ^{13}C NMR measurements. The fraction of L residues, $L/(D+L+T)$, is also important here because the internal hydroxyls on the L residues can be crosslinked to tune the deformability without changing surface properties, as discussed in Supporting Information 6.

Baille et al.[272] used pulsed gradient spsin echo NMR to measure diffusion of hyperbranched polyglycidol fractions in aqueous solutions of poly(vinyl alcohol) ranging from pure water to viscous gels. The hyperbranched polymers were characterized by SEC and mass spectroscopy. The branching structure was examined by ^{13}C-NMR. Diffusion and conformation were discussed in terms of Flory exponents.

Conclusion. Synthetic hyperbranched polymers, particularly hyperbranched polyglycerol, are appealing candidates as tracers or crowders. Hyperbranched polymers are less difficult to synthesize than a similar range of dendrimer sizes would be. One ought to be able to make a range of sizes with a statistically uniform structure. Just as with dendrimers, branching imposes approximate spherical symmetry and inhibits the diffusion-to-reptation transition. The main disadvantage is that the polydispersity must be dealt with by some combination of synthesis and purification.

Dendrigraft (Arborescent) and Related Polymers

We note briefly some other types of iteratively branched polymers. One class is dendrimers in which the branching structure is the same as in conventional dendrimers but the building blocks are linear polymers instead of small molecules. The advantages are that the overall size of the dendrimers is large, and the dendrimers can be made in a structurally precise manner.[273] The disadvantage is that the solution dynamics is likely to be intermediate between ordinary dendrimers and linear polymers, with tendencies to what Phillies[274] calls "teuthidic" (squid-like) motion. The same argument holds for hyperbranched polymers synthesized from linear polymer building blocks.

A related class of structures is the dendrigraft polymer.[275,276] These are random hyperbranched polymers synthesized from linear polymer building blocks, but here each linear polymer has many possible branch points so that the branching multiplicity is high, 10–15 instead of

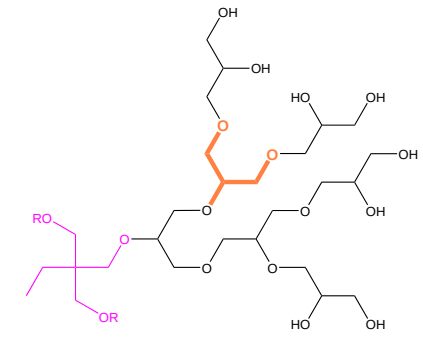

a. Dendritic polyglycerol

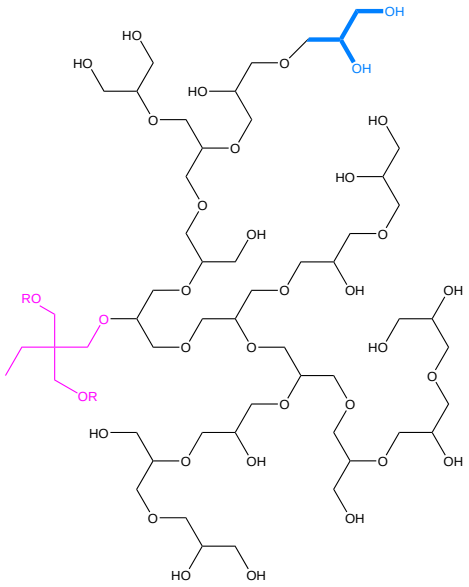

b. Hyperbranched polyglycerol

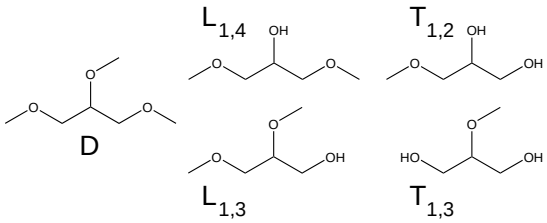

c. Structural units

Figure S4. Structure of dendritic and hyperbranched polyglycerol. *(a)* Dendritic polyglycerol. The core (magenta) is the compound commonly used, TMP, 1,1,1-tris(hydroxymethyl)propane. Only one dendron is shown, three generations. In a perfect dendrimer, two more dendrons (R) are bonded to the core. The repeating unit is shown in orange. No internal chemistry is possible; reactions occur only at the terminal hydroxyls. *(b)* An example of hyperbranched polyglycerol. The core is again TMP (magenta), and again only one dendron is shown. There are hydroxyl groups in the topological interior, so chemistry is allowed there. Reactions can be carried out on both interior and terminal hydroxyls. Terminal 1,2-diols (vicinal diols) (heavy blue bonds) can be distinguished chemically from isolated hydroxyls, making selective crosslinking or labeling possible, as discussed in Supporting Information 6. *(c)* The structural units of hyperbranched polyglycerol: linear $L_{1,3}$; linear $L_{1,4}$; dendritic D; terminal 1,2-diol $T_{1,2}$; and terminal 1,3-diol $T_{1,3}$. Terminal 1,3-diols are not found in the usual preparations of hyperbranched polyglycerol, as shown by ^{13}C NMR analysis[268], but were found in an alternative synthesis.[269] Further specificity would be provided by reactions that distinguish terminal 1,2-diols from terminal 1,3-diols.

2–3 for the conventional case. The building blocks are larger than in the usual hyperbranched polymers, so the dendrigraft polymers are large, in the potentially useful size range of 10 kDa to 100 MDa, 10 nm to a few hundred nm. Furthermore they are less polydisperse than hyperbranched polymers, $M_w/M_n < 1.1$. Measurements of solution properties of arborescent polystyrenes show them to be hard core, soft shell, with the outermost polymer layer forming the soft shell.

Star Polymers

Star polymers consist of a core to which unbranched linear arms are attached.[277–279] In star polymers, the core is much smaller than the arms, but in sterically stabilized nanospheres, the core is larger than the arms. These two cases can be treated as limits with a crossover.[280] The properties of star polymers depend on the length of the arms and the number of arms f. The $f = 1$ and $f = 2$ forms are linear polymers. As f increases, the inherent asymmetry decreases and the polymer becomes more spherelike. The polymer becomes more like a hard sphere on account of steric repulsion of arm segments near the core. Hard-sphere-like behavior is evident[281] for $f = 64$. Star polymers thus interpolate between linear polymers and sterically stabilized hard spheres. This behavior was shown in simulations of the effective potential between a pair of star polymers. As f was increased from 18 to 256, the potential steepened considerably.[277,282] Many star polymers are hydrophobic, such as those discussed by Likos[277]: polyisoprene stars, $f = 8$ and 18, and polybutadiene stars, $f = 32, 64, 128$, all monodisperse in the number of arms and the degree of polymerization. Hydrophilic star polymers may be based on PEG arms, as reviewed by Lapienis[278]. One route to PEG-based star polymers with large f is to use a dendrimer or hyperbranched polymer as the core.[278]

Fleischer et al.[283] used PFG NMR to measure self-diffusion of star polymers as a function of concentration and arm length; 128-arm polybutadiene star polymers in toluene were used, with R(hydro) of 14.1 to 31.2 nm.

PEG and Analogs

The extensive work done on PEG-related polymers presents an opportunity to examine the effects of polymer topology on diffusion using water-soluble, highly biocompatible polymers. Here PEG is poly(ethylene glycol). PEO, poly(ethylene oxide), is chemically the same. PEG is short enough that the end hydroxyls are significant; PEO is long enough that they are not. Fig. S5 compares PEG with linear polyglycerol, also called linear polyglycidol.

Star-shaped PEG polymers are reviewed by Lapienis[278]. Hyperbranched and dendrimeric forms are reviewed by various researchers.[233–235,257] Hyperbranched PEG has been prepared from random copolymerization of ethylene oxide and glycidol[284] and block copolymers of PEO and polyglycerol have been prepared.[285] Related polymers are discussed by Rele et al.[286], Feng et al.[287], and Taton et al.[273], and larger particles by Calderón et al.[263] and Steinhilber et al.[264] The missing type is the dendrigraft with many branch points per polymer building block. The form reported in the literature is an ordinary dendrimer made of polymer building blocks.

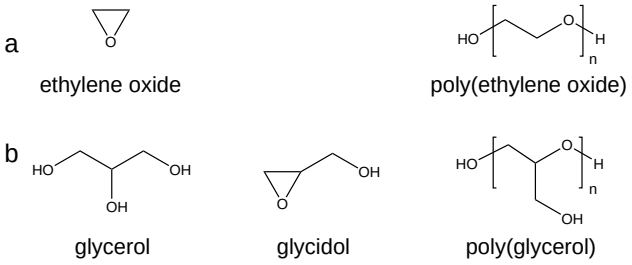

Figure S5. Poly(ethylene oxide) and linear polyglycerol. Both polymers are polyethers. *(a)* Ethylene oxide monomer and poly(ethylene oxide). *(b)* Glycerol monomer, glycidol monomer (2,3-epoxy-1-propanol, oxiranylmethanol), and linear polyglycerol (polyglycidol). In terms of the structural units in Fig. S4, linear polyglycerol is made up of $L_{1,3}$ units.

Significant progress has already been made on the diffusion problem. Wang et al.[288] used PGSE NMR to measure diffusion of PEG-like polymers in aqueous solutions of poly(vinyl alcohol) solutions ranging from pure water to poly(vinyl alcohol) gel. Behavior of linear, star, and dendritic forms were compared, and the M_r of each form was varied.

One disadvantage is labeling; a generic hydroxyl label must be used so the location and numbers of fluorophore are variable. A potentially more serious disadvantage is the protein-PEG interaction that has led to criticism of PEG as a crowder. The problem is the attraction between PEG and nonpolar or hydrophobic side chains on the protein surface. This protein-dependent attraction partially compensates for the excluded-volume repulsion underlying crowding. Other crowders – dextrans, Ficoll, hemoglobin, bovine serum albumin – do not have this attraction and are preferred.[289] For a contrary view see.[290] If a polyglycerol dendrimer or hyperbranched polymer is to be used as a crowder, it must be tested similarly.

Microgels

Microgels are crosslinked latex particles swollen by a good solvent. The particles are limited to the colloidal size range by carrying out the polymerization and crosslinking in microemulsions or emulsions. The particles swell in a good solvent but retain their spherical shape due to the crosslinking.[291] A common hydrophilic microgel – with various acronyms – is poly(*N*-isopropylacrylamide), made from *N*-isopropylacrylamide with *N,N′*-methylene-bis-acrylamide crosslinker and say 4-acrylamidofluorescein as a covalently linked fluorophore. There is considerable interest in this microgel because the swelling is strongly temperature-dependent, and the transition temperature is near body temperature. Paloli

et al.[292] used a similar microgel in a confocal microscopy study of colloid dynamics and glass formation. The diameter was 714 nm, the polydispersity 4%, the crosslinking 5 mol%, and the label rhodamine B. Bartsch et al.[293] used microgel particles as a model of glass formation. The particles were polystyrene or poly(*t*-butylacrylate), diameter 50–326 nm, in water or various organic solvents.

Microgel properties are strongly dependent on the density of p crosslinkers. The density affects the amount of swelling in a given solvent, and therefore the particle size, the deformability, and the viscosity of the solution. For example, Wolfe and Scopazzi[294] measured the size of PMMA microgels in a good organic solvent and the macroscopic viscosity of the solution. As the crosslinking density increased, the particles became smaller and the viscosity decreased.

Bartsch et al.[293] raise an important point affecting microgels as scalable tracers. As the density of crosslinkers increases, the length of polymer chains between crosslinks decreases, and likewise the chain length of loose polymer ends at the surface decreases. (Both lengths are taken to be the mean lengths assuming complete reaction of the crosslinker.) But these loose ends act as a steric stabilizing layer, and the hairy-sphere repulsion (Supporting Information 5) depends on the ratio of the length of the dangling ends to the particle radius. Thus microgels are not automatically scalable.

Wanted: Scalable Tracers for Diffusion Measurements

Supporting Information 5
Potentials

Michael J. Saxton

Now that we have described the different polymer structures of interest, we can discuss tracer-tracer interactions. The interactions are a fundamental part of the characterization of the tracers, and one measure of the softness of various types of tracer. A highly informative review by Likos [277] emphasizes potentials and another, by Vlassopoulos and Fytas [279], emphasizes structures, densities, and the tunability of the softness. Interactions in some mixed systems have been studied, for example between star polymers and hard colloidal particles. [277] The case of interest in cell biology – the interactions of candidate tracers with proteins – does not seem to have been studied much except in the crowding literature. [289]

In a very interesting experimental paper, Yethiraj and van Blaaderen [295] presented a model colloidal system in which the interaction was tunable from hard sphere to soft dipolar. The particles were sterically stabilized PMMA spheres, and a mixed organic solvent was used to match both density and refractive index. The potential was tuned by means of an external AC field. The high degree of control enabled these workers to map out a complex phase diagram. This work is an instructive example of experimental rigor, even if that level of rigor is not attainable in measurements on cells.

Conventional Potentials

Various conventional potentials are often assumed for protein-protein, polymer-polymer, and colloid-colloid interactions. In these potentials, r is the radial coordinate, ϵ is an energy in units of the thermal energy kT, r_{HS} is the hard-sphere radius, and r_0 is a characteristic radius of the order of the radius of gyration. In all, $V(r)$ is infinite as $r \to 0$.

1. Hard sphere

$$V(r) = \begin{cases} \infty & \text{if } r < r_{HS} \\ 0 & \text{if } r > r_{HS} \end{cases} \tag{S16}$$

2. Coulomb potential

$$V(r) = \epsilon(r_0/r) \tag{S17}$$

3. Inverse power law

$$V(r) = \epsilon(r_0/r)^n \tag{S18}$$

This form interpolates between the Coulomb potential for $n = 1$ and the hard-sphere potential for $n \to \infty$. In standard liquid theory, this is classified as a soft potential as distinguished from a hard-sphere potential, n is a measure of the steepness or stiffness, and $1/n$ a measure of the softness. [296]

4. Lennard-Jones potential

$$V(r) = \epsilon[(r_0/r)^{12} - (r_0/r)^6] \tag{S19}$$

5. Yukawa or screened Coulomb potential, usually with a hard-sphere core

$$V(r) = \begin{cases} \infty & \text{if } r < r_{HS} \\ \epsilon(\lambda/r)\exp(-r/\lambda) & \text{if } r > r_{HS} \end{cases} \tag{S20}$$

where λ is the Debye screening length.

6. The DLVO, Derjaguin-Landau-Verwey-Overbeek, potential for a pair of spherical colloidal particles in an electrolyte solution. One component of the DLVO is the van der Waals interaction for a macroscopic pair of spheres, more complicated than the $1/r^6$ term in the Lennard-Jones potential. The other component is a screened Coulomb potential from the interaction of the double layers around the particles, in the linearized Poisson-Boltzmann approximation. [297–299] DLVO is mentioned for completeness but I downplay polyelectrolytes here because charge complicates scalability.

7. The depletion interaction is an entropic attractive force between large particles in solution in the presence of small particles or small nonadsorbing polymers. In such a mixture, the small particles are excluded from a shell around each large particle. If the excluded regions overlap, the total excluded volume decreases, the entropy of the small particles increases, and the free energy of the system decreases, so there is an attractive potential. An alternative physical picture is that the small particles are excluded from the overlap region and exert an osmotic pressure on the large particles. The depletion interaction is short-range, with the range determined by the diameter of the small particles. The strength of the attraction is proportional to the concentration of small particles. Phillips et al. [300] give an elementary derivation and Likos [277] gives a detailed review. The attraction was observed directly in a colloid-polymer mixture. [301] Marenduzzo et al. [302] discussed the implications for cellular organization.

8. Atomistic. It is becoming practical to calculate a potential incorporating molecular detail, as in the work of McGuffee and Elcock [137] already mentioned. In another example, Chan et al. [303] computed an approximate interaction between two lysozyme molecules in their native folded states. The emphasis on was on charge effects, not on shape effects. Lysozyme was approximated as a sphere with charges at the proper angular locations from the molecular structure, but at a uniform and fixed distance below the sphere surface. The ionization states of the amino acids could change, and the difference in dielectric constants between water and protein was taken into account. Van der Waals forces and steric repulsion were approximated as a Lennard-Jones-like potential. The authors found the potential of mean force, Boltzmann-averaged over orientations. One main conclusion was that the DLVO potential overestimates electrostatic interactions on account of the uniform charge assumed; particles with nonuniform charge distributions align themselves favorably.

Ultrasoft Potentials

Polymer research has led to materials with much softer potentials than those discussed in the preceding section,

and some of these materials are appropriate candidate scalable tracers. Some have a soft potential until the cores required by the chemistry come into contact. Others have a logarithmic potential, described as "ultrasoft" because it increases more slowly than any power law. Others have a finite potential[277] even at $r = 0$. A finite potential at $r = 0$ may sound counterintuitive but Likos[277] gives a simple explanation. Consider the effective potential between two random coil polymers as a function of the distance between their centers of mass. The potential $V(0)$ is finite because two self-avoiding walks can have the same center of mass but can still avoid themselves and each other. There is simply an entropic cost to have the two self-avoiding walks in proximity. The finite $V(0)$ is a result of using center-of-mass coordinates. The value would be infinite if, for example, the distance between the middle monomer positions were chosen as the coordinate.

Random Coils

The potential for an isolated pair of random-coil polymers in a good solvent is to a good approximation a Gaussian

$$V(r) = \epsilon \exp(-r^2/r_0^2), \tag{S21}$$

the so-called Gaussian core model, and is approximately Gaussian at higher concentrations.[304,305] The potential is finite at all separations, with a maximum of 3 kT or less at $r = 0$. The potential goes to zero by $3R(gyr)$ for an isolated pair of random coils. Monte Carlo simulations examined in detail the effects of chain length, concentration, and monomer-monomer interaction.[306,307]

Hairy Spheres

Steric repulsion is a common method of stabilizing colloids against aggregation. Here polymer chains are attached to the colloid, causing a repulsive pair potential between the colloids. The interaction involves both osmotic and elastic repulsion, and is of the range of the polymer length. The expression for the potential is too complicated to include here; results and simulations are found in the literature.[279,298,308] Of particular interest are recent molecular dynamics simulations in which the polymer chains are treated by a bead-spring model. The spheres are repeatedly moved closer, the chains are allowed to equilibrate, and the interaction is calculated. At close approach, some of the chains are squeezed out into the plane perpendicular to the particle-particle axis, so the potential increases steeply even before the cores are in contact.[309]

The hairy sphere is related to other types of polymers. It is a star polymer in which the number of arms is large and the arms are shorter than the core radius. It is also a polymer brush in which the polymers are anchored to a sphere instead of a line or a plane.

We consider the case where the polymers are grafted to the colloid, that is, chemically attached, or strongly adsorbed via a unique site on the polymer.

Weak multiple adsorption sites complicate the system because desorption may occur, the polymer may bridge two colloids, and multiple binding sites lead to variation of the length of polymer in solution. We do not consider the case of stabilization by polyelectrolyte brushes. The equations for this case are conveniently summarized by Fritz et al.[310]

Star Polymers

A pair of star polymers in a good solvent interact by an ultrasoft potential[277,282]

$$V(r) = \begin{cases} \ln(r/\sigma) + \text{const} & \text{if } r < \sigma \\ 1 + \text{Yukawa potential} & \text{if } r < \sigma \end{cases} \tag{S22}$$

where σ is the corona diameter. As the number of arms in the star polymer increases, the repulsion grows longer-ranged and steeper. This form was confirmed by molecular dynamics calculations using a bead-spring model for the arms, though a hard-core repulsion must be included at small r to account for the cores. Calculations were for 5–50 arms, each of 50–200 beads.[309,311]

Dendrimers

Monte Carlo simulations[312] of two different generations of athermal dendrimers (entropic interactions only) yielded a potential of mean force, steeper for generation 5 than for generation 2. Götze et al.[313] obtained a Gaussian effective interaction between flexible dendrimers

$$V(r) \propto \exp[-3r^2/4R_{gyr}^2(\infty)] \tag{S23}$$

where $R_{gyr}(\infty)$ is the radius of gyration at infinite separation. The proportionality constant involves one free variable, the excluded-volume parameter. Interactions are discussed further in the review of Likos and Ballauff[314].

Effects of polymer topology on diffusivity and solution viscosity were examined by Bosko and Prakash[315]. They carried out Brownian dynamics calculations for dilute solutions of dendrimers, star polymers, and linear polymers of comparable molecular masses. The polymers were described by a bead-spring model and hydrodynamic interactions were included. The solutions were at the theta temperature.

Others

An important artificial soft potential is the form used in dissipative particle dynamics calculations[316]

$$V(r) = \begin{cases} \epsilon(1 - r/r_c)^2 & \text{if } r < r_c \\ 0 & \text{if } r > r_c \end{cases} \tag{S24}$$

There is no consensus yet on the potential between two uncharged microgel spheres.

Scalability

How does the potential affect the scalablity of tracers? For obstructed diffusion, the tracer-obstacle interaction must be considered, and for crowding, the tracer-tracer interaction. We give an elementary geometrical argument, mostly to make the point that this question warrants attention.

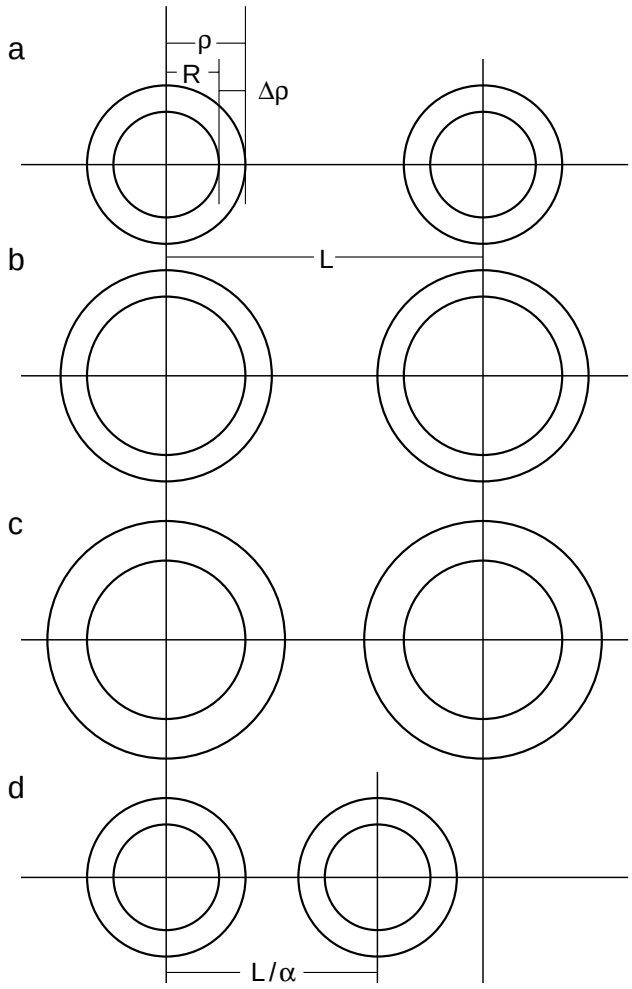

Figure S6. Scaling of a potential. *(a)* Starting point. Two particles of hard-sphere radius R, radius of the short-range potential ρ, width of the short-range potential $\Delta\rho$, and center-to-center distance L. *(b)* Correct rescaling. The width of the potential is the same as in panel a but the hard-sphere radius is increased. *(c)* Incorrect rescaling. Both R and ρ are rescaled by a factor of α. This rescaling gives a system identical to panel a but with the mean separation decreased from L to L/α, as shown in panel d. That is, the system is the same but the 3D number density is increased by a factor of α^3. *(d)* Panel c with all lengths rescaled by $1/\alpha$.

Assume that the system size is much larger than the particle size and the range of the potential, so that the system size can be neglected. For hard spheres, there are then two characteristic lengths, the particle radius R and the mean separation L and therefore only one parameter R/L. If n is the number density, then $L = 1/n^{1/3}$ in 3D.

Consider hard spheres with an added short-range potential of range ρ, forming a shell of thickness $\Delta\rho = \rho - R$ around the hard sphere. Then there are two parameters, R/L and ρ/L. Suppose these tracers are scaled by changing R by a factor of α. How should the potential be changed? As Fig. S6 shows, ρ should not be scaled by a factor of α, and $\Delta\rho$ should be kept constant. That is, one must change the hard-sphere radius but keep the short-range potential constant with respect to the particle surface.

Wanted: Scalable Tracers for Diffusion Measurements

Supporting Information 6
Tunable Deformability

Michael J. Saxton

Supporting Information 6 gives details on some methods of measuring molecular deformability and crosslinking chemistry to tune it.

Deformability Measurements

Several methods to measure deformability are available. I argue that ultrasonic measurements are best, though probably any of the methods would give useful relative values within a series of tracers differing only in crosslink density.

Ultrafiltration through Nanopores

Passage through well-defined pores has been used to characterize the deformability of microgel beads. Much of the work on the mechanics of microgel beads involves larger particles than those of interest here. An exception is the work of Hendrickson and Lyon [317] on filtration of microgel beads through track-etch membranes under a pressure difference similar to that in the kidney. The microgel was made of *N*-isopropylacrylamide and acrylic acid with various concentrations of *N,N′*-methylene-bisacrylamide crosslinker. Pore diameters were 10 and 100 nm; the hydrodynamic diameters of the microgel beads were 0.6–1.1 μm. Polystyrene beads were used as positive and negative controls. This work showed that the microgel beads can pass through pores even when the opening is a factor of 10 smaller than the unperturbed particle diameter.

Osmotic Compression

Some laboratories have measured deformability by measuring particle size as a function of osmotic pressure. Measurements for crowder macromolecules were described in the text. Work has also been done on microgel particles. In a study of the effect of softness on glass formation by microgel particles, Mattsson et al. [318] prepared particles of three different deformabilities, based on interpenetrating networks of poly(*N*-isopropylacrylamide) and polyacrylic acid. Particle size was measured by dynamic light scattering (DLS) for a range of osmotic pressures set by a dextran osmolyte, and the elasticity was characterized by the slope of the plot of size versus osmotic pressure. Fernández-Nieves et al. [319] measured the effect of osmotic pressure on the swelling of an ionic poly(2-vinylpyridine) microgel. Sierra-Martin et al. [320] used a dextran crowder to measure the bulk modulus of microgel particles with different degrees of crosslinking. This reference includes a useful discussion of potential artifacts.

To measure crosslinking effects, one would prepare a batch of scalable tracer with a prescribed fraction of crosslinker, and find $R(hydro)$ by DLS as a function of crowder concentration. The complexities in interpreting light scattering measurements in tracer-polymer mixtures are discussed by Phillies [274], Sierra-Martin et al. [320], and Streletzky and Phillies [321].

Two different experiments are possible, one using the tracer as the crowder and one using a distinct crowder. Both experiments assume that the entire change in diffusion coefficent is due to a change in particle size and not to, say, a change in solvent microviscosity. Increasing the crosslinking density may affect deformability through both the tracer-tracer penetrability and the overall elasticity of the tracer viewed as a macroscopic solid. If the tracer is used as the crowder, [322] the system is binary and interpretation is straightforward. The crowding depends on the tracer-tracer interaction. If a distinct crowder is used – say a protein crowder for a tracer to be used in a cell – crowding depends on the tracer-crowder interaction. One potential problem is that the system is ternary so the osmotic compressibility is involved. Parsegian et al. [323] pointed out the distinction between osmotic stress and hydrostatic pressure. Osmotic stress is imposed in an open system and there is a change in volume due to mass transfer. Hydrostatic pressure is imposed at fixed mass and the change in volume is due to material compressibility. See also later work by Parsegian et al. [324] Parsegian's objections can be met by the approach of Dijkstra et al. [325] who derived a potential of mean force for a ternary system, using a grand canonical ensemble to account for mass transfer. The example considered was the depletion interaction in a mixture of large and small spheres. Another potential problem is light scattering by the crowder, though in some systems light scattering by the crowder is negligible. Measurements on polystyrene latex spheres in high-molecular-mass hydroxypropylcellulose showed that scattering by the latex was predominant. [321] In synthetic polymer mixtures, refractive index matching has been used to make one polymer invisible. [326]

Ultrasound

The adiabatic compressibility β_S is readily measured in solution by ultrasonics. Many studies of β_S have been done for polymers and biomolecules. [327–330] There are three distinct contributions to molecular volume: (1) the atomic volume is constant and makes no contribution to the compressibility; (2) the volume of cavities makes a positive contribution given the sign convention; and (3) the hydration depends on pressure and makes a negative contribution. The compressibility of amino acid solutions is negative because there are no cavities, just hydration. Dextran solutions have a negative compressibility, suggesting hydration with negligible void volume. [331] In these experiments, dextrans in the range 2–44.5 kDa had the same β_S, and branching is not likely to be important in this mass range. Compressibilities of globular proteins are generally positive on account of voids. Gekko and Noguchi [328] calculated values of β_T from values of β_S for a few proteins; Gekko and Hasegawa [332] calculated values of β_T for more proteins assuming typical values of thermodynamic properties.

Some numerical values are shown in Table S3 to illustrate two main points. First, globular proteins are more compressible than metals, less compressible than solid plastics, and much less compressible than common solvents. Second, compressibilities can be small or negative, implying that both hydration and void volume are essential components. As a result, direct comparison of say proteins with polysaccharides may be questionable. For-

tunately, to construct a series of scalable tracers varying in deformability, it is sufficient to compare polymers that have the same general composition and surface properties, but differ only in crosslink density. Hydration effects are then likely to be approximately constant.

The discussion of compressibility in the protein literature is necessarily complex given the variation in primary and secondary structure in common globular proteins. The problem here is much simpler, measuring the effects of crosslinks or limited amino acid substitution on an otherwise constant structure.

Ultrasonic absorption measurements are also used to examine polymer dynamics in solution and interactions of polymers at high concentrations. For example, Dunbar et al.[341] studied polystyrene in toluene and cyclohexane.

In ultrasonic measurements on suspensions, a key quantity is the difference in density between particles and medium.[346,347]

Synthetic Polymers by Crosslinking

The text discussed one approach to crosslinking, in which Ficoll was treated with epichlorohydrin, the crosslinking agent used to produce Ficoll from sucrose.

Alternatively, a distinct secondary crosslinker could be used. Much work has been published on modification of dextrans and agarose as chromatography media, either to make stiffer beads with better fluid flow through the column, or to activate the substrate to attach ligands for affinity chromatography. For example, Porath et al.[348] crosslinked agarose with divinyl sulfone to improve the mechanics, and also varied the crosslink length. Sundberg and Porath[349] activated agarose with bifunctional oxiranes for ligand attachment. Interestingly, Matsumoto et al.[350] activated Sepharose with epichlorohydrin for ligand attachment, and noted that a problem with epichlorohydrin activation is that the Sepharose is simultaneously crosslinked. Crosslinking increases the stability and rigidity of the gel but decreases the permeability. Andersson et al.[351] used a sequence of crosslinkers to make an agarose column with more rigid beads, therefore improved flow. Lindgren[352] described methods of crosslinking Sepharose to improve flow properties. Another source of potential crosslinking methods is work on hydrogels.[353] An excellent general reference is the book of Hermanson[108]. This entire body of literature is a valuable source of reaction conditions and analytical methods, but the approach must be modified to favor intramolecular crosslinking over intermolecular, to maximize crosslinking rather than activation, and to measure deformability as a property of individual macromolecules instead of macroscopic flow in a chromatographic column.

The same chemistry can be used to randomly crosslink other macromolecules with multiple internal hydroxyls, to make for example "reinforced hyperbranched polyglycerol." In general, hyperbranched polymers show no distinguishable interior and periphery, unlike dendrimers.[354] But hyperbranched polyglycerol has chemically distinguishable hydroxyls as was shown in Fig. S4, so one can block the terminal 1,2-diols (vicinal diols), carry out a crosslinking reaction on the internal hydroxyls alone, and then unblock the diols.[355]

Table S3. Adiabatic and Isothermal Compressibilities (1/Mbar)

	β_S	β_T	
Ideal monatomic gas	$\frac{3}{5}\frac{1}{P}$	$\frac{1}{P}$	
Dextran 2–44.5 kDa in water	−7.3		[331]
Gelatin	−2.50	1.92	[332]
Subtilisin BPN	−1.11	3.22	[332]
Cytochrome c	0.066	4.27	[332]
Carbon (diamond)		0.18	[333]
Tungsten		0.35	[333]
Iron		0.58	[333]
Aluminum		1.27	[333]
Silica		2.82	[334]
Carbon (graphite)		3.0	[333]
Sodium chloride		4.27	[333]
Trypsin	0.92	5.16	[332]
Ribonuclease A	1.12	5.48	[332]
Peroxidase	2.36	6.70	[332]
α-Chymotrypsinogen A	4.05	6.95	[332]
Lysozyme	4.67	7.73	[332]
β-Lactoglobulin	8.45	11.8	[332]
Myoglobin	8.98	13.1	[332]
Ovalbumin	9.18	12.1	[332]
Bovine serum albumin	10.5	14.6	[332]
Hemoglobin	10.9	15.0	[332]
Ice, 0 C	11.4	11.8	[335]
PMMA, bulk solid		19.6	[336]
Polyethylene, bulk solid		20.7	[336]
Polystyrene, bulk solid		22.7	[336]
Glycerol	21.8	24.3	[337]
Poly(ethylene glycol) in water	33.3		
PEG-1000, 0.5 mol/kg			[338]
Water	45.91	45.895	[339,340]
Polystyrene in toluene	53.4 − 62.8		[341]
M_n 89 kDa, 0.01–0.40 g/cm^3			
Toluene	73.3	89.6	[335,342]
Ethanol	94.1	111.9	[335,343]
Methanol	98.6	121.4	[335,344]
Hexane	125.4	162.0	[345]

1 Mbar = 10^5 Pa = 0.987 atm

References

(1) Vinothkumar, K. R.; Henderson, R. Structures of Membrane Proteins. *Q. Rev. Biophys.* **2010**, *43*, 65–158.

(2) Perez-Aguilar, J. M.; Saven, J. G. Computational Design of Membrane Proteins. *Structure* **2012**, *20*, 5–14.

(3) Liang, J.; Naveed, H.; Jimenez-Morales, D.; Adamian, L.; Lin, M. Computational Studies of Membrane Proteins: Models and Predictions for Biological Understanding. *Biochim. Biophys. Acta Biomembr.* **2012**, *1818*, 927–941.

(4) Klingler, J. F.; McConnell, H. M. Brownian Motion and Fluid Mechanics of Lipid Monolayer Domains. *J. Phys. Chem.* **1993**, *97*, 6096–6100.

(5) Yanagisawa, M.; Imai, M.; Masui, T.; Komura, S.; Ohta, T. Growth Dynamics of Domains in Ternary Fluid Vesicles. *Biophys. J.* **2007**, *92*, 115–125.

(6) Cicuta, P.; Keller, S. L.; Veatch, S. L. Diffusion of Liquid Domains in Lipid Bilayer Membranes. *J. Phys. Chem. B* **2007**, *111*, 3328–3331.

(7) Petrov, E. P.; Petrosyan, R.; Schwille, P. Translational and Rotational Diffusion of Micrometer-Sized Solid Domains in Lipid Membranes. *Soft Matter* **2012**, *8*, 7552–7555.

(8) Lohmüller, T.; Triffo, S.; O'Donoghue, G. P.; Xu, Q.; Coyle, M. P.; Groves, J. T. Supported Membranes Embedded with Fixed Arrays of Gold Nanoparticles. *Nano Lett.* **2011**, *11*, 4912–4918.

(9) Wolf, D. E.; Schlessinger, J.; Elson, E. L.; Webb, W. W.; Blumenthal, R.; Henkart, P. Diffusion and Patching of Macromolecules on Planar Lipid Bilayer Membranes. *Biochemistry* **1977**, *16*, 3476–3483.

(10) Wolf, D. E.; Henkart, P.; Webb, W. W. Diffusion, Patching, and Capping of Stearoylated Dextrans on 3T3 Cell Plasma Membranes. *Biochemistry* **1980**, *19*, 3893–3904.

(11) Knight, J. D.; Lerner, M. G.; Marcano-Velázquez, J. G.; Pastor, R. W.; Falke, J. J. Single Molecule Diffusion of Membrane-Bound Proteins: Window into Lipid Contacts and Bilayer Dynamics. *Biophys. J.* **2010**, *99*, 2879–2887.

(12) Ziemba, B. P.; Knight, J. D.; Falke, J. J. Assembly of Membrane-Bound Protein Complexes: Detection and Analysis by Single Molecule Diffusion. *Biochemistry* **2012**, *51*, 1638–1647.

(13) Liu, C.; Paprica, A.; Petersen, N. O. Effects of Size of Macrocyclic Polyamides on Their Rate of Diffusion in Model Membranes. *Biophys. J.* **1997**, *73*, 2580–2587.

(14) Lee, C. C.; Petersen, N. O. The Lateral Diffusion of Selectively Aggregated Peptides in Giant Unilamellar Vesicles. *Biophys. J.* **2003**, *84*, 1756–1764.

(15) Nyholm, T. K. M.; Özdirekcan, S.; Killian, J. A. How Protein Transmembrane Segments Sense the Lipid Environment. *Biochemistry* **2007**, *46*, 1457–1465.

(16) Holt, A.; Killian, J. A. Orientation and Dynamics of Transmembrane Peptides: The Power of Simple Models. *Eur. Biophys. J.* **2010**, *39*, 609–621.

(17) Strandberg, E.; Esteban-Martín, S.; Ulrich, A. S.; Salgado, J. Hydrophobic Mismatch of Mobile Transmembrane Helices: Merging Theory and Experiments. *Biochim. Biophys. Acta Biomembr.* **2012**, *1818*, 1242–1249.

(18) Domański, J.; Marrink, S. J.; Schäfer, L. V. Transmembrane Helices Can Induce Domain Formation in Crowded Model Membranes. *Biochim. Biophys. Acta Biomembr.* **2012**, *1818*, 984–994.

(19) de Planque, M. R. R.; Bonev, B. B.; Demmers, J. A. A.; Greathouse, D. V.; Koeppe, R. E., II; Separovic, F.; Watts, A.; Killian, J. A. Interfacial Anchor Properties of Tryptophan Residues in Transmembrane Peptides Can Dominate over Hydrophobic Matching Effects in Peptide-Lipid Interactions. *Biochemistry* **2003**, *42*, 5341–5348.

(20) de Jesus, A. J.; Allen, T. W. The Determinants of Hydrophobic Mismatch Response for Transmembrane Helices. *Biochim. Biophys. Acta Biomembr.* **2013**, *1828*, 851–863.

(21) de Jesus, A. J.; Allen, T. W. The Role of Tryptophan Side Chains in Membrane Protein Anchoring and Hydrophobic Mismatch. *Biochim. Biophys. Acta Biomembr.* **2013**, *1828*, 864–876.

(22) Gambin, Y.; Reffay, M.; Sierecki, E.; Homblé, F.; Hodges, R. S.; Gov, N. S.; Taulier, N.; Urbach, W. Variation of the Lateral Mobility of Transmembrane Peptides with Hydrophobic Mismatch. *J. Phys. Chem. B* **2010**, *114*, 3559–3566.

(23) Ramadurai, S.; Holt, A.; Schäfer, L. V.; Krasnikov, V. V.; Rijkers, D. T. S.; Marrink, S. J.; Killian, J. A.; Poolman, B. Influence of Hydrophobic Mismatch and Amino Acid Composition on the Lateral Diffusion of Transmembrane Peptides. *Biophys. J.* **2010**, *99*, 1447–1454.

(24) Sparr, E.; Ash, W. L.; Nazarov, P. V.; Rijkers, D. T. S.; Hemminga, M. A.; Tieleman, D. P.; Killian, J. A. Self-Association of Transmembrane α-Helices in Model Membranes: Importance of Helix Orientation and Role of Hydrophobic Mismatch. *J. Biol. Chem.* **2005**, *280*, 39324–39331.

(25) MacKenzie, K. R. Folding and Stability of α-Helical Integral Membrane Proteins. *Chem. Rev.* **2006**, *106*, 1931–1977.

(26) Li, E.; Wimley, W. C.; Hristova, K. Transmembrane Helix Dimerization: Beyond the Search for Sequence Motifs. *Biochim. Biophys. Acta Biomembr.* **2012**, *1818*, 183–193.

(27) Fink, A.; Sal-Man, N.; Gerber, D.; Shai, Y. Transmembrane Domains Interactions Within the Membrane Milieu: Principles, Advances and Challenges. *Biochim. Biophys. Acta Biomembr.* **2012**, *1818*, 974–983.

(28) Chakrabarti, A.; Matko, J.; Rahman, N. A.; Barisas, B. G.; Edidin, M. Self-Association of Class I Major Histocompatibility Complex Molecules in

Liposome and Cell Surface Membranes. *Biochemistry* **1992**, *31*, 7182–7189.

(29) Ramadurai, S.; Holt, A.; Krasnikov, V.; van den Bogaart, G.; Killian, J. A.; Poolman, B. Lateral Diffusion of Membrane Proteins. *J. Am. Chem. Soc.* **2009**, *131*, 12650–12656.

(30) Crane, J. M.; Verkman, A. S. Long-Range Nonanomalous Diffusion of Quantum Dot-Labeled Aquaporin-1 Water Channels in the Cell Plasma Membrane. *Biophys. J.* **2008**, *94*, 702–713.

(31) Verkman, A. S.; Rossi, A.; Crane, J. M. Live-Cell Imaging of Aquaporin-4 Supramolecular Assembly and Diffusion. *Methods Enzymol.* **2012**, *504*, 341–354.

(32) Iacovache, I.; Bischofberger, M.; van der Goot, F. G. Structure and Assembly of Pore-Forming Proteins. *Curr. Opin. Struc. Biol.* **2010**, *20*, 241–246.

(33) Parker, M. W.; Feil, S. C. Pore-Forming Protein Toxins: From Structure to Function. *Prog. Biophys. Mol. Biol.* **2005**, *88*, 91–142.

(34) Tulumello, D. V.; Johnson, R. M.; Isupov, I.; Deber, C. M. Design, Expression, and Purification of De Novo Transmembrane "hairpin" Peptides. *Biopolymers (Pept. Sci.)* **2012**, *98*, 546–556.

(35) Korendovych, I. V.; Senes, A.; Kim, Y. H.; Lear, J. D.; Fry, H. C.; Therien, M. J.; Blasie, J. K.; Walker, F. A.; DeGrado, W. F. De Novo Design and Molecular Assembly of a Transmembrane Diporphyrin-Binding Protein Complex. *J. Am. Chem. Soc.* **2010**, *132*, 15516–15518.

(36) Lichtenstein, B. R. et al. Engineering Oxidoreductases: Maquette Proteins Designed from Scratch. *Biochem. Soc. Trans.* **2012**, *40*, 561–566.

(37) Gambin, Y.; Lopez-Esparza, R.; Reffay, M.; Sierecki, E.; Gov, N. S.; Genest, M.; Hodges, R. S.; Urbach, W. Lateral Mobility of Proteins in Liquid Membranes Revisited. *Proc. Natl. Acad. Sci. USA* **2006**, *103*, 2098–2102.

(38) Luckey, M. *Membrane Structural Biology: With Biochemical and Biophysical Foundations*; Cambridge: Cambridge University Press, 2008; pp 113–124.

(39) Koebnik, R.; Locher, K. P.; Van Gelder, P. Structure and Function of Bacterial Outer Membrane Proteins: Barrels in a Nutshell. *Mol. Microbiol.* **2000**, *37*, 239–253.

(40) Schulz, G. E. β-Barrel Membrane Proteins. *Curr. Opin. Struc. Biol.* **2000**, *10*, 443–447.

(41) Schulz, G. E. The Structure of Bacterial Outer Membrane Proteins. *Biochim. Biophys. Acta Biomembr.* **2002**, *1565*, 308–317.

(42) Wimley, W. C. The Versatile β-Barrel Membrane Protein. *Curr. Opin. Struc. Biol.* **2003**, *13*, 404–411.

(43) Galdiero, S.; Galdiero, M.; Pedone, C. β-Barrel Membrane Bacterial Proteins: Structure, Function, Assembly and Interaction with Lipids. *Curr. Protein Pept. Sci.* **2007**, *8*, 63–82.

(44) Murzin, A. G.; Lesk, A. M.; Chothia, C. Principles Determining the Structure of β-Sheet Barrels in Proteins. I. a Theoretical Analysis. *J. Mol. Biol.* **1994**, *236*, 1369–1381.

(45) Reboul, C. F.; Mahmood, K.; Whisstock, J. C.; Dunstone, M. A. Predicting Giant Transmembrane β-Barrel Architecture. *Bioinformatics* **2012**, *28*, 1299–1302.

(46) Freeman, T. C., Jr.; Wimley, W. C. A Highly Accurate Statistical Approach for the Prediction of Transmembrane β-Barrels. *Bioinformatics* **2010**, *26*, 1965–1974.

(47) Freeman, T. C., Jr.; Wimley, W. C. TMBB-DB: a Transmembrane β-Barrel Proteome Database. *Bioinformatics* **2012**, *28*, 2425–2430.

(48) Fairman, J. W.; Noinaj, N.; Buchanan, S. K. The Structural Biology of β-Barrel Membrane Proteins: A Summary of Recent Reports. *Curr. Opin. Struc. Biol.* **2011**, *21*, 523–531.

(49) Pautsch, A.; Schulz, G. E. Structure of the Outer Membrane Protein A Transmembrane Domain. *Nat. Struct. Biol.* **1998**, *5*, 1013–1017.

(50) Vogt, J.; Schulz, G. E. The Structure of the Outer Membrane Protein OmpX from *Escherichia Coli* Reveals Possible Mechanisms of Virulence. *Structure* **1999**, *7*, 1301–1309.

(51) Zeth, K.; Thein, M. Porins in Prokaryotes and Eukaryotes: Common Themes and Variations. *Biochem. J.* **2010**, *431*, 13–22.

(52) Mohammad, M. M.; Iyer, R.; Howard, K. R.; McPike, M. P.; Borer, P. N.; Movileanu, L. Engineering a Rigid Protein Tunnel for Biomolecular Detection. *J. Am. Chem. Soc.* **2012**, *134*, 9521–9531.

(53) Remaut, H.; Tang, C.; Henderson, N. S.; Pinkner, J. S.; Wang, T.; Hultgren, S. J.; Thanassi, D. G.; Waksman, G.; Li, H. Fiber Formation Across the Bacterial Outer Membrane by the Chaperone/usher Pathway. *Cell* **2008**, *133*, 640–652.

(54) Ellena, J. F.; Lackowicz, P.; Mongomery, H.; Cafiso, D. S. Membrane Thickness Varies Around the Circumference of the Transmembrane Protein BtuB. *Biophys. J.* **2011**, *100*, 1280–1287.

(55) White, S. H. Biophysical Dissection of Membrane Proteins. *Nature* **2009**, *459*, 344–346.

(56) Johansson, M. U.; Alioth, S.; Hu, K.; Walser, R.; Koebnik, R.; Pervushin, K. A Minimal Transmembrane β-Barrel Platform Protein Studied by Nuclear Magnetic Resonance. *Biochemistry* **2007**, *46*, 1128–1140.

(57) Naveed, H.; Jimenez-Morales, D.; Tian, J.; Pasupuleti, V.; Kenney, L. J.; Liang, J. Engineered Oligomerization State of OmpF Protein Through Computational Design Decouples Oligomer Dissociation from Unfolding. *J. Mol. Biol.* **2012**, *419*, 89–101.

(58) Arnold, T.; Poynor, M.; Nussberger, S.; Lupas, A. N.; Linke, D. Gene Duplication of the Eight-

Stranded β-Barrel OmpX Produces a Functional Pore: A Scenario for the Evolution of Transmembrane β-Barrels. *J. Mol. Biol.* **2007**, *366*, 1174–1184.

(59) Lolicato, M.; Reina, S.; Messina, A.; Guarino, F.; Winterhalter, M.; Benz, R.; De Pinto, V. Generation of Artificial Channels by Multimerization of β-Strands from Natural Porin. *Biol. Chem.* **2011**, *392*, 617–624.

(60) Krewinkel, M.; Dworeck, T.; Fioroni, M. Engineering of an *E. Coli* Outer Membrane Protein FhuA with Increased Channel Diameter. *J. Nanobiotechnol.* **2011**, *9*, 33.

(61) Muhammad, N.; Dworeck, T.; Fioroni, M.; Schwaneberg, U. Engineering of the *E. Coli* Outer Membrane Protein FhuA to Overcome the Hydrophobic Mismatch in Thick Polymeric Membranes. *J. Nanobiotechnol.* **2011**, *9*, 8.

(62) Mohammad, M. M.; Howard, K. R.; Movileanu, L. Redesign of a Plugged β-Barrel Membrane Protein. *J. Biol. Chem.* **2011**, *286*, 8000–8013.

(63) Gouaux, E. α-Hemolysin from *Staphylococcus Aureus*: An Archetype of β-Barrel, Channel-Forming Toxins. *J. Struct. Biol.* **1998**, *121*, 110–122.

(64) Tweten, R. K. Cholesterol-Dependent Cytolysins, a Family of Versatile Pore-Forming Toxins. *Infect. Immun.* **2005**, *73*, 6199–6209.

(65) Tilley, S. J.; Orlova, E. V.; Gilbert, R. J. C.; Andrew, P. W.; Saibil, H. R. Structural Basis of Pore Formation by the Bacterial Toxin Pneumolysin. *Cell* **2005**, *121*, 247–256.

(66) Dunstone, M. A.; Tweten, R. K. Packing a Punch: The Mechanism of Pore Formation by Cholesterol Dependent Cytolysins and Membrane Attack Complex/perforin-like Proteins. *Curr. Opin. Struc. Biol.* **2012**, *22*, 342–349.

(67) Hale, C. M.; Sun, S. X.; Wirtz, D. Resolving the Role of Actoymyosin Contractility in Cell Microrheology. *PLoS One* **2009**, *4*, e7054.

(68) Duits, M. H. G.; Li, Y.; Vanapalli, S. A.; Mugele, F. Mapping of Spatiotemporal Heterogeneous Particle Dynamics in Living Cells. *Phys. Rev. E* **2009**, *79*, 051910.

(69) Poon, W. C. K.; Weeks, E. R.; Royall, C. P. On Measuring Colloidal Volume Fractions. *Soft Matter* **2012**, *8*, 21–30.

(70) Royall, C. P.; Poon, W. C. K.; Weeks, E. R. In Search of Colloidal Hard Spheres. *Soft Matter* **2013**, *9*, 17–27.

(71) Schärtl, W. Crosslinked Spherical Nanoparticles with Core-Shell Topology. *Adv. Mater.* **2000**, *12*, 1899–1908.

(72) Kogan, M.; Dibble, C. J.; Rogers, R. E.; Solomon, M. J. Viscous Solvent Colloidal System for Direct Visualization of Suspension Structure, Dynamics and Rheology. *J. Colloid Interface Sci.* **2008**, *318*, 252–263.

(73) Rousseau, G.; Fensterbank, H.; Baczko, K.; Cano, M.; Allard, E.; Larpent, C. Azido-Coated Nanoparticles: A Versatile Clickable Platform for the Preparation of Fluorescent Polystyrene Core-PAMAM Shell Nanoparticles. *Macromolecules* **2012**, *45*, 3513–3522.

(74) Pfaff, A.; Müller, A. H. E. Hyperbranched Glycopolymer Grafted Microspheres. *Macromolecules* **2011**, *44*, 1266–1272.

(75) Pfaff, A.; Shinde, V. S.; Lu, Y.; Wittemann, A.; Ballauff, M.; Müller, A. H. E. Glycopolymer-Grafted Polystyrene Nanospheres. *Macromol. Biosci.* **2011**, *11*, 199–210.

(76) van der Vlist, J.; Schönen, I.; Loos, K. Utilization of Glycosyltransferases for the Synthesis of a Densely Packed Hyperbranched Polysaccharide Brush Coating As Artificial Glycocalyx. *Biomacromolecules* **2011**, *12*, 3728–3732.

(77) Tolić-Nørrelykke, I. M.; Munteanu, E.-L.; Thon, G.; Oddershede, L.; Berg-Sørensen, K. Anomalous Diffusion in Living Yeast Cells. *Phys. Rev. Lett.* **2004**, *93*, 078102.

(78) He, Y.; Burov, S.; Metzler, R.; Barkai, E. Random Time-Scale Invariant Diffusion and Transport Coefficients. *Phys. Rev. Lett.* **2008**, *101*, 058101.

(79) Selhuber-Unkel, C.; Yde, P.; Berg-Sørensen, K.; Oddershede, L. B. Variety in Intracellular Diffusion During the Cell Cycle. *Phys. Biol.* **2009**, *6*, 025015.

(80) Jeon, J.-H.; Tejedor, V.; Burov, S.; Barkai, E.; Selhuber-Unkel, C.; Berg-Sørensen, K.; Oddershede, L.; Metzler, R. *in Vivo* Anomalous Diffusion and Weak Ergodicity Breaking of Lipid Granules. *Phys. Rev. Lett.* **2011**, *106*, 048103.

(81) Leijnse, N.; Jeon, J.-H.; Loft, S.; Metzler, R.; Oddershede, L. B. Diffusion Inside Living Human Cells. *Eur. Phys. J.: Spec. Top.* **2012**, *204*, 75–84.

(82) Saka, H. A.; Valdivia, R. Emerging Roles for Lipid Droplets in Immunity and Host-Pathogen Interactions. *Annu. Rev Cell Dev. Biol.* **2012**, *28*, 411–437.

(83) Digel, M.; Ehehalt, R.; Füllekrug, J. Lipid Droplets Lighting Up: Insights from Live Microscopy. *FEBS Lett.* **2010**, *584*, 2168–2175.

(84) Fujimoto, T.; Parton, R. G. Not Just Fat: The Structure and Function of the Lipid Droplet. *Cold Spring Harbor Perspect. Biol.* **2011**, *3*, a004838.

(85) Terasaki, M.; Jaffe, L. A. Organization of the Sea Urchin Egg Endoplasmic Reticulum and Its Reorganization at Fertilization. *J. Cell Biol.* **1991**, *114*, 929–940.

(86) Pinaud, F.; Clarke, S.; Sittner, A.; Dahan, M. Probing Cellular Events, One Quantum Dot at a Time. *Nat. Methods* **2010**, *7*, 275–285.

(87) Smith, A. M.; Nie, S. Semiconductor Nanocrystals: Structure, Properties, and Band Gap Engineering. *Acc. Chem. Res.* **2010**, *43*, 190–200.

(88) Howarth, M.; Liu, W.; Puthenveetil, S.; Zheng, Y.; Marshall, L. F.; Schmidt, M. M.; Wittrup, K. D.; Bawendi, M. G.; Ting, A. Y. Monovalent, Reduced-Size Quantum Dots for Imaging Receptors on Living Cells. *Nat. Methods* **2008**, *5*, 397–399.

(89) Cordes, T.; Maiser, A.; Steinhauer, C.; Schermelleh, L.; Tinnefeld, P. Mechanisms and Advancement of Antifading Agents for Fluorescence Microscopy and Single-Molecule Spectroscopy. *Phys. Chem. Chem. Phys.* **2011**, *13*, 6699–6709.

(90) Nadeau, J. L.; Carlini, L.; Suffern, D.; Ivanova, O.; Bradforth, S. E. Effects of β-Mercaptoethanol on Quantum Dot Emission Evaluated from Photoluminescence Decays. *J. Phys. Chem. C* **2012**, *116*, 2728–2739.

(91) Wang, X.; Ren, X.; Kahen, K.; Hahn, M. A.; Rajeswaran, M.; Maccagnano-Zacher, S.; Silcox, J.; Cragg, G. E.; Efros, A. L.; Krauss, T. D. Non-Blinking Semiconductor Nanocrystals. *Nature* **2009**, *459*, 686–689.

(92) Mahler, B.; Spinicelli, P.; Buil, S.; Quelin, X.; Hermier, J.-P.; Dubertret, B. Towards Non-Blinking Colloidal Quantum Dots. *Nat. Mater.* **2008**, *7*, 659–664.

(93) Chen, Y.; Vela, J.; Htoon, H.; Casson, J. L.; Werder, D. J.; Bussian, D. A.; Klimov, V. I.; Hollingsworth, J. A. "Giant" Multishell CdSe Nanocrystal Quantum Dots with Suppressed Blinking. *J. Am. Chem. Soc.* **2008**, *130*, 5026–5027.

(94) Li, J. J.; Wang, Y. A.; Guo, W.; Keay, J. C.; Mishima, T. D.; Johnson, M. B.; Peng, X. Large-Scale Synthesis of Nearly Monodisperse CdSe/CdS Core/shell Nanocrystals Using Air-Stable Reagents Via Successive Ion Layer Adsorption and Reaction. *J. Am. Chem. Soc.* **2003**, *125*, 12567–12575.

(95) Brovelli, S.; Schaller, R. D.; Crooker, S. A.; García-Santamaría, F.; Chen, Y.; Viswanatha, R.; Hollingsworth, J. A.; Htoon, H.; Klimov, V. I. Nano-Engineered Electron-Hole Exchange Interaction Controls Exciton Dynamics in Core-Shell Semiconductor Nanocrystals. *Nat. Commun.* **2011**, *2*, 280.

(96) Ghosh, Y.; Mangum, B. D.; Casson, J. L.; Williams, D. J.; Htoon, H.; Hollingsworth, J. A. New Insights into the Complexities of Shell Growth and the Strong Influence of Particle Volume in Nonblinking "Giant" Core/Shell Nanocrystal Quantum Dots. *J. Am. Chem. Soc.* **2012**, *134*, 9634–9643.

(97) Guo, Y.; Marchuk, K.; Sampat, S.; Abraham, R.; Fang, N.; Malko, A. V.; Vela, J. Unique Challenges Accompany Thick-Shell CdSe/n CdS ($n >$ 10) Nanocrystal Synthesis. *J. Phys. Chem. C* **2012**, *116*, 2791–2800.

(98) Galland, C.; Ghosh, Y.; Steinbrück, A.; Sykora, M.; Hollingsworth, J. A.; Klimov, V. I.; Htoon, H. Two Types of Luminescence Blinking Revealed by Spectroelectrochemistry of Single Quantum Dots. *Nature* **2011**, *479*, 203–U75.

(99) Arnspang, E. C.; Brewer, J. R.; Lagerholm, B. C. Multi-Color Single Particle Tracking with Quantum Dots. *PLoS One* **2012**, *7*, e48521.

(100) Cutler, P. J.; Malik, M. D.; Liu, S.; Byars, J. M.; Lidke, D. S.; Lidke, K. A. Multi-Color Quantum Dot Tracking Using a High-Speed Hyperspectral Line-Scanning Microscope. *PLoS One* **2013**, *8*, e64320.

(101) Lees, E. E.; Gunzburg, M. J.; Nguyen, T.-L.; Howlett, G. J.; Rothacker, J.; Nice, E. C.; Clayton, A. H. A.; Mulvaney, P. Experimental Determination of Quantum Dot Size Distributions, Ligand Packing Densities, and Bioconjugation Using Analytical Ultracentrifugation. *Nano Lett.* **2008**, *8*, 2883–2890.

(102) Carney, R. P.; Kim, J. Y.; Qian, H.; Jin, R.; Mehenni, H.; Stellacci, F.; Bakr, O. M. Determination of Nanoparticle Size Distribution Together with Density or Molecular Weight by 2D Analytical Ultracentrifugation. *Nat. Commun.* **2011**, *2*, 335.

(103) Sperling, R. A.; Pellegrino, T.; Li, J. K.; Chang, W. H.; Parak, W. J. Electrophoretic Separation of Nanoparticles with a Discrete Number of Functional Groups. *Adv. Funct. Mater.* **2006**, *16*, 943–948.

(104) Lin, C.-A. J.; Sperling, R. A.; Li, J. K.; Yang, T.-Y.; Li, P.-Y.; Zanella, M.; Chang, W. H.; Parak, W. J. Design of an Amphiphilic Polymer for Nanoparticle Coating and Functionalization. *Small* **2008**, *4*, 334–341.

(105) Pellach, M.; Goldshtein, J.; Ziv-Polat, O.; Margel, S. Functionalised, Photostable, Fluorescent Polystyrene Nanoparticles of Narrow Size-Distribution. *J. Photochem. Photobiol. A* **2012**, *228*, 60–67.

(106) Burns, A.; Ow, H.; Wiesner, U. Fluorescent Core-Shell Silica Nanoparticles: Towards "Lab on a Particle" Architectures for Nanobiotechnology. *Chem. Soc. Rev.* **2006**, *35*, 1028–1042.

(107) Sokolova, V.; Epple, M. Synthetic Pathways to Make Nanoparticles Fluorescent. *Nanoscale* **2011**, *3*, 1957–1962.

(108) Hermanson, G. T. *Bioconjugate Techniques*, 2nd ed.; Amsterdam: Academic Press, 2008; 1202 pages.

(109) Kegel, W. K.; van Blaaderen, A. Direct Observation of Dynamical Heterogeneities in Colloidal Hard-Sphere Suspensions. *Science* **2000**, *287*, 290–293.

(110) Demirörs, A. F.; van Blaaderen, A.; Imhof, A. A General Method to Coat Colloidal Particles with Titania. *Langmuir* **2010**, *26*, 9297–9303.

(111) Viravathana, P.; Marr, D. W. M. Optical Trapping of Titania/silica Core-Shell Colloidal Particles. *J. Colloid Interface Sci.* **2000**, *221*, 301–307.

(112) Nunes, J. de S.; Asua, J. M. Theory-Guided Strategy for Nanolatex Synthesis. *Langmuir* **2012**, *28*, 7333–7342.

(113) Dullens, R. P. A. Colloidal Hard Spheres: Cooking and Looking. *Soft Matter* **2006**, *2*, 805–810.

(114) Velikov, K. P.; Zegers, G. E.; van Blaaderen, A. Synthesis and Characterization of Large Colloidal Silver Particles. *Langmuir* **2003**, *19*, 1384–1389.

(115) Dullens, R. P. A.; Claesson, M.; Derks, D.; van Blaaderen, A.; Kegel, W. K. Monodisperse Core-

Shell Poly(methyl Methacrylate) Latex Colloids. *Langmuir* **2003**, *19*, 5963–5966.

(116) Peng, B.; van der Wee, E.; Imhof, A.; van Blaaderen, A. Synthesis of Monodisperse, Highly Cross-Linked, Fluorescent PMMA Particles by Dispersion Polymerization. *Langmuir* **2012**, *28*, 6776–6785.

(117) Blechinger, J.; Herrmann, R.; Kiener, D.; García-García, F. J.; Scheu, C.; Reller, A.; Bräuchle, C. Perylene-Labeled Silica Nanoparticles: Synthesis and Characterization of Three Novel Silica Nanoparticle Species for Live-Cell Imaging. *Small* **2010**, *6*, 2427–2435.

(118) Ow, H.; Larson, D. R.; Srivastava, M.; Baird, B. A.; Webb, W. W.; Wiesner, U. Bright and Stable Core-Shell Fluorescent Silica Nanoparticles. *Nano Lett.* **2005**, *5*, 113–117.

(119) Larson, D. R.; Ow, H.; Vishwasrao, H. D.; Heikal, A. A.; Wiesner, U.; Webb, W. W. Silica Nanoparticle Architecture Determines Radiative Properties of Encapsulated Fluorophores. *Chem. Mater.* **2008**, *20*, 2677–2684.

(120) Burns, A. A.; Vider, J.; Ow, H.; Herz, E.; Penate-Medina, O.; Baumgart, M.; Larson, S. M.; Wiesner, U.; Bradbury, M. Fluorescent Silica Nanoparticles with Efficient Urinary Excretion for Nanomedicine. *Nano Lett.* **2009**, *9*, 442–448.

(121) Cho, E.-B.; Volkov, D. O.; Sokolov, I. Ultrabright Fluorescent Mesoporous Silica Nanoparticles. *Small* **2010**, *6*, 2314–2319.

(122) Yu, S.-J.; Kang, M.-W.; Chang, H.-C.; Chen, K.-M.; Yu, Y.-C. Bright Fluorescent Nanodiamonds: No Photobleaching and Low Cytotoxicity. *J. Am. Chem. Soc.* **2005**, *127*, 17604–17605.

(123) Aharonovich, I.; Castelletto, S.; Simpson, D. A.; Su, C.-H.; Greentree, A. D.; Prawer, S. Diamond-Based Single-Photon Emitters. *Rep. Prog. Phys.* **2011**, *74*, 076501.

(124) Shang, L.; Dong, S.; Nienhaus, G. U. Ultra-Small Fluorescent Metal Nanoclusters: Synthesis and Biological Applications. *Nano Today* **2011**, *6*, 401–418.

(125) Estrada, L. C.; Gratton, E. Spectroscopic Properties of Gold Nanoparticles at the Single-Particle Level in Biological Environments. *ChemPhysChem* **2012**, *13*, 1087–1092.

(126) Graf, C.; Vossen, D. L. J.; Imhof, A.; van Blaaderen, A. A General Method to Coat Colloidal Particles with Silica. *Langmuir* **2003**, *19*, 6693–6700.

(127) De Brabander, M.; Geerts, H.; Nuyens, R.; Nuydens, R.; Cornelissen, F. In *Electronic Light Microscopy*; Shotton, D., Ed.; New York: Wiley-Liss, 1993; pp 141–155.

(128) Kusumi, A.; Nakada, C.; Ritchie, K.; Murase, K.; Suzuki, K.; Murakoshi, H.; Kasai, R. S.; Kondo, J.; Fujiwara, T. Paradigm Shift of the Plasma Membrane Concept from the Two-Dimensional Continuum Fluid to the Partitioned Fluid: High-Speed Single-Molecule Tracking of Membrane Molecules. *Annu. Rev. Biophys. Biomol. Struct.* **2005**, *34*, 351–U54.

(129) Cantor, C. R.; Schimmel, P. R. *Biophysical Chemistry*; New York: W. H. Freeman and Co., 1980; Vol. II; pp 557–558,560–565.

(130) Hunter, R. J. *Foundations of Colloid Science*, 2nd ed.; Oxford: Oxford University Press, 2001; pp 185–187.

(131) García de la Torre, J.; Huertas, M. L.; Carrasco, B. Calculation of Hydrodynamic Properties of Globular Proteins from Their Atomic-Level Structure. *Biophys. J.* **2000**, *78*, 719–730.

(132) Ortega, A.; Amorós, D.; García de la Torre, J. Prediction of Hydrodynamic and Other Solution Properties of Rigid Proteins from Atomic- and Residue-Level Models. *Biophys. J.* **2011**, *101*, 892–898.

(133) Aragon, S. R. Recent Advances in Macromolecular Hydrodynamic Modeling. *Methods* **2011**, *54*, 101–114.

(134) Tyn, M. T.; Gusek, T. W. Prediction of Diffusion Coefficients of Proteins. *Biotechnol. Bioeng.* **1990**, *35*, 327–338.

(135) Dill, K. A.; Ghosh, K.; Schmit, J. D. Physical Limits of Cells and Proteomes. *Proc. Natl. Acad. Sci. USA* **2011**, *108*, 17876–17882.

(136) Hong, L.; Lei, J. Scaling Law for the Radius of Gyration of Proteins and Its Dependence on Hydrophobicity. *J. Polym. Sci., Part B: Polym. Phys.* **2009**, *47*, 207–214.

(137) McGuffee, S. R.; Elcock, A. H. Diffusion, Crowding & Protein Stability in a Dynamic Molecular Model of the Bacterial Cytoplasm. *PLoS Comput. Biol.* **2010**, *6*, e1000694.

(138) Kalwarczyk, T.; Tabaka, M.; Holyst, R. Biologistics – Diffusion Coefficients for Complete Proteome of *Escherichia Coli*. *Bioinformatics* **2012**, *28*, 2971–2978.

(139) Kumar, M.; Mommer, M. S.; Sourjik, V. Mobility of Cytoplasmic, Membrane, and DNA-Binding Proteins in *Escherichia Coli*. *Biophys. J.* **2010**, *98*, 552–559.

(140) Nenninger, A.; Mastroianni, G.; Mullineaux, C. W. Size Dependence of Protein Diffusion in the Cytoplasm of *Escherichia Coli*. *J. Bacteriol.* **2010**, *192*, 4535–4540.

(141) Tanner, D. E.; Ma, W.; Chen, Z.; Schulten, K. Theoretical and Computational Investigation of Flagellin Translocation and Bacterial Flagellum Growth. *Biophys. J.* **2011**, *100*, 2548–2556.

(142) Adams, M. J.; Antoniw, J. F. DPVweb: a Comprehensive Database of Plant and Fungal Virus Genes and Genomes. *Nucleic Acids Res.* **2006**, *34*, D382–D385.

(143) Carrillo-Tripp, M.; Shepherd, C. M.; Borelli, I. A.; Venkataraman, S.; Lander, G.; Natarajan, P.; Johnson, J. E.; Brooks, C. L., III; Reddy, V. S. VIPERdb^2: an Enhanced and Web API Enabled

Relational Database for Structural Virology. *Nucleic Acids Res.* **2009**, *37*, D436–D442.

(144) O'Connell, J. E.; Grinberg, V. Ya.; de Kruif, C. G. Association Behavior of β-Casein. *J. Colloid Interface Sci.* **2003**, *258*, 33–39.

(145) Dodd, J.; Hill, W. E. Physical Characteristics of Ribosomal Protein S4 from *Escherichia Coli*. *J. Biol. Chem.* **1987**, *262*, 2478–2484.

(146) Aragon, S.; Hahn, D. K. Precise Boundary Element Computation of Protein Transport Properties: Diffusion Tensors, Specific Volume, and Hydration. *Biophys. J.* **2006**, *91*, 1591–1603.

(147) Brookes, E.; Demeler, B.; Rocco, M. Developments in the US-SOMO Bead Modeling Suite: New Features in the Direct Residue-To-Bead Method, Improved Grid Routines, and Influence of Accessible Surface Area Screening. *Macromol. Biosci.* **2010**, *10*, 746–753.

(148) Robertson, R. M.; Laib, S.; Smith, D. E. Diffusion of Isolated DNA Molecules: Dependence on Length and Topology. *Proc. Natl. Acad. Sci. USA* **2006**, *103*, 7310–7314.

(149) Amorós, D.; Ortega, A.; García de la Torre, J. Hydrodynamic Properties of Wormlike Macromolecules: Monte Carlo Simulation and Global Analysis of Experimental Data. *Macromolecules* **2011**, *44*, 5788–5797.

(150) Pavlov, G.; Finet, S.; Tatarenko, K.; Korneeva, E.; Ebel, C. Conformation of Heparin Studied with Macromolecular Hydrodynamic Methods and X-Ray Scattering. *Eur. Biophys. J.* **2003**, *32*, 437–449.

(151) Nishinari, K.; Kohyama, K.; Williams, P. A.; Phillips, G. O.; Burchard, W.; Ogino, K. Solution Properties of Pullulan. *Macromolecules* **1991**, *24*, 5590–5593.

(152) Nordmeier, E. Static and Dynamic Light-Scattering Solution Behavior of Pullulan and Dextran in Comparison. *J. Phys. Chem.* **1993**, *97*, 5770–5785.

(153) Rolland-Sabaté, A.; Mendez-Montealvo, M. G.; Colonna, P.; Planchot, V. Online Determination of Structural Properties and Observation of Deviations from Power Law Behavior. *Biomacromolecules* **2008**, *9*, 1719–1730.

(154) Santos, N. C.; Castanho, M. A. R. B. Teaching Light Scattering Spectroscopy: The Dimension and Shape of Tobacco Mosaic Virus. *Biophys. J.* **1996**, *71*, 1641–1650.

(155) Terry, B. R.; Matthews, E. K.; Haseloff, J. Molecular Characterization of Recombinant Green Fluorescent Protein by Fluorescence Correlation Microscopy. *Biochem. Biophys. Res. Commun.* **1995**, *217*, 21–27.

(156) Durchschlag, H.; Zipper, P. Modeling the Hydration of Proteins: Prediction of Structural and Hydrodynamic Parameters from X-Ray Diffraction and Scattering Data. *Eur. Biophys. J.* **2003**, *32*, 487–502.

(157) Peschek, J.; Braun, N.; Franzmann, T. M.; Georgalis, Y.; Haslbeck, M.; Weinkauf, S.; Buchner, J. The Eye Lens Chaperone α-Crystallin Forms Defined Globular Assemblies. *Proc. Natl. Acad. Sci. USA* **2009**, *106*, 13272–13277.

(158) Marrero, A.; Duquerroy, S.; Trapani, S.; Goulas, T.; Guevara, T.; Andersen, G. R.; Navaza, J.; Sottrup-Jensen, L.; Gomis-Rüth, F. X. The Crystal Structure of Human α_2-Macroglobulin Reveals a Unique Molecular Cage. *Angew. Chem. Int. Ed.* **2012**, *51*, 3340–3344.

(159) Kleman, M.; Lavrentovich, O. D. *Soft Matter Physics: An Introduction*; New York: Springer, 2003; pp 560–603.

(160) Rubinstein, M.; Colby, R. H. *Polymer Physics*; Oxford: Oxford University Press., 2003; pp 140–146.

(161) Wilkins, D. K.; Grimshaw, S. B.; Receveur, V.; Dobson, C. M.; Jones, J. A.; Smith, L. J. Hydrodynamic Radii of Native and Denatured Proteins Measured by Pulse Field Gradient NMR Techniques. *Biochemistry* **1999**, *38*, 16424–16431.

(162) Kohn, J. E.; Millett, I. S.; Jacob, J.; Zagrovic, B.; Dillon, T. M.; Cingel, N.; Dothager, R. S.; Seifert, S.; Thiyagarajan, P.; Sosnick, T. R.; Hasan, M. Z.; Pande, V. S.; Ruczinski, I.; Doniach, S.; Plaxco, K. W. Random-Coil Behavior and the Dimensions of Chemically Unfolded Proteins. *Proc. Natl. Acad. Sci. USA* **2004**, *101*, 12491–12496.

(163) de Belder, A. N. *Dextran*, AA ed.; Uppsala: Amersham Biosciences, 2003; 64 pages.

(164) Theodorou, D. N.; Suter, U. W. Shape of Unperturbed Linear Polymers: Polypropylene. *Macromolecules* **1985**, *18*, 1206–1214.

(165) Dima, R. I.; Thirumalai, D. Asymmetry in the Shapes of Folded and Denatured States of Proteins. *J. Phys. Chem. B* **2004**, *108*, 6564–6570.

(166) Griep, S.; Hobohm, U. PDBselect 1992-2009 and PDBfilter-Select. *Nucleic Acids Res.* **2010**, *38*, D318–D319.

(167) Saffman, P. G.; Delbrück, M. Brownian Motion in Biological Membranes. *Proc. Natl. Acad. Sci. USA* **1975**, *72*, 3111–3113.

(168) Blaber, M.; Lee, J. Designing Proteins from Simple Motifs: Opportunities in Top-down Symmetric Deconstruction. *Curr. Opin. Struc. Biol.* **2012**, *22*, 442–450.

(169) Regan, L.; DeGrado, W. F. Characterization of a Helical Protein Designed from First Principles. *Science* **1988**, *241*, 976–978.

(170) Robertson, D. E.; Farid, R. S.; Moser, C. C.; Urbauer, J. L.; Mulholland, S. E.; Pidikiti, R.; Lear, J. D.; Wand, A. J.; DeGrado, W. F.; Dutton, P. L. Design and Synthesis of Multi-Haem Proteins. *Nature* **1994**, *368*, 425–431.

(171) Discher, B. M.; Koder, R. L.; Moser, C. C.; Dutton, P. L. Hydrophilic to Amphiphilic Design in Redox Protein Maquettes. *Curr. Opin. Chem. Biol.* **2003**, *7*, 741–748.

(172) Samish, I.; MacDermaid, C. M.; Perez-Aguilar, J. M.; Saven, J. G. Theoretical and Computational Protein Design. *Annu. Rev. Phys. Chem.* **2011**, *62*, 129–149.

(173) Flower, D. R.; North, A. C. T.; Sansom, C. E. The Lipocalin Protein Family: Structural and Sequence Overview. *Biochim. Biophys. Acta, Protein Struct. Mol. Enzymol.* **2000**, *1482*, 9–24.

(174) Grzyb, J.; Latowski, D.; Strzałka, K. Lipocalins – a Family Portrait. *J. Plant Physiol.* **2006**, *163*, 895–915.

(175) Schlehuber, S.; Skerra, A. Lipocalins in Drug Discovery: From Natural Ligand-Binding Proteins to 'anticalins'. *Drug Discovery Today* **2005**, *10*, 23–33.

(176) Branden, C.; Tooze, J. *Introduction to Protein Structure*, 2nd ed.; New York: Garland Pub., 1999; pp 47–65, 67–88.

(177) Lai, Y.-T.; King, N. P.; Yeates, T. O. Principles for Designing Ordered Protein Assemblies. *Trends Cell Biol.* **2012**, *22*, 653–661.

(178) Naessens, M.; Cerdobbel, A.; Soetaert, W.; Vandamme, E. J. *Leuconostoc* Dextransucrase and Dextran: Production, Properties, and Applications. *J. Chem. Technol. Biotechnol.* **2005**, *80*, 845–860.

(179) Striegel, A. M. Multiple Detection in Size-Exclusion Chromatography of Macromolecules. *Analyt. Chem.* **2005**, *77*, 104A–113A.

(180) Burchard, W. Solution Properties of Branched Macromolecules. *Adv. Polym. Sci.* **1999**, *143*, 113–194.

(181) Vilaplana, F.; Gilbert, R. G. Characterization of Branched Polysaccharides Using Multiple-Detection Size Separation Techniques. *J. Sep. Sci.* **2010**, *33*, 3537–3554.

(182) Gaborieau, M.; Castignolles, P. Size-Exclusion Chromatography (SEC) of Branched Polymers and Polysaccharides. *Analyt. Bioanalyt. Chem.* **2011**, *399*, 1413–1423.

(183) Chang, T. Polymer Characterization by Interaction Chromatography. *J. Polym. Sci., Part B: Polym. Phys.* **2005**, *43*, 1591–1607.

(184) Hutchings, L. R. Complex Branched Polymers for Structure-Property Correlation Studies: the Case for Temperature Gradient Interaction Chromatography Analysis. *Macromolecules* **2012**, *45*, 5621–5639.

(185) Potschka, M. Inverse Size Exclusion Chromatography and Universal Calibration. *Macromol. Symp.* **1996**, *110*, 121–154.

(186) Kostanski, L. K.; Keller, D. M.; Hamielec, A. E. Size-Exclusion Chromatography – a Review of Calibration Methodologies. *J. Biochem. Biophys. Methods* **2004**, *58*, 159–186.

(187) Ioan, C. E.; Aberle, T.; Burchard, W. Structure Properties of Dextran. 3. Shrinking Factors of Individual Clusters. *Macromolecules* **2001**, *34*, 3765–3771.

(188) Guo, X.; Condra, M.; Kimura, K.; Berth, G.; Dautzenberg, H.; Dubin, P. L. Determination of Molecular Weight of Heparin by Size Exclusion Chromatography with Universal Calibration. *Anal. Biochem.* **2003**, *312*, 33–39.

(189) Rolland-Sabaté, A.; Guilois, S.; Jaillais, B.; Colonna, P. Molecular Size and Mass Distributions of Native Starches Using Complementary Separation Methods: Asymmetrical Flow Field Flow Fractionation (A4F) and Hydrodynamic and Size Exclusion Chromatography (HDC-SEC). *Analyt. Bioanalyt. Chem.* **2011**, *399*, 1493–1505.

(190) Stokke, B. T.; Elgsaeter, A.; Hara, C.; Kitamura, S.; Takeo, K. Physicochemical Properties of $(1 \rightarrow 6)$-Branched $(1 \rightarrow 3)$-β-D-Glucans. 1. Physical Dimensions Estimated from Hydrodynamic and Electron Microscopic Data. *Biopolymers* **1993**, *33*, 561–573.

(191) Dubin, P. L. Nonionic Polysaccharides As Calibration Standards for Aqueous Size Exclusion Chromatography. *Carbohydr. Polym.* **1994**, *25*, 295–303.

(192) Adolphi, U.; Kulicke, W.-M. Coil Dimensions and Conformation of Macromolecules in Aqueous Media from Flow Field-Flow Fractionation/multi-Angle Laser Light Scattering Illustrated by Studies on Pullulan. *Polymer* **1997**, *38*, 1513–1519.

(193) Yanaki, T.; Norisuye, T.; Fujita, H. Triple Helix of *Schizophyllum Commune* Polysaccharide in Dilute Solution. 3. Hydrodynamic Properties in Water. *Macromolecules* **1980**, *13*, 1462–1466.

(194) Kashiwagi, Y.; Norisuye, T.; Fujita, H. Triple Helix of *Schizophyllum Commune* Polysaccharide in Dilute Solution. 4. Light Scattering and Viscosity in Dilute Aqueous Sodium Hydroxide. *Macromolecules* **1981**, *14*, 1220–1225.

(195) Kuge, T.; Kobayashi, K.; Kitamura, S.; Tanahashi, H. GPC Analyses of Polysaccharides. 2. Degrees of Long-Chain Branching in Dextrans. *Carbohydr. Res.* **1987**, *160*, 205–214.

(196) Billmeyer, F. W., Jr The Molecular Structure of Polyethylene. III. Determination of Long Chain Branching. *J. Am. Chem. Soc.* **1953**, *75*, 6118–6122.

(197) Berry, G. C.; Orofino, T. A. Branched Polymers. III. Dimensions of Chains with Small Excluded Volume. *J. Chem. Phys.* **1964**, *40*, 1614–1621.

(198) Heinze, T.; Liebert, T.; Heublein, B.; Hornig, S. Functional Polymers Based on Dextran. *Adv. Polym. Sci.* **2006**, *205*, 199–291.

(199) Larm, O.; Lindberg, B.; Svensson, S. Studies on the Length of Side Chains of the Dextran Elaborated by *Leuconostoc Mesenteroides* NRRL B-512. *Carbohydr. Res.* **1971**, *20*, 39–48.

(200) Ioan, C. E.; Aberle, T.; Burchard, W. Structure Properties of Dextran. 2. Dilute Solution. *Macromolecules* **2000**, *33*, 5730–5739.

(201) Vollmer, A.; Voiges, K.; Bork, C.; Fiege, K.; Cuber, K.; Mischnick, P. Comprehensive Analysis of the Substitution Pattern in Dextran Ethers with

Respect to the Reaction Conditions. *Analyt. Bioanalyt. Chem.* **2009**, *395*, 1749–1768.

(202) Venturoli, D.; Rippe, B. Ficoll and Dextran Vs. Globular Proteins As Probes for Testing Glomerular Permselectivity: Effects of Molecular Size, Shape, Charge, and Deformability. *Am. J. Physiol.: Renal Physiol.* **2005**, *288*, F605–F613.

(203) Oliver, J. D., III; Deen, W. M. Random-Coil Model for Glomerular Sieving of Dextran. *Bull. Math. Biol.* **1994**, *56*, 369–389.

(204) Weiss, M.; Elsner, M.; Kartberg, F.; Nilsson, T. Anomalous Subdiffusion Is a Measure for Cytoplasmic Crowding in Living Cells. *Biophys. J.* **2004**, *87*, 3518–3524.

(205) Tomalia, D. A.; Fréchet, J. M. J. In *Dendrimers and Other Dendritic Polymers*; Fréchet, J. M. J., Tomalia, D. A., Eds.; Chichester: Wiley, 2001; pp 3–44.

(206) Carlmark, A.; Hawker, C.; Hult, A.; Malkoch, M. New Methodologies in the Construction of Dendritic Materials. *Chem. Soc. Rev.* **2009**, *38*, 352–362.

(207) Flodin, P. G. M.; Ingelman, B. G.-A. Sucrose ether copolymerizates. 1967; US Patent 3,300,474.

(208) Holmberg, L.; Lindberg, B.; Lindqvist, B. The Reaction Between Epichlorohydrin and Polysaccharides: Part 1, Syntheses of Some Model Substances with Non-Cyclic Substituents. *Carbohydr. Res.* **1994**, *262*, 213–221.

(209) Holmberg, L.; Lindberg, B.; Lindqvist, B. The Reaction Between Epichlorohydrin and Polysaccharides: Structural Elements in a Cross-Linked Dextran, Sephadex ® G-25. *Carbohydr. Res.* **1995**, *272*, 203–211.

(210) De Miguel, I.; Rieumajou, V.; Betbeder, D. New Methods to Determine the Extent of Reaction of Epichlorohydrin with Maltodextrins. *Carbohydr. Res.* **1999**, *319*, 17–23.

(211) Hamdi, G.; Ponchel, G.; Duchène, D. Formulation of Epichlorohydrin Cross-Linked Starch Microspheres. *J. Microencapsulation* **2001**, *18*, 373–383.

(212) Holmberg, L.; Lindberg, B.; Lindqvist, B. The Reaction Between Epichlorohydrin and Polysaccharides: Part 2, Synthesis of Some Model Substances, with Cyclic Substituents. *Carbohydr. Res.* **1995**, *268*, 47–56.

(213) Laurent, T. C.; Granath, K. A. Fractionation of Dextran and Ficoll by Chromatography on Sephadex G-200. *Biochim. Biophys. Acta* **1967**, *136*, 191–198.

(214) Groszek, J.; Li, L.; Ferrell, N.; Smith, R.; Zorman, C. A.; Hofmann, C. L.; Roy, S.; Fissell, W. H. Molecular Conformation and Filtration Properties of Anionic Ficoll. *Am. J. Physiol.: Renal Physiol.* **2010**, *299*, F752–F757.

(215) Fissell, W. H.; Hofmann, C. L.; Smith, R.; Chen, M. H. Size and Conformation of Ficoll As Determined by Size-Exclusion Chromatography Followed by Multiangle Light Scattering. *Am. J. Physiol.: Renal Physiol.* **2010**, *298*, F205–F208.

(216) Lavrenko, P. N.; Mikryukova, O. I.; Didenko, S. A. Hydrodynamic Properties and the Shape of the Molecules of the Polysaccharide Ficoll-400 in Solution. *Polym. Sci. USSR* **1986**, *28*, 576–584.

(217) Georgalis, Y.; Philipp, M.; Aleksandrova, R.; Krüger, J. K. Light Scattering Studies on Ficoll PM70 Solutions Reveal Two Distinct Diffusive Modes. *J. Colloid Interface Sci.* **2012**, *386*, 141–147.

(218) Wang, Y.; Dubin, P. L. Observation of Ficoll Charge Using Size-Exclusion Chromatography. *J. Chromatog. A* **1998**, *800*, 181–185.

(219) Asgeirsson, D.; Venturoli, D.; Fries, E.; Rippe, B.; Rippe, C. Glomerular Sieving of Three Neutral Polysaccharides, Polyethylene Oxide and Bikunin in Rat. Effects of Molecular Size and Conformation. *Acta Physiol.* **2007**, *191*, 237–246.

(220) Fissell, W. H.; Manley, S.; Dubnisheva, A.; Glass, J.; Magistrelli, J.; Eldridge, A. N.; Fleischman, A. J.; Zydney, A. L.; Roy, S. Ficoll Is Not a Rigid Sphere. *Am. J. Physiol.: Renal Physiol.* **2007**, *293*, F1209–F1213.

(221) Bohrer, M. P.; Patterson, G. D.; Carroll, P. J. Hindered Diffusion of Dextran and Ficoll in Microporous Membranes. *Macromolecules* **1984**, *17*, 1170–1173.

(222) Dubin, P. L.; Edwards, S. L.; Kaplan, J. I.; Mehta, M. S.; Tomalia, D.; Xia, J. Carboxylated Starburst Dendrimers As Calibration Standards for Aqueous Size Exclusion Chromatography. *Analyt. Chem.* **1992**, *64*, 2344–2347.

(223) Hussain, S.; Mehta, M. S.; Kaplan, J. I.; Dubin, P. L. Experimental Evaluation of Conflicting Models for Size Exclusion Chromatography. *Analyt. Chem.* **1991**, *63*, 1132–1138.

(224) Oliver, J. D., III; Anderson, S.; Troy, J. L.; Brenner, B. M.; Deen, W. M. Determination of Glomerular Size-Selectivity in the Normal Rat with Ficoll. *J. Am. Soc. Nephrol.* **1992**, *3*, 214–228.

(225) Clark, C. G., Jr.; Wenzel, R. J.; Andreitchenko, E. V.; Steffen, W.; Zenobi, R.; Müllen, K. Controlled MegaDalton Assembly with Locally Stiff but Globally Flexible Polyphenylene Dendrimers. *J. Am. Chem. Soc.* **2007**, *129*, 3292–3301.

(226) Ruiz, J.; Lafuente, G.; Marcen, S.; Ornelas, C.; Lazare, S.; Cloutet, E.; Blais, J.-C.; Astruc, D. Construction of Giant Dendrimers Using a Tripodal Building Block. *J. Am. Chem. Soc.* **2003**, *125*, 7250–7257.

(227) Tomalia, D. A.; Naylor, A. M.; Goddard, W. A., III Starburst Dendrimers: Molecular-Level Control of Size, Shape, Surface Chemistry, Topology, and Flexibility from Atoms to Macroscopic Matter. *Angew. Chem. Int. Ed.* **1990**, *29*, 138–175.

(228) Astruc, D.; Boisselier, E.; Ornelas, C. Dendrimers Designed for Functions: From Physical, Photophysical, and Supramolecular Properties to Applica-

tions in Sensing, Catalysis, Molecular Electronics, Photonics, and Nanomedicine. *Chem. Rev.* **2010**, *110*, 1857–1959.

(229) Konkolewicz, D.; Monteiro, M. J.; Perrier, S. Dendritic and Hyperbranched Polymers from Macromolecular Units: Elegant Approaches to the Synthesis of Functional Polymers. *Macromolecules* **2011**, *44*, 7067–7087.

(230) Boas, U.; Christensen, J. B.; Heegaard, P. M. H. *Dendrimers in Medicine and Biotechnology: New Molecular Tools*; Cambridge: Royal Society of Chemistry, 2006; pp 1–27.

(231) Tomalia, D. A.; Fréchet, J. M. J. Discovery of Dendrimers and Dendritic Polymers: A Brief Historical Perspective. *J. Polym. Sci., Part A: Polym. Chem.* **2002**, *40*, 2719–2728.

(232) Türp, D.; Nguyen, T.-T.-T.; Baumgarten, M.; Müllen, K. Uniquely Versatile: Nano-Site Defined Materials Based on Polyphenylene Dendrimers. *New J. Chem.* **2012**, *36*, 282–298.

(233) Heek, T.; Fasting, C.; Rest, C.; Zhang, X.; Würthner, F.; Haag, R. Highly Fluorescent Water-Soluble Polyglycerol-Dendronized Perylene Bisimide Dyes. *Chem. Commun.* **2010**, *46*, 1884–1886.

(234) Zill, A. T.; Licha, K.; Haag, R.; Zimmerman, S. C. Synthesis and Properties of Fluorescent Dyes Conjugated to Hyperbranched Polyglycerols. *New J. Chem.* **2012**, *36*, 419–427.

(235) Yang, S. K.; Zimmerman, S. C. Polyglycerol-Dendronized Perylenediimides As Stable, Water-Soluble Fluorophores. *Adv. Funct. Mater.* **2012**, *22*, 3023–3028.

(236) Weil, T.; Vosch, T.; Hofkens, J.; Peneva, K.; Müllen, K. The Rylene Colorant Family–Tailored Nanoemitters for Photonics Research and Applications. *Angew. Chem. Int. Ed.* **2010**, *49*, 9068–9093.

(237) Zill, A.; Rutz, A. L.; Kohman, R. E.; Alkilany, A. M.; Murphy, C. J.; Kong, H.; Zimmerman, S. C. Clickable Polyglycerol Hyperbranched Polymers and Their Application to Gold Nanoparticles and Acid-Labile Nanocarriers. *Chem. Commun.* **2011**, *47*, 1279–1281.

(238) Pérignon, N.; Marty, J.-D.; Mingotaud, A.-F.; Dumont, M.; Rico-Lattes, I.; Mingotaud, C. Hyperbranched Polymers Analogous to PAMAM Dendrimers for the Formation and Stabilization of Gold Nanoparticles. *Macromolecules* **2007**, *40*, 3034–3041.

(239) Scott, R. W. J.; Wilson, O. M.; Crooks, R. M. Synthesis, Characterization, and Applications of Dendrimer-Encapsulated Nanoparticles. *J. Phys. Chem. B* **2005**, *109*, 692–704.

(240) Boisselier, E.; Diallo, A. K.; Salmon, L.; Ornelas, C.; Ruiz, J.; Astruc, D. Encapsulation and Stabilization of Gold Nanoparticles with "Click" Polyethyleneglycol Dendrimers. *J. Am. Chem. Soc.* **2010**, *132*, 2729–2742.

(241) Daniel, M.-C.; Grow, M. E.; Pan, H.; Bednarek, M.; Ghann, W. E.; Zabetakis, K.; Cornish, J. Gold Nanoparticle-Cored Poly(propyleneimine) Dendrimers As a New Platform for Multifunctional Drug Delivery Systems. *New J. Chem.* **2011**, *35*, 2366–2374.

(242) Zheng, J.; Zhang, C.; Dickson, R. M. Highly Fluorescent, Water-Soluble, Size-Tunable Gold Quantum Dots. *Phys. Rev. Lett.* **2004**, *93*, 077402.

(243) Zheng, J.; Nicovich, P. R.; Dickson, R. M. Highly Fluorescent Noble-Metal Quantum Dots. *Annu. Rev. Phys. Chem.* **2007**, *58*, 409–431.

(244) Striegel, A. M.; Plattner, R. D.; Willett, J. L. Dilute Solution Behavior of Dendrimers and Polysaccharides: SEC, ESI-MS, and Computer Modeling. *Analyt. Chem.* **1999**, *71*, 978–986.

(245) Hawker, C. J.; Malmström, E. E.; Frank, C. W.; Kampf, J. P. Exact Linear Analogs of Dendritic Polyether Macromolecules: Design, Synthesis, and Unique Properties. *J. Am. Chem. Soc.* **1997**, *119*, 9903–9904.

(246) Hay, G.; Mackay, M. E.; Hawker, C. J. Thermodynamic Properties of Dendrimers Compared with Linear Polymers: General Observations. *J. Polym. Sci., Part B: Polym. Phys.* **2001**, *39*, 1766–1777.

(247) Stiriba, S.-E.; Kautz, H.; Frey, H. Hyperbranched Molecular Nanocapsules: Comparison of the Hyperbranched Architecture with the Perfect Linear Analogue. *J. Am. Chem. Soc.* **2002**, *124*, 9698–9699.

(248) Ballauff, M.; Likos, C. N. Dendrimers in Solution: Insight from Theory and Simulation. *Angew. Chem. Int. Ed.* **2004**, *43*, 2998–3020.

(249) Likos, C. N. Soft Matter with Soft Particles. *Soft Matter* **2006**, *2*, 478–498.

(250) Yu, K.; Russo, P. S. Light Scattering and Fluorescence Photobleaching Recovery Study of Poly(amidoamine) Cascade Polymers in Aqueous Solution. *J. Polym. Sci., Part B: Polym. Phys.* **1996**, *34*, 1467–1475.

(251) McCain, K. S.; Schluesche, P.; Harris, J. M. Poly(amidoamine) Dendrimers As Nanoscale Diffusion Probes in Sol-Gel Films Investigated by Total Internal Reflection Fluorescence Spectroscopy. *Analyt. Chem.* **2004**, *76*, 939–946.

(252) Cheng, Y.; Prud'homme, R. K.; Thomas, J. L. Diffusion of Mesoscopic Probes in Aqueous Polymer Solutions Measured by Fluorescence Recovery After Photobleaching. *Macromolecules* **2002**, *35*, 8111–8121.

(253) Fritzinger, B.; Scheler, U. Scaling Behaviour of PAMAM Dendrimers Determined by Diffusion NMR. *Macromol. Chem. Phys.* **2005**, *206*, 1288–1291.

(254) Jiménez, V. A.; Gavin, J. A.; Alderete, J. B. Scaling Trend in Diffusion Coefficients of Low Generation G0–G3 PAMAM Dendrimers in Aqueous Solution at High and Neutral pH. *Struct. Chem.* **2012**, *23*, 123–128.

(255) del Río Echenique, G.; Rodríguez Schmidt, R.; Freire, J. J.; Hernández Cifre, J. G.; García de la Torre, J. A Multiscale Scheme for the Simulation of Conformational and Solution Properties of Different Dendrimer Molecules. *J. Am. Chem. Soc.* **2009**, *131*, 8548–8556.

(256) Kainthan, R. K.; Muliawan, E. B.; Hatzikiriakos, S. G.; Brooks, D. E. Synthesis, Characterization, and Viscoelastic Properties of High Molecular Weight Hyperbranched Polyglycerols. *Macromolecules* **2006**, *39*, 7708–7717.

(257) Wilms, D.; Stiriba, S.-E.; Frey, H. Hyperbranched Polyglycerols: From the Controlled Synthesis of Biocompatible Polyether Polyols to Multipurpose Applications. *Acc. Chem. Res.* **2010**, *43*, 129–141.

(258) Senti, F. R.; Hellman, N. N.; Ludwig, N. H.; Babcock, G. E.; Tobin, R.; Glass, C. A.; Lamberts, B. L. Viscosity, Sedimentation, and Light-Scattering Properties of Fractions of an Acid-Hydrolyzed Dextran. *J. Polym. Sci.* **1955**, *17*, 527–546.

(259) Ryu, J.-H.; Drain, J.; Kim, J. H.; McGee, S.; Gray-Weale, A.; Waddington, L.; Parker, G. J.; Hargreaves, M.; Yoo, S.-H.; Stapleton, D. Comparative Structural Analyses of Purified Glycogen Particles from Rat Liver, Human Skeletal Muscle and Commercial Preparations. *Int. J. Biol. Macromol.* **2009**, *45*, 478–482.

(260) Sullivan, M. A.; Vilaplana, F.; Cave, R. A.; Stapleton, D.; Gray-Weale, A. A.; Gilbert, R. G. Nature of α and β Particles in Glycogen Using Molecular Size Distributions. *Biomacromolecules* **2010**, *11*, 1094–1100.

(261) Fernandez, C.; Rojas, C. C.; Nilsson, L. Size, Structure and Scaling Relationships in Glycogen from Various Sources Investigated with Asymmetrical Flow Field-Flow Fractionation and ^{1}H NMR. *Int. J. Biol. Macromol.* **2011**, *49*, 458–465.

(262) Pérez, S.; Bertoft, E. The Molecular Structures of Starch Components and Their Contribution to the Architecture of Starch Granules: A Comprehensive Review. *Starch/Stärke* **2010**, *62*, 389–420.

(263) Calderón, M.; Quadir, M. A.; Sharma, S. K.; Haag, R. Dendritic Polyglycerols for Biomedical Applications. *Adv. Mater.* **2010**, *22*, 190–218.

(264) Steinhilber, D.; Seiffert, S.; Heyman, J. A.; Paulus, F.; Weitz, D. A.; Haag, R. Hyperbranched Polyglycerols on the Nanometer and Micrometer Scale. *Biomaterials* **2011**, *32*, 1311–1316.

(265) Sisson, A. L.; Haag, R. Polyglycerol Nanogels: Highly Functional Scaffolds for Biomedical Applications. *Soft Matter* **2010**, *6*, 4968–4975.

(266) de Belder, A. N.; Granath, K. Preparation and Properties of Fluorescein-Labelled Dextrans. *Carbohydr. Res.* **1973**, *30*, 375–378.

(267) Hobson, L. J.; Feast, W. J. Poly(amidoamine) Hyperbranched Systems: Synthesis, Structure and Characterization. *Polymer* **1999**, *40*, 1279–1297.

(268) Sunder, A.; Hanselmann, R.; Frey, H.; Mülhaupt, R. Controlled Synthesis of Hyperbranched Polyglycerols by Ring-Opening Multibranching Polymerization. *Macromolecules* **1999**, *32*, 4240–4246.

(269) Rokicki, G.; Rakoczy, P.; Parzuchowski, P.; Sobiecki, M. Hyperbranched Aliphatic Polyethers Obtained from Environmentally Benign Monomer: Glycerol Carbonate. *Green Chem.* **2005**, *7*, 529–539.

(270) Garamus, V. M.; Maksimova, T. V.; Kautz, H.; Barriau, E.; Frey, H.; Schlotterbeck, U.; Mecking, S.; Richtering, W. Hyperbranched Polymers: Structure of Hyperbranched Polyglycerol and Amphiphilic Poly(glycerol Ester)s in Dilute Aqueous and Nonaqueous Solution. *Macromolecules* **2004**, *37*, 8394–8399.

(271) Konkolewicz, D.; Perrier, S.; Stapleton, D.; Gray-Weale, A. Modeling Highly Branched Structures: Description of the Solution Structures of Dendrimers, Polyglycerol, and Glycogen. *J. Polym. Sci., Part B: Polym. Phys.* **2011**, *49*, 1525–1538.

(272) Baille, W. E.; Zhu, X. X.; Fomine, S. Study of Self-Diffusion of Hyperbranched Polyglycidols in Poly(vinyl Alcohol) Solutions and Gels by Pulsed-Field Gradient NMR Spectroscopy. *Macromolecules* **2004**, *37*, 8569–8576.

(273) Taton, D.; Feng, X.; Gnanou, Y. Dendrimer-like Polymers: A New Class of Structurally Precise Dendrimers with Macromolecular Generations. *New J. Chem.* **2007**, *31*, 1097–1110.

(274) Phillies, G. D. J. *Phenomenology of Polymer Solution Dynamics*; Cambridge: Cambridge University Press, 2011; pp 45–47,462–463.

(275) Teertstra, S. J.; Gauthier, M. Dendrigraft Polymers: Macromolecular Engineering on a Mesoscopic Scale. *Prog. Polym. Sci.* **2004**, *29*, 277–327.

(276) Gauthier, M. Arborescent Polymers and Other Dendrigraft Polymers: A Journey into Structural Diversity. *J. Polym. Sci., Part A: Polym. Chem.* **2007**, *45*, 3803–3810.

(277) Likos, C. N. Effective Interactions in Soft Condensed Matter Physics. *Phys. Rep.* **2001**, *348*, 267–439.

(278) Lapienis, G. Star-Shaped Polymers Having PEO Arms. *Prog. Polym. Sci.* **2009**, *34*, 852–892.

(279) Vlassopoulos, D.; Fytas, G. From Polymers to Colloids: Engineering the Dynamic Properties of Hairy Particles. *Adv. Polym. Sci.* **2010**, *236*, 1–54.

(280) Marla, K. T.; Meredith, J. C. Simulation of Interaction Forces Between Nanoparticles: End-Grafted Polymer Modifiers. *J. Chem. Theory Comput.* **2006**, *2*, 1624–1631.

(281) Roovers, J. Colloidal Properties of Star Polymers. *Macromol. Symp.* **1997**, *121*, 89–93.

(282) Likos, C. N.; Löwen, H.; Watzlawek, M.; Abbas, B.; Jucknischke, O.; Allgaier, J.; Richter, D. Star Polymers Viewed As Ultrasoft Colloidal Particles. *Phys. Rev. Lett.* **1998**, *80*, 4450–4453.

(283) Fleischer, G.; Fytas, G.; Vlassopoulos, D.; Roovers, J.; Hadjichristidis, N. Self-Diffusion of Multiarm Star Polymers in Solution Far from and Near the Ordering Transition. *Physica A* **2000**, *280*, 266–278.

(284) Wilms, D.; Schömer, M.; Wurm, F.; Hermanns, M. I.; Kirkpatrick, C. J.; Frey, H. Hyperbranched PEG by Random Copolymerization of Ethylene Oxide and Glycidol. *Macromol. Rapid Commun.* **2010**, *31*, 1811–1815.

(285) Wurm, F.; Nieberle, J.; Frey, H. Double-Hydrophilic Linear-Hyperbranched Block Copolymers Based on Poly(ethylene Oxide) and Poly(glycerol). *Macromolecules* **2008**, *41*, 1184–1188.

(286) Rele, S. M.; Cui, W. X.; Wang, L. C.; Hou, S. J.; Barr-Zarse, G.; Taton, D.; Gnanou, Y.; Esko, J. D.; Chaikof, E. L. Dendrimer-like PEO Glycopolymers Exhibit Anti-Inflammatory Properties. *J. Am. Chem. Soc.* **2005**, *127*, 10132–10133.

(287) Feng, X.-S.; Taton, D.; Chaikof, E. L.; Gnanou, Y. Toward an Easy Access to Dendrimer-like Poly(ethylene Oxide)s. *J. Am. Chem. Soc.* **2005**, *127*, 10956–10966.

(288) Wang, Y.; Therien-Aubin, H.; Baille, W. E.; Luo, J. T.; Zhu, X. X. Effect of Molecular Architecture on the Self-Diffusion of Polymers in Aqueous Systems: A Comparison of Linear, Star, and Dendritic Poly(ethylene Glycol)s. *Polymer* **2010**, *51*, 2345–2350.

(289) Zhou, H.-X.; Rivas, G.; Minton, A. P. Macromolecular Crowding and Confinement: Biochemical, Biophysical, and Potential Physiological Consequences. *Annu. Rev. Biophys.* **2008**, *37*, 375–397.

(290) Phillip, Y.; Schreiber, G. Formation of Protein Complexes in Crowded Environments - From In Vitro to In Vivo. *FEBS Lett.* **2013**, *587*, 1046–1052.

(291) Saunders, B. R.; Vincent, B. Microgel Particles As Model Colloids: Theory, Properties and Applications. *Adv. Colloid Interface Sci.* **1999**, *80*, 1–25.

(292) Paloli, D.; Mohanty, P. S.; Crassous, J. J.; Zaccarelli, E.; Schurtenberger, P. Fluid-Solid Transitions in Soft-Repulsive Colloids. *Soft Matter* **2013**, *9*, 3000–3004.

(293) Bartsch, E.; Kirsch, S.; Lindner, P.; Scherer, T.; Stölken, S. Spherical Microgel Colloids – Hard Spheres from Soft Matter. *Ber. Bunsen-Ges. Phys. Chem.* **1998**, *102*, 1597–1602.

(294) Wolfe, M. S.; Scopazzi, C. Rheology of Swellable Microgel Dispersions: Influence of Crosslink Density. *J. Colloid Interface Sci.* **1989**, *133*, 265–277.

(295) Yethiraj, A.; van Blaaderen, A. A Colloidal Model System with an Interaction Tunable from Hard Sphere to Soft and Dipolar. *Nature* **2003**, *421*, 513–517.

(296) Heyes, D. M.; Brańka, A. C. Physical Properties of Soft Repulsive Particle Fluids. *Phys. Chem. Chem. Phys.* **2007**, *9*, 5570–5575.

(297) Russel, W. B.; Saville, D. A.; Schowalter, W. R. *Colloidal Dispersions*, 1st ed.; Cambridge: Cambridge University Press, 1991; pp 115–120.

(298) Hiemenz, P. C.; Rajagopalan, R. *Principles of Colloid and Surface Chemistry*, 3rd ed.; New York: Marcel Dekker, 1997; pp 585–592.

(299) Israelachvili, J. N. *Intermolecular and Surface Forces*, 2nd ed.; San Diego, CA: Academic Press, 1992; pp 246–254.

(300) Phillips, R.; Kondev, J.; Theriot, J.; Garcia, H. G. *Physical Biology of the Cell*, 2nd ed.; New York: Garland Science, 2013; pp 554–559.

(301) de Hoog, E. H. A.; Kegel, W. K.; van Blaaderen, A.; Lekkerkerker, H. N. W. Direct Observation of Crystallization and Aggregation in a Phase-Separating Colloid-Polymer Suspension. *Phys. Rev. E* **2001**, *64*, 021407.

(302) Marenduzzo, D.; Finan, K.; Cook, P. R. The Depletion Attraction: An Underappreciated Force Driving Cellular Organization. *J. Cell Biol.* **2006**, *175*, 681–686.

(303) Chan, H. Y.; Lankevich, V.; Vekilov, P. G.; Lubchenko, V. Anisotropy of the Coulomb Interaction Between Folded Proteins: Consequences for Mesoscopic Aggregation of Lysozyme. *Biophys. J.* **2012**, *102*, 1934–1943.

(304) Louis, A. A.; Bolhuis, P. G.; Hansen, J. P. Mean-Field Fluid Behavior of the Gaussian Core Model. *Phys. Rev. E* **2000**, *62*, 7961–7972.

(305) Louis, A. A.; Bolhuis, P. G.; Finken, R.; Krakoviack, V.; Meijer, E. J.; Hansen, J. P. Coarse-Graining Polymers As Soft Colloids. *Physica A* **2002**, *306*, 251–261.

(306) Dautenhahn, J.; Hall, C. K. Monte Carlo Simulation of Off-Lattice Polymer Chains: Effective Pair Potentials in Dilute Solution. *Macromolecules* **1994**, *27*, 5399–5412.

(307) Bolhuis, P. G.; Louis, A. A.; Hansen, J. P.; Meijer, E. J. Accurate Effective Pair Potentials for Polymer Solutions. *J. Chem. Phys.* **2001**, *114*, 4296–4311.

(308) Genz, U.; D'Aguanno, B.; Mewis, J.; Klein, R. Structure of Sterically Stabilized Colloids. *Langmuir* **1994**, *10*, 2206–2212.

(309) Lo Verso, F.; Yelash, L.; Egorov, S. A.; Binder, K. Interactions Between Polymer Brush-Coated Spherical Nanoparticles: The Good Solvent Case. *J. Chem. Phys.* **2011**, *135*, 214902.

(310) Fritz, G.; Schädler, V.; Willenbacher, N.; Wagner, N. J. Electrosteric Stabilization of Colloidal Dispersions. *Langmuir* **2002**, *18*, 6381–6390.

(311) Jusufi, A.; Watzlawek, M.; Löwen, H. Effective Interaction Between Star Polymers. *Macromolecules* **1999**, *32*, 4470–4473.

(312) Lue, L. Volumetric Behavior of Athermal Dendritic Polymers: Monte Carlo Simulation. *Macromolecules* **2000**, *33*, 2266–2272.

(313) Götze, I. O.; Harreis, H. M.; Likos, C. N. Tunable Effective Interactions Between Dendritic Macromolecules. *J. Chem. Phys.* **2004**, *120*, 7761–7771.

(314) Likos, C. N.; Ballauff, M. Equilibrium Structure of Dendrimers: Results and Open Questions. *Topics Curr. Chem.* **2005**, *245*, 239–252.

(315) Bosko, J. T.; Prakash, J. R. Effect of Molecular Topology on the Transport Properties of Dendrimers in Dilute Solution at Θ Temperature: A Brownian Dynamics Study. *J. Chem. Phys.* **2008**, *128*, 034902.

(316) Warren, P. B. Dissipative Particle Dynamics. *Curr. Opin. Colloid Interface Sci.* **1998**, *3*, 620–624.

(317) Hendrickson, G. R.; Lyon, L. A. Microgel Translocation Through Pores Under Confinement. *Angew. Chem. Int. Ed.* **2010**, *49*, 2193–2197.

(318) Mattsson, J.; Wyss, H. M.; Fernandez-Nieves, A.; Miyazaki, K.; Hu, Z.; Reichman, D. R.; Weitz, D. A. Soft Colloids Make Strong Glasses. *Nature* **2009**, *462*, 83–86.

(319) Fernández-Nieves, A.; Fernández-Barbero, A.; Vincent, B.; de las Nieves, F. J. Osmotic De-Swelling of Ionic Microgel Particles. *J. Chem. Phys.* **2003**, *119*, 10383–10388.

(320) Sierra-Martin, B.; Frederick, J. A.; Laporte, Y.; Markou, G.; Lietor-Santos, J. J.; Fernandez-Nieves, A. Determination of the Bulk Modulus of Microgel Particles. *Colloid Polym. Sci.* **2011**, *289*, 721–728.

(321) Streletzky, K. A.; Phillies, G. D. J. Translational Diffusion of Small and Large Mesoscopic Probes in Hydroxypropylcellulose-Water in the Solution-like Regime. *J. Chem. Phys.* **1998**, *108*, 2975–2988.

(322) Harve, K. S.; Raghunath, M.; Lareu, R. R.; Rajagopalan, R. Macromolecular Crowding in Biological Systems: Dynamic Light Scattering (DLS) to Quantify the Excluded Volume Effect (EVE). *Biophys. Rev. Lett.* **2006**, *1*, 317–325.

(323) Parsegian, V. A.; Rand, R. P.; Fuller, N. L.; Rau, D. C. Osmotic Stress for the Direct Measurement of Intermolecular Forces. *Methods Enzymol.* **1986**, *127*, 400–416.

(324) Parsegian, V. A.; Rand, R. P.; Rau, D. C. Macromolecules and Water: Probing with Osmotic Stress. *Methods Enzymol.* **1995**, *259*, 43–94.

(325) Dijkstra, M.; van Roij, R.; Evans, R. Effective Interactions, Structure, and Isothermal Compressibility of Colloidal Suspensions. *J. Chem. Phys.* **2000**, *113*, 4799–4807.

(326) Cantor, A. S.; Pecora, R. Dynamics of Flexible Coils in an Isorefractive Rod/coil Composite Liquid. 2. Ternary Solutions. *Macromolecules* **1994**, *27*, 6817–6833.

(327) Gavish, B.; Gratton, E.; Hardy, C. J. Adiabatic Compressibility of Globular Proteins. *Proc. Natl. Acad. Sci. USA* **1983**, *80*, 750–754.

(328) Gekko, K.; Noguchi, H. Compressibility of Globular Proteins in Water at 25 °C. *J. Phys. Chem.* **1979**, *83*, 2706–2714.

(329) Kharakoz, D. P.; Sarvazyan, A. P. Hydrational and Intrinsic Compressibilities of Globular Proteins. *Biopolymers* **1993**, *33*, 11–26.

(330) Paci, E.; Velikson, B. On the Volume of Macromolecules. *Biopolymers* **1997**, *41*, 785–797.

(331) Gekko, K.; Noguchi, H. Physicochemical Studies of Oligodextran. I. Molecular Weight Dependence of Intrinsic Viscosity, Partial Specific Compressibility and Hydrated Water. *Biopolymers* **1971**, *10*, 1513–1524.

(332) Gekko, K.; Hasegawa, Y. Compressibility-Structure Relationship of Globular Proteins. *Biochemistry* **1986**, *25*, 6563–6571.

(333) Vinogradov, B. V. In *Handbook of Physical Quantities*; Grigoriev, I. S., Meilikhov, E. Z., Eds.; Boca Raton, FL: CRC Press, 1997; pp 97–113.

(334) Corning Inc., *HPFS® Fused Silica Standard Grade brochure*; 2003.

(335) Haynes, W. M., Lide, D. R., Eds. *CRC Handbook of Chemistry and Physics*; Boca Raton, FL: CRC Press, 2011; pp 6-12, 6-156–6-157.

(336) Warfield, R. W.; Cuevas, J. E.; Barnet, F. R. Single Specimen Determination of Young's and Bulk Moduli of Polymers. *Rheol. Acta* **1970**, *9*, 439–46.

(337) Zorębski, E.; Nurek, J. Ultrasonic Speeds, Molar Excess Volumes and Adiabatic Compressibilities of the 1-Butanol + Glycerol System at 298.15 K. *Z. Phys. Chem.* **2002**, *216*, 895–904.

(338) Kushare, S. K.; Terdale, S. S.; Dagade, D. H.; Patil, K. J. Compressibility and Volumetric Studies of Polyethylene-Glycols in aqueous, methanolic, and benzene solutions at T = 298.15 K. *J. Chem. Thermodyn.* **2007**, *39*, 1125–1131.

(339) Kell, G. S. Precise Representation of Volume Properties of Water at One Atmosphere. *J. Chem. Eng. Data* **1967**, *12*, 66–69.

(340) Kell, G. S. Isothermal Compressibility of Liquid Water at 1 Atm. *J. Chem. Eng. Data* **1970**, *15*, 119–122.

(341) Dunbar, J. I.; North, A. M.; Pethrick, R. A.; Steinhauer, D. B. Acoustic Absorption and Dynamic Compressibility Studies of Dilute and Concentrated Solutions of Polystyrene in Toluene and Cyclohexane. *J. Polym. Sci. Polym. Phys* **1977**, *15*, 263–277.

(342) Nath, J.; Dixit, A. P. Ultrasonic Velocities In, and Adiabatic Compressibilities For, Binary Liquid Mixtures of Acetone with Benzene, Toluene, *P*-Xylene, and Mesitylene at 308.15 K. *J. Chem. Eng. Data* **1984**, *29*, 320–321.

(343) Onori, G. Adiabatic Compressibility and Structure of Aqueous Solutions of Ethyl Alcohol. *J. Chem. Phys.* **1988**, *89*, 4325–4332.

(344) Onori, G. Adiabatic Compressibility and Structure of Aqueous Solutions of Methyl-Alcohol. *J. Chem. Phys.* **1987**, *87*, 1251–1255.

(345) Nath, J. Speeds of Sound in and Isentropic Compressibilities of (*N*-Butanol + *N*-Pentane, or *N*-Hexane, or *N*-Heptane, or *N*-Octane, or 2,2,4-

trimethylpentane, or carbon tetrachloride) at T = 293.15 K. *J. Chem. Thermodyn.* **1997**, *29*, 853–863.

(346) McClements, D. J.; Povey, M. J. W. Ultrasonic Velocity As a Probe of Emulsions and Suspensions. *Adv. Colloid Interface Sci.* **1987**, *27*, 285–316.

(347) Challis, R. E.; Povey, M. J. W.; Mather, M. L.; Holmes, A. K. Ultrasound Techniques for Characterizing Colloidal Dispersions. *Rep. Prog. Phys.* **2005**, *68*, 1541–1637.

(348) Porath, J.; Aspberg, K.; Drevin, H.; Axén, R. Preparation of Cyanogen Bromide-Activated Agarose Gels. *J. Chromatog.* **1973**, *86*, 53–56.

(349) Sundberg, L.; Porath, J. Preparation of Adsorbents for Biospecific Affinity Chromatography. I. Attachment of Group-Containing Ligands to Insoluble Polymers by Means of Bifunctional Oxiranes. *J. Chromatog.* **1974**, *90*, 87–98.

(350) Matsumoto, I.; Mizuno, Y.; Seno, N. Activation of Sepharose with Epichlorohydrin and Subsequent Immobilization of Ligand for Affinity Adsorbent. *J. Biochem.* **1979**, *85*, 1091–1098.

(351) Andersson, T.; Carlsson, M.; Hagel, L.; Pernemalm, P.-Ä.; Janson, J.-C. Agarose-Based Media for High-Resolution Gel Filtration of Biopolymers. *J. Chromatog.* **1985**, *326*, 33–44.

(352) Lindgren, G. E. S. Method of cross-linking a porous polysaccharide gel. 1990; US Patent 4,973,683.

(353) Hennink, W. E.; van Nostrum, C. F. Novel Crosslinking Methods to Design Hydrogels. *Adv. Drug Delivery Rev.* **2002**, *54*, 13–36.

(354) Frey, H.; Haag, R. Dendritic Polyglycerol: A New Versatile Biocompatible Material. *Rev. Molec. Biotech.* **2002**, *90*, 257–267.

(355) Haag, R.; Stumbé, J. F.; Sunder, A.; Frey, H.; Hebel, A. An Approach to Core-Shell-Type Architectures in Hyperbranched Polyglycerols by Selective Chemical Differentiation. *Macromolecules* **2000**, *33*, 8158–8166.